UNIVERSITÉ DU QUÉBEC À TROIS-RIVIÈRES

# VERS UN CHASSIS DE BIOLOGIE SYNTHÉTIQUE POUR LA PRODUCTION DE PRÉCURSEURS D'ALCALOÏDES D'AMARYLLIDACEAE : CARACTÉRISATION DE LA TYROSINE DÉCARBOXYLASE1 DE *NARCISSUS PSEUDONARCISSUS* ET EXPRESSION HÉTÉROLOGUE DANS *CHLAMYDOMONAS REINHARDTII*

# TOWARDS A SYNTHETIC BIOLOGY PLATFORM TO PRODUCE AMARYLLIDACEAE ALKALOID PRECURSORS: CHARACTERIZATION OF TYROSINE DECARBOXYLASE1 FROM *NARCISSUS PSEUDONARCISSUS* AND ITS HETEROLOGOUS EXPRESSION IN *CHLAMYDOMONAS REINHARDTII*

THÈSE PRÉSENTÉE

COMME EXIGENCE PARTIELLE DE LA

DU DOCTORAT EN BIOLOGIE CELLULAIRE ET MOLÉCULAIRE

PAR

ARGHAVAN ARJMANDI

AOÛT 2026

Université du Québec à Trois-Rivières

Service de la bibliothèque

Avertissement

L'auteur de ce mémoire, de cette thèse ou de cet essai a autorisé l'Université du Québec à Trois-Rivières à diffuser, à des fins non lucratives, une copie de son mémoire, de sa thèse ou de son essai.

Cette diffusion n'entraîne pas une renonciation de la part de l'auteur à ses droits de propriété intellectuelle, incluant le droit d'auteur, sur ce mémoire, cette thèse ou cet essai. Notamment, la reproduction ou la publication de la totalité ou d'une partie importante de ce mémoire, de cette thèse et de son essai requiert son autorisation.

UNIVERSITÉ DU QUÉBEC À TROIS-RIVIÈRES

BIOLOGIE CELLULAIRE ET MOLÉCULAIRE (DOCTORAT)

**Direction de recherche** :

**Isabel Desgagné-Penix**

Prénom et nom — Directeur de recherche

**Jury d'évaluation**

**Isabel Desgagné-Penix**

Prénom et nom — Directeur de recherche

**Hugo Germain**

Prénom et nom — Président du jury

**Tagnon Missihoun**

Prénom et nom — Évaluateur interne

**Guanqun (Gavin) Chen**

Prénom et nom — Évaluateur externe

## Résumé en français:

Les alcaloïdes des Amaryllidacées (AmAs) constituent un groupe de plus de 650 métabolites spécialisés végétaux d'une importance pharmacologique significative, notamment la galanthamine, utilisée cliniquement pour traiter les symptômes de la maladie d'Alzheimer, ainsi que la lycorine et la chérylline, qui présentent respectivement des activités anticancéreuses et antivirales. Tous les AmAs partagent une origine biosynthétique commune et dérivent de la norbelladine, elle-même formée par la condensation de la tyramine et du 3,4-dihydroxybenzaldéhyde. La tyramine est produite par la décarboxylation de la L-tyrosine par la tyrosine décarboxylase (TyDC), une enzyme dépendante du pyridoxal 5'-phosphate qui catalyse la première étape engagée dans la biosynthèse des AmAs. Malgré son rôle central, l'enzyme TyDC responsable de la production de tyramine chez *Narcissus pseudonarcissus* 'King Alfred' n'avait pas été caractérisée expérimentalement avant ce travail. De plus, le potentiel des microorganismes photosynthétiques en tant qu'hôtes hétérologues pour la reconstruction des premières étapes de la voie des AmAs n'avait pas été évalué pour cette espèce. Par conséquent, cette thèse visait à caractériser les isoformes TyDC de *N. pseudonarcissus* et à évaluer *Chlamydomonas reinhardtii* comme châssis pour la biosynthèse hétérologue de tyramine.

Deux isoformes TyDC complètes, *NpTyDC1* et *NpTyDC2*, ont été identifiées à partir des données du transcriptome de *N. pseudonarcissus*, clonées et exprimées de manière hétérologue dans *E. coli*. L'analyse *in silico* a placé *Np*TyDC1 au sein d'un clade phylogénétique bien soutenu, aux côtés d'enzymes TyDC caractérisées provenant d'espèces de *Lycoris* productrices de galanthamine. La modélisation par homologie et l'amarrage moléculaire ont révélé une poche de liaison au PLP compatible avec la liaison de la L-tyrosine, et des motifs conservés caractéristiques de la famille des décarboxylases d'acides aminés aromatiques ont été identifiés.

Des tests enzymatiques couplés à la HPLC-MS/MS ont confirmé que *Np*TyDC1 décarboxyle la L-tyrosine en tyramine, avec une préférence claire pour ce substrat par rapport à la L-phénylalanine, au L-tryptophane et au L-DOPA. L'analyse cinétique a donné un $K_m$ de 109 µM, un *kcat* de 0,02337 $s^{-1}$ et une $V_{max}$ de 0,23 nkat $mg^{-1}$, des valeurs cohérentes avec un rôle de gardien à faible flux à l'entrée de la biosynthèse des AmAs et conformes à celles rapportées pour les enzymes TyDC de *Lycoris* apparentées. En revanche, *Np*TyDC2 n'a montré aucune activité tyrosine décarboxylase détectable dans les conditions testées, et son rôle physiologique demeure incertain. Des études de localisation subcellulaire dans *Nicotiana benthamiana* ont placé les deux isoformes dans le compartiment nucléocytoplasmique. Ensemble, ces résultats établissent *Np*TyDC1 comme l'isoforme principale dirigeant la L-tyrosine vers le réseau biosynthétique des AmAs et fournissent la première caractérisation biochimique et cinétique d'une TyDC issue de *N. pseudonarcissus*.

*C. reinhardtii* a ensuite été évaluée comme châssis photosynthétique pour la biosynthèse de tyramine. L'analyse bioinformatique de la séquence endogène unique de type décarboxylase d'acides aminés aromatiques chez *C. reinhardtii* a révélé un résidu glycine à la position de sélectivité du substrat et un placement phylogénétique plus proche des synthases du 4-hydroxyphénylacétaldéhyde que des TyDCs végétales, et aucune tyramine n'a été détectée dans les extraits métaboliques de l'algue, confirmant l'absence d'activité décarboxylase endogène. Des tests de croissance ont montré que *C. reinhardtii* tolère la L-tyrosine exogène jusqu'à sa limite de solubilité sans altération de la croissance, et tolère la tyramine à de faibles concentrations, une inhibition de croissance n'étant observée qu'à partir de 16 mM. *Np*TyDC1 optimisé pour les codons et marqué à la mVenus a été assemblé sous le promoteur *PsaD* et introduit dans la souche UVM4 de *C. reinhardtii* par transformation nucléaire. L'imagerie de

colonies a indiqué une fluorescence mVenus ; cependant, les tests quantitatifs en plaques et la cytométrie en flux n'ont pas détecté de population fluorescente stable en culture liquide, et aucune accumulation de tyramine n'a été observée dans les extraits algaux transformés. La cause sous-jacente n'a pas pu être déterminée à partir de ces seules données. Le silençage des transgènes nucléaires constitue une explication possible. Les effets de position découlant d'une intégration par jonction d'extrémités non homologues pourraient également avoir contribué. Collectivement, ce travail établit *Np*TyDC1 comme un gardien biochimiquement défini de la biosynthèse des AmAs, démontre la compatibilité métabolique de *C. reinhardtii* avec le substrat et le produit de cette réaction, et identifie la stabilité de l'expression des transgènes nucléaires comme le principal obstacle à la production de tyramine dans cet hôte photosynthétique.

## Abstract:

Amaryllidaceae alkaloids (AmAs) are a group of more than 650 specialized plant metabolites with significant pharmacological importance, including galanthamine, which is clinically used to treat the symptoms of Alzheimer's disease, and lycorine and cherylline, which display anticancer and antiviral activities, respectively. All AmAs share a common biosynthetic origin and derive from norbelladine, which is itself formed from the condensation of tyramine and 3,4-dihydroxybenzaldehyde. Tyramine is produced by the decarboxylation of L-tyrosine by tyrosine decarboxylase (TyDC), a pyridoxal 5'-phosphate-dependent enzyme that catalyzes the first committed step in AmA biosynthesis. Despite its central role, the TyDC enzyme responsible for tyramine production in *Narcissus pseudonarcissus* 'King Alfred' had not been experimentally characterized prior to this work. Furthermore, the potential of photosynthetic microorganisms as heterologous hosts for early AmA pathway reconstruction had not been evaluated for this species. Consequently, this thesis aimed to characterize the TyDC isoforms from *N. pseudonarcissus* and to evaluate *Chlamydomonas reinhardtii* as a chassis for heterologous tyramine biosynthesis.

Two full-length TyDC isoforms, *NpTyDC1* and *NpTyDC2*, were identified from *N. pseudonarcissus* transcriptome data, cloned, and heterologously expressed in *E. coli*. *In silico* analysis placed *Np*TyDC1 within a well-supported phylogenetic clade alongside characterized TyDC enzymes from galanthamine-producing *Lycoris* species. Homology modelling and molecular docking revealed a PLP-binding pocket compatible with L-tyrosine binding, and conserved motifs characteristic of the aromatic amino acid decarboxylase family were identified. Enzymatic assays coupled with HPLC-MS/MS confirmed that *Np*TyDC1 decarboxylates L-tyrosine to tyramine, with a clear preference for this substrate over L-

phenylalanine, L-tryptophan, and L-DOPA. Kinetic analysis yielded a $K_m$ of 109 μM, a *kcat* of 0.02337 $s^{-1}$, and a $V_{max}$ of 0.23 nkat $mg^{-1}$, values consistent with a low-flux gatekeeper role at the entry point of AmA biosynthesis and in line with those reported for related *Lycoris* TyDC enzymes. In contrast, *Np*TyDC2 showed no detectable tyrosine decarboxylase activity under the conditions tested, and its physiological role remains unclear. Subcellular localization studies in *Nicotiana benthamiana* placed both isoforms in the nucleocytoplasmic compartment. Together, these findings establish *Np*TyDC1 as the principal isoform between the two isoforms in this study to direct L-tyrosine into the AmA biosynthetic network and provide the first biochemical and kinetic characterization of a TyDC from *N. pseudonarcissus*.

*C. reinhardtii* was then evaluated as a photosynthetic chassis for tyramine biosynthesis. Bioinformatic analysis of the single endogenous aromatic amino acid decarboxylase-like sequence in *C. reinhardtii* revealed a glycine residue at the substrate-selectivity position and a phylogenetic placement closer to 4-hydroxyphenylacetaldehyde synthase-type aldehyde synthases than to plant TyDCs, and no tyramine was detected in algal metabolite screens, confirming the absence of endogenous decarboxylase activity. Growth assays showed that *C. reinhardtii* tolerates exogenous L-tyrosine up to its solubility limit without growth impairment and tolerates tyramine at low concentrations, with growth inhibition observed only at 16 mM and above. A codon-optimized, mVenus-tagged *Np*TyDC1 construct was assembled under the *PsaD* promoter and introduced into the *C. reinhardtii* UVM4 strain via nuclear transformation. Colony imaging indicated mVenus fluorescence; however, quantitative plate assays and flow cytometry did not detect a stable fluorescent population in liquid culture, and no tyramine accumulation was observed in transformed algal extracts. The underlying cause could not be determined from these data alone. Nuclear transgene silencing is one possible explanation.

Position effects arising from non-homologous end-joining integration may have also contributed. Collectively, this work establishes *Np*TyDC1 as a biochemically defined gatekeeper of AmA biosynthesis, demonstrates the metabolic compatibility of *C. reinhardtii* with the substrate and product of this reaction, and identifies nuclear transgene expression stability as the main barrier to tyramine production in this photosynthetic host.

## Acknowledgments:

First and foremost, I would like to thank my lovely husband. I also wish to express how grateful I am for my parents and my amazing aunt. My mother and her sister, Mina and Nahid, both bring a profound and tangible sense of joy and warmth, and even though they are so far away, I always felt their love and presence with me. I would also like to thank my Canadian family. My sweet mother-in-law who treated me as her own daughter and made my first winter in Canada not only bearable, but also warm and cozy with homemade food and board games. My adoptive Canadian aunts and uncles, Auntie Esther, Auntie Judy, Uncle Frankie, Uncle Michel, and his lovely wife Diane. And France, who has been like an older sister to me. I take infinite delight in being part of such a wonderful family so far away from my home country.

I extend my deepest gratitude to my supervisor, Pr. Isabel Desgagné-Penix, for in my most difficult moments, the light of her knowledge illuminated my path. I was fortunate to witness her analytical mind at work and to learn from it. She consistently was available for a scientific chat when I needed her guidance, even though her schedule was always so full. I am also incredibly grateful to her right hand, Dr. Natacha Mérindol, whose presence was a constant source of warmth and encouragement. Her scientific insights were always helpful, on point, and sharp. She represents a perfect harmony of kindness and intelligence, meaning that in her presence, asking questions never felt overwhelming. I am also incredibly thankful to Dr. Karen Cristine Gonçalves dos Santos for familiarizing me with the world of coding and R. She was an extraordinary teacher that I was privileged to have, and her brilliance makes every conversation a genuinely interesting one.

I also wish to thank the many wonderful friends I made along the way during my PhD journey: Dr. Vahid Karimzadegan, Dr. Nicolas Sene, Ms. Negar Noorbakhsh, Dr. Sameera Liyanage,

Dr. Snehi Gazal, Mr. Sajjad Sobhanverdi and his lovely wife Melika Ghaziani, Zahra Naderian, and Dr. Elisa Fantino. Pursuing a PhD can be an isolating experience, and having each of you nearby made all the difference. You turned long lab days into shared adventures and laughter, and I am deeply grateful for the countless small moments together that made this chapter of my life so rich.

Finally, I dedicate this thesis to my incredible husband, Bryan, who has been by my side supporting me through this rollercoaster of a journey. Your selflessness and kindness are the reason I was able to finish my studies in a foreign country with ease, feeling safe and unburdened, because you were there for me every step of the way, whether to protect me or to offer words of encouragement on the days I could not see a light at the end of the tunnel. You were not only a source of support, but also a force that pushed me to go higher, to be better, and to surpass my own limits. I am forever thankful for having you by my side, my love.

Statement on the Use of Artificial Intelligence

During the preparation of this thesis, AI-based language tools were used to assist with editing for grammar, clarity, and flow, and for initial literature searches. These tools were used only as an aid: all AI-assisted text was reviewed, verified, and edited by the author, and all sources identified with AI assistance were independently located, read, added to the library, and cited in their original form. The research design, data analysis, interpretation of results, and all scientific conclusions presented in this thesis are entirely the author's own. Full responsibility for the content of this work rests with the author.

1. Introduction ..... 6

1.1. Specialized Metabolites in Plants ..... 7

1.1.1. Nitrogen-Free Plant Metabolites ..... 8

1.1.2. Nitrogen-Containing Metabolites ..... 10

1.1.2.1. Non-Alkaloid Nitrogen-Containing Metabolites ..... 10

1.1.2.2. Alkaloids ..... 10

1.1.2.1.1. Amaryllidaceae Alkaloids ..... 14

1.2. Amaryllidaceae ..... 15

1.2.1. *Narcissus pseudonarcissus* ..... 18

1.3. Amaryllidaceae Alkaloid Biosynthesis ..... 20

1.3.1. Amaryllidaceae alkaloid biosynthetic pathway ..... 20

1.3.1.1. Tyrosine Decarboxylase ..... 21

1.3.1.2. Norbelladine Synthase (NBS) ..... 22

1.3.2. Shikimate pathway ..... 23

1.3.3. Phenylpropanoid pathway ..... 24

1.4. Synthetic Biology Approaches for Plant Alkaloid Production ..... 29

1.5. *Chlamydomonas reinhardtii* ..... 31

1.5.1. Gene expression in *C. reinhardtii* ..... 34

1.5.1.1.1. UV-mutagenized strains, specifically UVM4 and UVM11 ..... 36
1.5.1.1.2. Codon optimization ..... 36
1.5.1.1.3. Inclusion of endogenous introns ..... 37
1.5.1.1.4. Promoter engineering: *HSP70A* and *PsaD* promoters. ..... 37
1.6. Problematic, Hypothesis and Objectives ..... 38
1.6.1. Problematic ..... 38
1.6.2. Research hypotheses ..... 40
1.6.3. Objectives ..... 40
1.6.3.1. Objective 1: Biochemical characterization of TyDCs from *N. pseudonarcissus* 'King Alfred' 40
1.6.3.2. Objective 2: Evaluation of *C. reinhardtii* as a chassis for *Np*TyDC1 expression and tyramine production. ..... 41
2. Chapter 2 ..... 44
2.1. Highlights ..... 47
2.2. Keywords ..... 47
2.3. Graphical abstract ..... 47
2.4. Abstract ..... 48
2.4. Introduction ..... 49
2.5. Results and Discussion ..... 53
2.5.1. Phylogenetic analysis supports that *Np*TyDC1 is evolutionarily close to other alkaloid-producing plants. ..... 53
2.5.2. Docking analysis suggests that *Np*TyDC1 and *Np*TyDC2 could bind multiple substrates ..... 56
2.5.3. Both *Np*TyDC1 and *Np*TyDC2 localize to the cytoplasm and nucleus ..... 59

*2.5.4. Np*TyDC1 exhibits high substrate specificity for L-tyrosine compared to *Np*TyDC2 ..... 60

2.5.5. Optimization of enzymatic assay conditions for *Np*TyDC1 ..... 63

2.6. Materials and Methods ..... 68

2.6.1. Conserved domain search ..... 68

2.6.2. Phylogenetic analysis ..... 68

2.6.3. Structural modelling and docking ..... 69

2.6.4. Bacterial strains and growth conditions ..... 70

2.6.5. RNA extraction, cDNA synthesis, and cloning of *Np*TyDC isoforms ..... 70

*2.6.6. Agrobacterium* transformation and transient expression for subcellular localization in *Nicotiana benthamiana* ..... 72

2.6.7. Expression of MBP fusion proteins in *E. coli* ..... 73

2.6.8. Protein quantification ..... 73

2.6.9. SDS-PAGE ..... 74

2.6.10. Protein purification and desalination ..... 74

2.6.11. Enzymatic assays ..... 75

2.6.12 HPLC-MS/MS analysis ..... 76

2.7. Conclusion ..... 78

2.8. Funding ..... 79

2.9. Acknowledgement ..... 79

2.10. Authors Contribution ..... 79

2.11. Declaration of Interest ..... 80

3. Chapter 3 ..... 81

3.1. Highlights ..... 83

3.2. Keywords ..... 83

3.3. Abstract ..... 84

3.4. Introduction ..... 86

3.4.1. Tyramine as a precursor of pharmacologically important plant alkaloids ..... 86

3.5. Materials and methods ..... 88

3.5.1. Bioinformatic Identification of AAAD-Like Proteins ..... 88

3.5.2. Conserve Domain and Phylogenetic Analysis ..... 89

3.5.3. *C. reinhardtii* Culture Conditions ..... 89

3.5.4. Toxicity Assays ..... 89

3.5.5. Endogenous Metabolite Production ..... 90

3.5.6. Metabolite Production Over a Course of Time ..... 90

3.5.7. Permeability to Substrate ..... 91

3.5.8. Assembly of the Construct ..... 91

3.5.9. Transformation ..... 92

3.6. Results ..... 94

3.6.1. The only AAAD-like protein from *C. reinhardtii* is likely not a tyrosine decarboxylase ..... 94

3.6.2. Tyramine and tyrosine supplementation do not affect the growth of *C. reinhardtii* UVM strains . 97

3.6.3. *C. reinhardtii* does not produce detectable tyramine or Amaryllidaceae alkaloids under standard growth conditions ..... 98

3.6.4. Supplemented tyrosine is taken up and retained by *C. reinhardtii* cells ..... 99

3.7. Discussion ..... 107

3.8. Conclusion ..... 113

4. Chapter 4 - Discussion, Conclusion and Perspective ..... 114

4.1. Overview ..... 115

4.2. *Np*TyDC1 within the broader TyDC landscape ..... 116

4.3. *C. reinhardtii* against an alternative chassis option ..... 120

4.4. *C. reinhardtii*: a metabolically clean but transcriptionally challenging chassis ..... 124

4.5. Contributions to the field ..... 126

4.6. Future Direction ..... 128

Chapter 5 - Annex ..... 130

4. Chapter 6 - References ..... 147

# 1. Introduction

## 1.1. Specialized Metabolites in Plants

Plants cannot move or flee from danger. So, it is only logical that they would have some systems in place that would defend them against possible threats. An important adaptation to achieve this goal involves plants utilizing powerful but small molecules (Wink, Ashour, and Botschen 2010). These compounds differ from primary metabolites in both their chemical nature and their distribution across species. While primary metabolites are found in nearly all plant species, specialized metabolites are far less widespread, and closely related species within the same genus, family, or order may have very different sets of these compounds. These metabolites are "specialized" to accomplish particular objectives, whether serving as protective mechanisms against disease-causing organisms and herbivorous animals or addressing various forms of environmental stress that plants may encounter (Wink, Ashour, and Botschen 2010). Their production stems from amino acids such as $_{L}$-phenylalanine and $_{L}$-tyrosine or shared precursor molecules like shikimic acid and acetyl-coenzyme A (acetyl-CoA) (Dias, Urban, and Roessner 2012).

These specialized metabolites, typically consisting of small and chemically reactive molecules, hold considerable pharmacological importance for human health (Wink, Ashour, and Botschen 2010). Well-known instances of medicine derived from natural sources include morphine, a powerful analgesic, and codeine, obtained from *Papaver somniferum* (Ziegler and Facchini 2008); aspirin, vincristine and vinblastine, which are both potent anticancer drugs, derived from *Catharanthus roseus* (Qu, Safonova, and De Luca 2019); and tetrahydrocannabinol, an active compound found in *Cannabis sativa* (Hanus et al. 2016) Beyond their pharmaceutical applications, specialized metabolites serve various industrial purposes as well, including use as

flavouring agents, cosmetic ingredients, dyes, and nutritional supplements (Garagounis, Delkis, and Papadopoulou 2021).

Specialized metabolites include a wide range of structurally diverse compounds, and one common way to organize them is based on whether their carbon skeleton contains nitrogen. This approach separates them into two broad classes. The first class, nitrogen-free metabolites, includes terpenoids and phenolics. The second class, nitrogen-containing metabolites, includes alkaloids along with other nitrogen-bearing compounds. The following sections review each class in turn and gradually narrow the focus toward alkaloids, and within that group, the Amaryllidaceae alkaloids.

### 1.1.1. Nitrogen-Free Plant Metabolites

Nitrogen-free plant metabolites can be devided in three subgroups (Figure 1). Terpenoids form the largest and most structurally diverse group of plant metabolites that do not have any nitrogen in their structure, unified by their isoprenoid biosynthetic origin (Cheng et al. 2007; Camara et al. 2024). Monoterpenes and sesquiterpenes are often volatile, contributing to plant scent and direct or indirect defence, and are widely studied for antimicrobial, anti-inflammatory, and anticancer activity (Gershenzon and Dudareva 2007; Patil et al. 2025; Sharifi-Rad et al. 2021). Diterpenes form more rigid polycyclic frameworks and include major drug scaffolds such as paclitaxel (Cheng et al. 2007; Yang et al. 2020). Triterpenes, steroids, and saponins all derive from the triterpenoid pathway via squalene cyclization, with saponins combining a hydrophobic aglycone with sugar chains to disrupt pathogen membranes, and the broader group shows anticancer, anti-inflammatory, and immunomodulatory properties (Phillips et al. 2006; Liu et al. 2024; Renda, Gokkaya, and Sohretoglu 2022). Tetraterpenes are represented mainly by carotenoids, whose extended conjugated structure supports photoprotection in plants and

antioxidant and anti-inflammatory effects in human health research (Wurtzel 2019). Phenolics and polyketides are aromatic compounds, but they originate from distinct biosynthetic routes. Phenylpropanoids, flavonoids, coumarins, tannins, lignins, and lignans derive primarily from the shikimate pathway via L-phenylalanine, though flavonoids are one of the notable exceptions in that they additionally incorporate malonyl-CoA extensions, placing them at the intersection of both pathways (Vogt 2010; Ferrer et al. 1999). Phenylpropanoids function broadly in pigmentation, UV screening, and defence and have yielded antioxidant, antimicrobial, anticoagulant, and antitumor leads (Motyka et al. 2023). Polyketides, in contrast, are assembled primarily by malonyl-CoA condensation chemistry, contributing to pigmentation and antimicrobial defence and showing antioxidant, anticancer, and phytoestrogen-related activities (Vogt 2010; Yu and Jez 2008). Lipid-derived compounds include polyacetylenes, fatty acids, and waxes. Polyacetylenes serve as antimicrobial compounds and are investigated for anti-inflammatory and anticancer effects (Xie and Wang 2022).

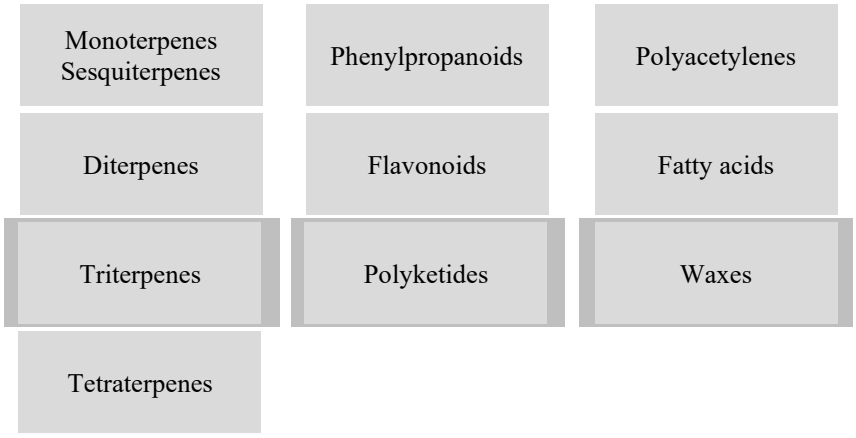



Figure 1. Nitrogen-free plant metabolites.

## 1.1.2. Nitrogen-Containing Metabolites

### 1.1.2.1. Non-Alkaloid Nitrogen-Containing Metabolites

Non-protein amino acids and amines are the structurally simplest members of the nitrogen-containing specialized metabolites, especially when compared to alkaloids. Non-protein amino acids serve several roles, including defence, signalling, nitrogen storage, and stress response (Bell 2003; Huang, Jander, and de Vos 2011). Many of them act as antimetabolites, they resemble standard metabolites closely enough to be taken up by enzymes or incorporated into proteins yet differ enough to disrupt normal function in herbivores and pathogens. Amines, formed through amino acid decarboxylation, contribute to growth regulation, stress responses, and physiological signalling (Alcazar, Bueno, and Tiburcio 2020). Furthermore, plants store certain nitrogen-containing compounds as inactive glycosidic precursors that become toxic only upon tissue disruption (Gleadow and Moller 2014). Cyanogenic glycosides release hydrogen cyanide through enzymatic hydrolysis and raise notable food-safety concerns, though some members show preliminary anticancer potential (Pirselova and Jakubcinova 2025). Glucosinolates, characteristic of Brassicales, follow the same activation principle, and release isothiocyanates such as sulforaphane, which appear to exert anti-inflammatory, cytoprotective, and anticancer effects, making them one of the most studied plant chemo-preventive compounds (Orouji et al. 2023). The nitrogen-containing compounds show great diversity. For example, alkamides are lipophilic amide-containing molecules with fatty-acid-derived chains. They participate in defence and signaling and are studied for anti-inflammatory and antimicrobial effects (Greger 2015; Mendez-Bravo et al. 2011).

### 1.1.2.2. Alkaloids

Alkaloids are nitrogen-containing plant specialized metabolites whose basic chemical character arises primarily from a protonatable nitrogen atom (Aniszewski 2007). In most cases, nitrogen is incorporated into a heterocyclic ring that forms the structural core of the molecule (Bhambhani, Kondhare, and Giri 2021). In plants, alkaloids function primarily as defence compounds, as their strong biological activity allows them to target the nervous systems and key enzymes of herbivores and pathogens (Sarvananda et al. 2025). Consequently, this same potency makes them highly valuable as pharmacological agents in medicine (Thawabteh et al. 2024). The classification of alkaloids includes three main types: true alkaloids, protoalkaloids, and pseudoalkaloids. True alkaloids are derived from amino acids (Aniszewski 2007; Wink, Ashour, and Botschen 2010). They function in plant defence against herbivores and pathogens and have contributed the majority of clinically important plant-derived drugs (Wink, Ashour, and Botschen 2010).

| **Betalains** | **Non-Protein Amino Acids** | **Alkaloids** |
|---|---|---|
| Cyanogenic Glycosides | Asparate Pathway | Protoalkaloids |
| Glucosinolates | Glutamate Pathway | Pseudoalkaloids |
| Triterpenes | Shikimate Pathway | True Alkaloids |
| Tetraterpenes | | |

Figure 2. Nitrogen-containing plant metabolites

Among pharmacologically significant subgroups, are indole alkaloids derived from tryptophan, which include the antitumor vinblastine and vincristine, as well as the antihypertensive

compound reserpine (Zhu et al. 2014). Isoquinoline alkaloids derive from L-tyrosine and encompass structurally diverse subclasses, including benzylisoquinolines, aporphines, protoberberines, morphinans, and bisbenzylisoquinolines (Yang et al. 2024). In addition, a large number of nitrogen-containing alkaloids are built on monocyclic scaffolds such as pyridine, piperidine, pyrrolidine, and imidazole, while more complex members incorporate bicyclic systems such as pyrrolizidine, quinoline, and quinazoline. (Aniszewski 2007). Collectively, true alkaloids cover a broad spectrum of therapeutic applications, including analgesic, antitumor, antimalarial, antimicrobial, anticholinergic, antihypertensive, and central nervous system activities (Thawabteh et al. 2024). Protoalkaloids are also derived from amino acids, but their nitrogen atom sits in an open side chain rather than a ring, which makes them structurally simpler than true alkaloids (Thawabteh et al. 2024). Phenethylamine-type alkaloids are their main representatives and arise from L-phenylalanine or L-tyrosine via decarboxylation. The phenethylamine scaffold includes many neuroactive, cardiovascular, and psychoactive compounds, such as endogenous catecholamines, and remains a widely explored platform in medicinal chemistry (Thawabteh et al. 2024).

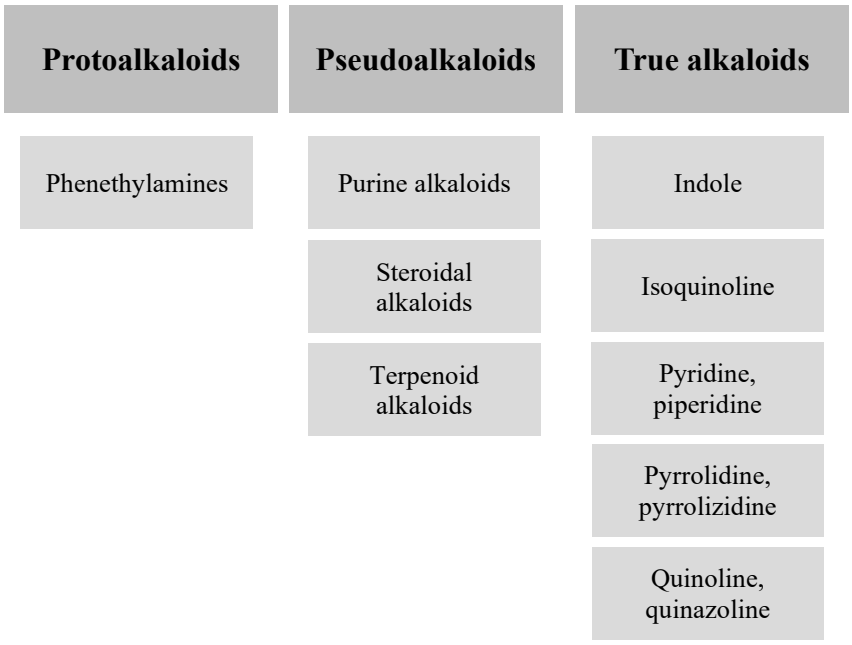



Figure 3. Classification of alkaloids.

Pseudoalkaloids do not derive their carbon skeleton from amino acids; instead, they arise from terpenoid, steroid, or purine biosynthetic pathways, with the nitrogen atom usually incorporated by transamination (Aniszewski 2007). This group includes purine alkaloids, derived from methylated xanthine synthesized from purine nucleotide catabolism products, such as caffeine, theobromine, and theophylline (Ashihara, Sano, and Crozier 2008). Steroidal alkaloids, which are prominent in Solanaceae, carry both alkaloid and steroid properties and appear to have relevant anticancer and anti-inflammatory activity (Dey et al. 2019). Furthermore, terpenoid alkaloids, notably the highly polycyclic diterpenoid alkaloids from *Aconitum* and *Delphinium*, exhibit analgesic and antiarrhythmic properties, yet their therapeutic application remains limited by significant cardiotoxicity (Wang et al. 2024; Zong et al. 2019).

Alkaloids are produced in a variety of plant tissues, including leaves, roots, bark, and seeds, and then transported to specific tissues where they perform a defensive function. These compounds protect plants by preventing and combating abiotic and biotic stresses like pests, fungi, bacteria,

and insect larvae. Furthermore, alkaloids have allelopathic properties, which prevent the growth of nearby competing plants. Through these mechanisms, alkaloids play an important role in plant survival and defence, contributing to the plant's ability to thrive in its environment. (Kilgore and Kutchan 2016; Bhambhani, Kondhare, and Giri 2021). Among the true alkaloids, the isoquinoline group derived from L-tyrosine is particularly notable in plant natural product chemistry (Yang et al. 2024). It includes a structurally rich set of subclasses and contains several clinically important compounds (Bastida et al. 2011). The Amaryllidaceae alkaloids are closely related to this group and form a distinct family with their own biosynthetic logic (Kilgore and Kutchan 2016; Desgagné-Penix 2021). Their structural diversity and pharmacological relevance are the focus of the following section.

### 1.1.2.1.1. Amaryllidaceae Alkaloids

Amaryllidaceae alkaloids (AmAs) are a structurally distinct group of more than 650 specialized plant metabolites. Their biosynthesis and classification have been covered in several reviews (Desgagné-Penix 2021; Bastida et al. 2011; Kilgore and Kutchan 2016; Liyanage et al. 2024). They all share a common biosynthetic origin, deriving from the central precursor norbelladine, which is formed through the condensation of tyramine and 3,4-dihydroxybenzaldehyde (Singh et al. 2018). Norbelladine then undergoes *O*-methylation and the resulting 4′-*O*-methylnorbelladine subsequently undergoes intramolecular oxidative phenol coupling reactions (Kilgore, Augustin, Starks, O'Neil-Johnson, et al. 2014). These reactions follow three main modes of carbon coupling, para-para', ortho-para', and para-ortho', each generating a different core ring system. The diversity of coupling modes, together with downstream structural rearrangements, accounts for the large number of distinct alkaloid skeletons found within this

family. The main structural types include the lycorine-, crinine-, haemanthamine-, narciclasine-, tazettine-, montanine-, and galanthamine-type alkaloids.

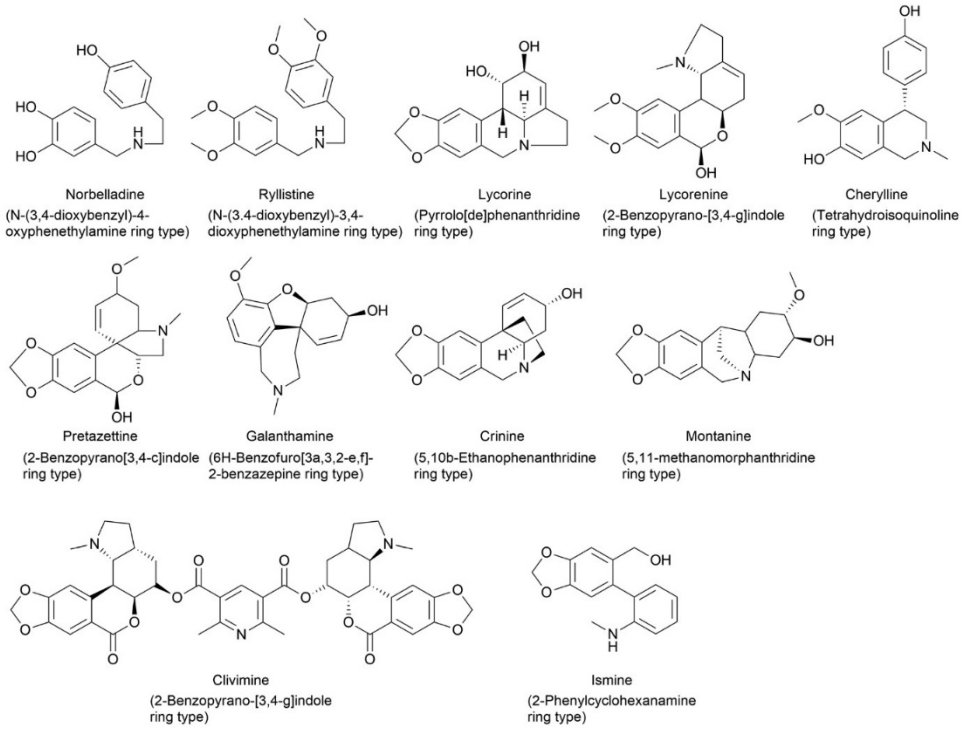



Figure 4. Amaryllidaceae alkaloids classification based on ring type as seen in (Jayawardena et al. 2024).

In plants, AmAs function primarily as defence compounds (Wink, Ashour, and Botschen 2010). Galanthamine acts as a selective acetylcholinesterase (AChE) inhibitor and is clinically approved for treating the symptoms of Alzheimer's disease (Lim, Schneider, and Loy 2024). Furthermore, lycorine has demonstrated both antiviral and anticancer activity, while other subclasses are actively being investigated for antimicrobial, anti-inflammatory, and cytotoxic effects (Roy et al. 2018; Thawabteh et al. 2024; Nair, Bastida, and Van Stadena 2016).

## 1.2. Amaryllidaceae

Amaryllidaceae is a primarily tropical family that is widely distributed throughout the world, from South America and South Africa to the Mediterranean region (Meerow and Snijman 1998). Amaryllidaceae members are perennials and are mostly bulbous. Although some are aquatic or epiphytic, most of them grow in soil. Leaves may be annual or persistent and show clear variation in form. The leaves can be sessile and linear to strap-shaped or petiolate. They can range from lanceolate to broadly elliptic. Their positions are usually arranged in two ranks or in a spiral. In some genera, they form sheaths at the base, which can form an aerial pseudostem. The surfaces of leaves are usually glabrous and rarely have trichomes. The flower has six segments called tepals, arranged in two groups of three. These tepals are usually fused at the base to form a short or long tube. The inner tepals are generally shorter than the outer ones.




Figure 5. Morphological features of representative Amaryllidaceae species. A. Habitat of *Narcissus pseudonarcissus*. B. Flower of *Hippeastrum papilio* showing six tepals. C. Cross-section of a tunicate bulb and leaves of *Hippeastrum aulicum*. D. Trumpet-shaped corona of *Narcissus pseudonarcissus*. E. Flower of *Galanthus nivalis* showing the reduced inner segments. F. Mature seeds with black phytomelanous testa. Image credits: **A,** Chris Manteling **B,** Tommy Tree **C,** A. P. Fontana/Instituto Nacional da Mata Atlântica - INMA **D,** Björn S. **E,** Małgorzata Ptaszek **F,** Juan Carlos Fonseca Mata. Creative Commons Attribution-Share Alike 4.0 International licenses for A, B, C, E, F. Creative Commons Attribution-Share Alike 2.0 Generic license for D.

A corona, a central petal-like structure, may form as an outgrowth of the tepals. In other instances, a smaller structure may be present at the opening of the floral tube. Seeds typically have a black or brown phytomelanous testa; they are globose to subglobose, fleshy, or hard, or flattened and winged. The endosperm contains hemicellulose and lipids and, in the more derived genera, is rich in water and/or starch (Meerow and Snijman 1998). Based on the latest classification, the Amaryllidaceae family consists of three subfamilies: Allioideae, Agapanthoideae, and Amaryllidoideae. Agapanthoideae is monotypic and endemic to South Africa, representing the earliest diverging lineage in the family. Allioideae contains around 1,200 species distributed predominantly across the Northern Hemisphere, while Amaryllidoideae encompasses over 1,100 species with a mostly pantropical distribution (Meerow 2023). Amaryllidoideae is uniquely defined by a family-specific isoquinoline-based alkaloid chemistry absent from the other two subfamilies; over 650 structurally diverse alkaloids have been reported from about 350 species within this subfamily (Liyanage et al. 2024).

### 1.2.1. *Narcissus pseudonarcissus*

*Narcissus pseudonarcissus* L. from the section Pseudonarcissus within the genus *Narcissus*, commonly referred to as the true daffodils, is distinguished by a well-developed, cylindrical, trumpet-shaped corona that is notably longer than it is wide. The taxonomy of section Pseudonarcissus has been very confusing throughout the years, and it remains incompletely resolved due to high phenotypic variability caused by extensive natural hybridization (Hanks 2002). It is a springtime geophyte, typically reaching 30 cm in height, bearing single-coloured or bi-coloured white and yellow flowers with a broadly conical perianth tube and spreading perianth segments; its corona is not widely expanded or frilled, and its leaves are grey-green

and flat (Hanks 2002). These plants exhibit considerable longevity, with half-lives of adult plants recorded at 12 to 18 years (Barkham and Hance 1982).



Figure 6. Pictures of *Narcissus pseudonarcissus* **A,** Close up of the flower of *Narcissus pseudonarcissus* 'king alfred' by Jacky M. **B,** leaves, and flowers of wild *Narcissus pseudonarcissus* by Brian Gratwicke. Creative Commons Attribution-Share Alike 4.0 International licenses for both images.

This species is native to Spain, southern France, and northern Italy (Meerow and Snijman 1998; Hanks 2002). Ecologically, *N. pseudonarcissus* represents one of the most intensively studied species within the genus, with its natural population dynamics documented extensively over several decades (Hanks 2002; Barkham and Hance 1982). From a phytochemical perspective, *N. pseudonarcissus* is a significant source of AmAs. The cultivar 'King Alfred' in particular has served as a principal experimental system in alkaloid biosynthesis research, with feeding experiments using isotopically labelled precursors elucidating key steps in the formation of lycorine-type, homolycorine-type, and galanthamine-type alkaloids from the shared precursor norbelladine via oxidative phenol coupling pathways (Hanks 2002). The 'King Alfred' cultivar was produced in Devon, England, through hybridization of *Narcissus* 'Emperor' and *Narcissus* 'Maximus' and introduced commercially in 1900. It is classified as RHS Division 1 (trumpet daffodils) and bears a uniformly golden yellow flower with oblong, twisted, overlapping perianth segments and a cylindrical corona with a widely flanged, deeply notched rim (Kington 2008). Among the alkaloids documented in 'King Alfred,' galanthamine, haemanthamine,

lycorine, and several others have been isolated and characterized (Eichhorn et al. 1998; Takos and Rook 2013; Cortes et al. 2015; Kilgore and Kutchan 2016).

## 1.3. Amaryllidaceae Alkaloid Biosynthesis

### 1.3.1. Amaryllidaceae alkaloid biosynthetic pathway

Even though the therapeutic properties of AmAs have been extensively studied, a full understanding of the biosynthetic pathway and the characterization of enzymes responsible for catalyzing different biosynthetic reactions need more effort. The combined application of early labelling studies followed by omics strategies has accelerated the discovery of AmAs biosynthetic enzymes (El Tahchy et al. 2011; Li et al. 2021). After the discovery of the biosynthetic route of different intermediates, many biosynthetic enzymes were predicted based on the nature of the biochemical reaction and homology with enzymes involved in the alkaloid biosynthesis in other plant families. The pathway to produce AmAs has been elucidated throughout the years using databases generated from transcriptomic and metabolic analysis of several Amaryllidaceae (Singh and Desgagné-Penix 2017; Hotchandani, de Villers, and Desgagne-Penix 2019; Park et al. 2019; Ferdausi et al. 2020; Li et al. 2021; Tousignant, Diaz-Garza, Majhi, Gélinas, Singh, and Desgagné-Penix 2022). Biosynthesis of AmAs involves a series of biochemical reactions such as bond formation, rearrangement, breakage, functional group addition, and modifications to connect primary metabolism to Amaryllidaceae alkaloid metabolism. Early labelling studies reveal that 4'-*O*-methylnorbelladine is involved in the biosynthesis of other AmAs downstream in this pathway, such as lycorine, haemanthamine, and galanthamine (El Tahchy et al. 2011). 4'-*O*-methylnorbelladine is the methylated form of norbelladine, which is produced by the condensation of tyramine and 3,4-DHBA (Park 2014; Singh et al. 2018). In order to produce tyramine, L-tyrosine is decarboxylated to produce

tyramine. While production of the second building block, 3,4-DHBA, is achieved from the phenylpropanoid pathway (Singh et al. 2018).

### 1.3.1.1. Tyrosine Decarboxylase

TyDC catalyzes the pyridoxal 5′-phosphate-dependent (PLP-dependent) decarboxylation of L-tyrosine to tyramine. In plants, TyDCs have been characterized in several species that produce tyrosine-derived alkaloids. The first plant TyDC was cloned from *Papaver somniferum*, where it supplies tyramine for benzylisoquinoline alkaloid biosynthesis (Facchini and De Luca 1994). In Amaryllidaceae, TyDC activity has been detected in *Lycoris* species, and candidate sequences have been reported in transcriptomic studies of AmA-producing tissues (Park et al. 2019; Wang et al. 2019). Additional TyDCs have been characterized in *Petroselinum crispum*, *Arabidopsis thaliana*, and *Thalictrum flavum*, among others (Kawalleck et al. 1993; Lehmann and Pollmann 2009; Facchini, Huber-Allanach, and Tari 2000). TyDC therefore occupies a committed branch point that channels primary aromatic amino acid metabolism toward specialized alkaloid biosynthesis. Two TyDC isoforms, *Np*TyDC1 and *Np*TyDC2, were previously identified from transcriptome data of *N. pseudonarcissus* 'King Alfred' (Singh and Desgagné-Penix 2017); however, their substrate preferences, kinetic properties, and individual roles in AmAs biosynthesis have not been experimentally characterized. These two enzymes share the canonical aromatic L-amino acid decarboxylase fold and the conserved catalytic lysine that anchors the pyridoxal 5′-phosphate cofactor. Mechanistically, TyDC belongs to the group II pyridoxal 5′-phosphate-dependent aromatic amino acid decarboxylases (AAADs) family, which also includes decarboxylases acting on tryptophan and dihydroxyphenylalanine. AAADs in plants typically function as homodimers, with the PLP cofactor covalently bound to a conserved lysine residue in the active site (Torrens-Spence et al. 2020b). Plant AAADs differ

in their substrate preference, and even small changes in active-site residues can shift activity between L-tyrosine, L-dopa, and L-phenylalanine (Torrens-Spence et al. 2020b). A second functional class within the same family, the aromatic acetaldehyde synthases (AASs), acts on the same substrates but produces aldehydes rather than amines through a coupled decarboxylation–deamination reaction (Torrens-Spence et al. 2013). The two classes share a common fold and high sequence identity (Torrens-Spence et al. 2020b).

### 1.3.1.2. Norbelladine Synthase (NBS)

All gene candidates that encode enzymes that catalyze biochemical reactions involved in the synthesis of precursor molecules of AmAs and some of their precursors have been identified (Singh et al. 2018; Hotchandani, de Villers, and Desgagne-Penix 2019). Norbelladine is considered the precursor of the first common intermediate of all AmAs, 4'-*O*-methylnorbelladine. This reaction is catalyzed by NBS and noroxomaritidine/norcraugsodine reductase (NR) (Kilgore and Kutchan 2016; Majhi et al. 2023). Furthermore, NBS and NR are shown to be localized in the nucleus and cytosol, and their observed physical interaction in yeast and plants indicates that both NR and NBS are involved in the biosynthesis of norbelladine (Tousignant, Diaz-Garza, Majhi, Gélinas, Singh, and Desgagné-Penix 2022; Majhi et al. 2023).

After its synthesis, norbelladine is converted to 4′-*O*-methylnorbelladine by norbelladine 4′-*O*-methyltransferase (N4OMT), which methylates the 4′ hydroxyl group of norbelladine using S-adenosyl-L-methionine as the methyl donor (Kilgore, Augustin, Starks, O'Neil-Johnson, et al. 2014; Koirala et al. 2024). Recent kinetic and structural characterization of N4OMT has shown that the enzyme accepts norbelladine as its preferred substrate (Koirala et al. 2024). Additional *O*-methyltransferases with overlapping activity have been reported in *Lycoris aurea* and other Amaryllidaceae, suggesting some functional redundancy in the methylation step (Sun et al.

2018; Li et al. 2019). The recent reconstitution of the early AmA pathway in *Nicotiana benthamiana* and the characterization of the enzyme network in *Leucojum aestivum* have confirmed the sequential action of NBS, NR, and N4OMT in the production of 4′-*O*-methylnorbelladine *in planta* (Majhi et al. 2023; Lamichhane et al. 2025; Mehta et al. 2024).

4′-O-methylnorbelladine then undergoes intramolecular oxidative phenol coupling, which establishes the carbon skeletons that distinguish the major AmA classes (Kilgore and Kutchan 2016; Desgagné-Penix 2021). CYP96T1 is a cytochrome P450 monooxygenase in *Narcissus* sp. aff. *pseudonarcissus* which produces the noroxomaritidine and norcraugsodine scaffolds (Kilgore et al. 2016). Substrate flexibility studies on NBS and NR have further shown that both enzymes accept a range of aldehyde substrates (Hnin, Nakashima, and Morita 2024).

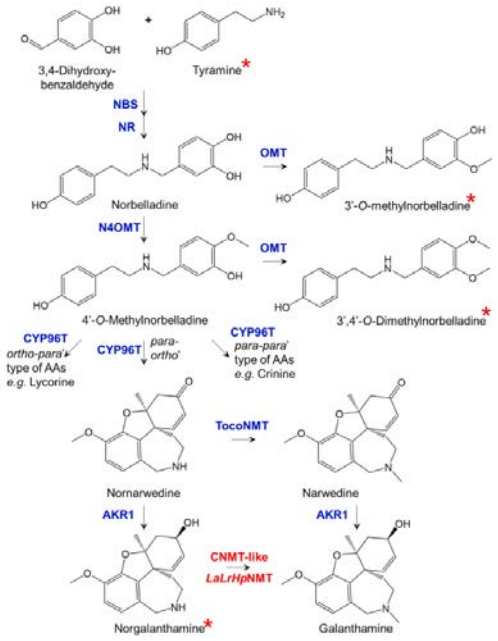



Figure 7. Biosynthetic pathway from tyramine and 3,4-DHBA to galanthamine. Enzymes identified in Amaryllidaceae are shown in bold. Reproduced from (Liyanage et al. 2025)

## 1.3.2. Shikimate pathway

The shikimate pathway consists of seven sequential enzymatic reactions that connect central carbon metabolism to the aromatic amino acid (AAA) biosynthetic network. (Herrmann and Weaver 1999). The pathway was named after its first identified intermediate, shikimate, which was isolated from the fruit of *Illicium religiosum*, commonly known as the Japanese star anise (Eijkman 1885). All enzymes of the shikimate pathway have been biochemically characterized in other plants, and their corresponding genes identified from both microbes and plants (Shende, Bauman, and Moore 2024). In vascular plants, at least 30% of photosynthetically fixed carbon is directed into this pathway, reflecting its central importance in plant primary and specialized metabolism (Vogt 2010). The first committed step is catalyzed by 3-deoxy-D-arabino-heptulosonate 7-phosphate (DAHP) synthase (Shende, Bauman, and Moore 2024; Vogt 2010). Other steps can be seen in Figure 8, along with the last step in which chorismate synthase (CS) catalyzes the 1,4-anti-elimination of the 3-phosphate and the C6-pro-R hydrogen of 5-enolpyruvylshikimate-3-phosphate, thereby introducing the second double bond in the ring and forming chorismate (Vogt 2010). Biosynthesis of both precursor amino acids begins with chorismate, the final product from the shikimate pathway, occurring inside the plastid (Desgagné-Penix 2021). Chorismate is then transformed into prephenate then arogenate by chorismate mutase and an aminotransferase, respectively. From arogenate, under the action of arogenate dehydratase, L-phenylalanine is synthesized, whereas the arogenate dehydrogenase catalyzes L-tyrosine synthesis (Maeda and Dudareva 2012; Kilgore and Kutchan 2016; Facchini, Huber-Allanach, and Tari 2000).

### 1.3.3. Phenylpropanoid pathway

The phenylpropanoid pathway is a major metabolic cascade that generates a diverse range of specialized metabolites from L-phenylalanine or, in some cases, L-tyrosine. This pathway, which

dates back to early plant evolution, is critical for carbon assimilation and the synthesis of a variety of phenolic compounds required for plant growth, defence, and environmental adaptation (Ortiz and Sansinenea 2023; Zhao et al. 2023; Zhang and Liu 2015). Multiple downstream branches diverge from this pathway, each producing a unique class of phenolic compounds, most notably flavonoids, lignin, coumarins, and phenolic acids. Phenylpropanoid-derived metabolites serve as signaling molecules, facilitating intercellular communication, and regulating physiological processes. Their role in signal transduction emphasizes the importance of coordinating adaptive responses to environmental change (Vogt 2010; Ortiz and Sansinenea 2023). In Amaryllidaceae plants, the phenylpropanoid pathway is thought to connect to the Amaryllidaceae alkaloid pathway via DHBA. This pathway is started by phenylalanine ammonia-lyase (PAL), and it connects to the shikimate pathway, which converts carbon into aromatic amino acids. PAL activity is common in plants and microorganisms but not in animals (Hyun et al. 2011; Desgagné-Penix 2021). The enzymes that catalyze the reactions that convert L-phenylalanine into the aldehyde precursor 3,4-DHBA are not fully known. According to studies, 3,4-DHBA is produced via the phenylpropanoid pathway (Barton et al. 1963; Karimzadegan et al. 2024; Kilgore and Kutchan 2016). The biosynthetic pathway from L-phenylalanine to 3,4-DHBA was determined by feeding radiolabeled precursors to *N. pseudonarcissus* and measuring haemanthamine production (Suhadolnik, Fischer, and Zulalia 1963). These experiments established the following order: L-phenylalanine, trans-cinnamic acid, 4-hydroxycinnamic acid, 3,4-dihydroxycinnamic acid or 4-hydroxybenzaldehyde, and 3,4-DHBA (Suhadolnik, Fischer, and Zulalia 1963). These findings suggest that the phenylpropanoid pathway's early reactions and biosynthetic enzymes help to synthesize 3,4-DHBA (Desgagné-Penix 2021). The functional characterization of PAL and C4H from *Lycoris*

sp. was reported using heterologous expression in *E. coli* (Li, Li, Qian, et al. 2018; Jiang et al. 2011). Several PAL transcripts have been identified in Amaryllidaceae species (Hotchandani, de Villers, and Desgagne-Penix 2019; Singh and Desgagné-Penix 2017).

The tyrosine pool is then split among several paths (Figure 9). Protein synthesis is one of the ways that L-tyrosine is used by cells. However, some of the L-tyrosine pool is recovered through protein turnover. Another portion enters the 4-hydroxyphenylpyruvate dioxygenase (HPPD) branch. This branch produces tocopherols and plastoquinone. These products support the production of vitamin E and photosynthesis. A smaller portion is decarboxylated by TyDC to form tyramine, and as a result of that, AmAs. Tyrosine must therefore be shared between primary demand and specialized metabolism. This partition places TyDC at the entry point of AmA biosynthesis.

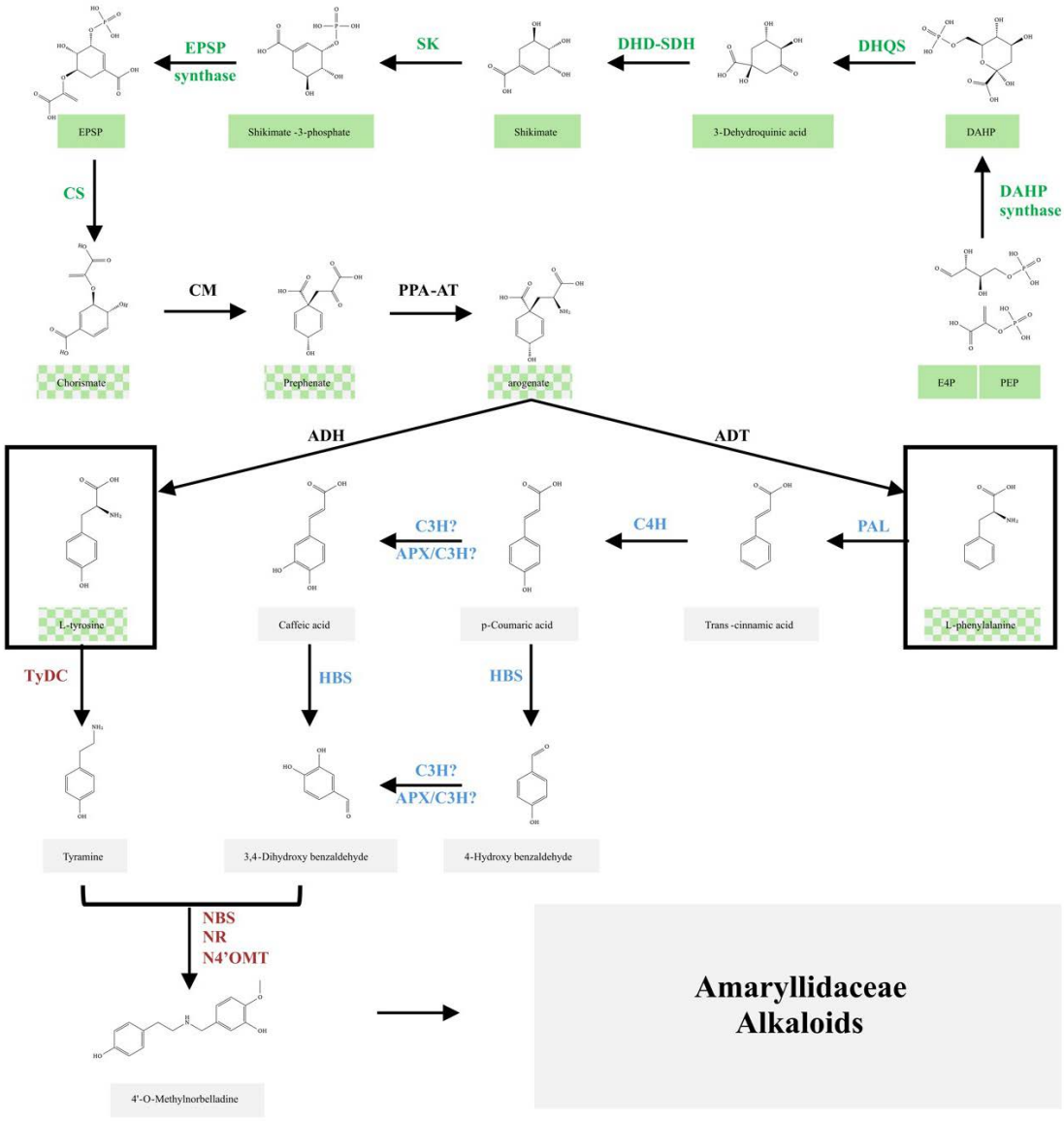



Figure 8. Comprehensive summary of the shikimate and phenylpropanoid pathways, leading to Amaryllidaceae alkaloid biosynthesis pathway. Compounds in a green background can be found in plastids; green and white backgrounds can be found in both plastids and cytosol; white backgrounds are present in cytosol. This figure is a compilation of data from (Maeda and Dudareva 2012; Desgagné-Penix 2021; Karimzadegan et al. 2024; Majhi et al. 2023; Singh et al. 2018; Li et al. 2019; Li, Li, Qian, et al. 2018; Suhadolnik, Fischer, and Zulalia 1963; Park 2014). DAHP synthase - 3-deoxy-D-arabino-heptulosonate 7-phosphate synthase, DHQS - 3-dehydroquinate synthase, DHD-SDH - 3-dehydroquinate dehydratase / shikimate dehydrogenase (bifunctional), SK - shikimate kinase, EPSP synthase - 5-enolpyruvylshikimate 3-phosphate synthase, CS - chorismate synthase, CM - chorismate mutase, PPA-AT - prephenate aminotransferase, ADH - Arogenate dehydrogenase, ADT - Arogenate dehydratase, PAL - Phenylalanine ammonia lyase, C4H - Cinnamate 4-hydroxylase, C3H / APX/C3H - Coumarate 3-hydroxylase / Ascorbate peroxidase-Coumarate 3-hydroxylase, HBS - Hydroxybenzaldehyde synthase, TYDC - Tyrosine decarboxylase, NBS - Norbelladine synthase, NR - Noroxomaritidine reductase, N4'OMT - Norbelladine 4'-O-methyltransferase. Enzymes in green belong to the shikimate pathway, enzymes in blue belong to the phenylpropanoid pathway, and enzymes in red belong to the Amaryllidaceae alkaloid biosynthesis pathway.

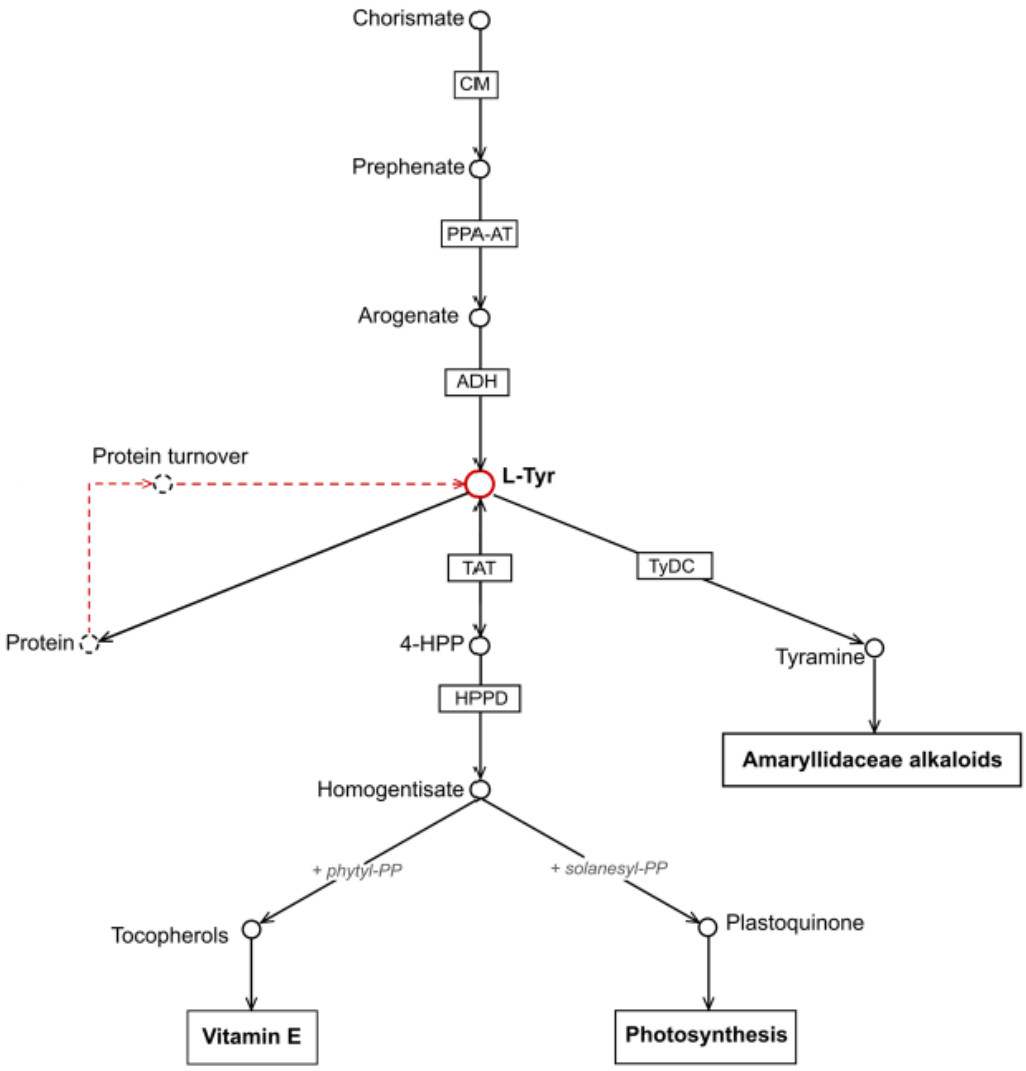



Figure 9. Tyrosine as a central branch point in *N. pseudonarcissus* metabolism. L-tyrosine is produced from chorismate through the arogenate route (CM, PPA-AT, ADH). It is drawn upon by four fates: incorporation into protein, recovery from protein turnover (dashed), the HPPD branch to tocopherols (vitamin E) and plastoquinone, and decarboxylation by TyDC to tyramine. Tyramine condenses with 3,4-DHBA to enter the Amaryllidaceae alkaloid pathway. Circles denote metabolites and boxes denote enzymes. The tyrosine - 4-HPP step (TAT) is reversible.

## 1.4. Synthetic Biology Approaches for Plant Alkaloid Production

Although using plants to produce alkaloids has been researched in recent decades, the yield is often low (Diamond and Desgagné-Penix 2016; Salim et al. 2023; Koirala et al. 2022). As a result, a solution to the challenge of limited natural product availability from native plants is necessary. In this sense, synthetic biology offers great opportunities for the synthesis of specialized metabolites, including alkaloids (Cho et al. 2022). Organisms such as bacteria, yeast, or microalgae can be metabolically engineered to produce a wide range of scientifically important molecules in a cost-effective and time-efficient manner (Sreenikethanam et al. 2022; Galanie et al. 2015). The successful production of high-value compounds such as vinblastine and opioids in microbial hosts reflects the considerable advances made in this field (Galanie et al. 2015). For instance, the biosynthesis of vinblastine and vincristine precursor molecules was reconstituted in yeast by introducing the complete biosynthetic pathway, enabling the production of pathway precursors, intermediates, and end products in a single heterologous host (Zhang et al. 2022). In addition, noscapine and its halogenated anticancer derivatives were produced in *S. cerevisiae* by assembling 30 biosynthetic enzymes from plant, bacterial, mammalian, and yeast sources, including seven plant endoplasmic reticulum-localized proteins (Li, Li, Thodey, et al. 2018).

The selection of an appropriate host organism is the critical first step in synthetic biology strategies. The host should either naturally produce or be capable of taking up the precursor molecules required for the target pathway, such as phenylalanine and tyrosine in the case of Amaryllidaceae alkaloid biosynthesis (Shen et al. 2025; Koirala et al. 2022). Host selection further depends on ease of genetic manipulation, the availability of established cloning tools, well-characterized culture conditions, and scalability to industrial requirements. For example,

microbial hosts such as *S. cerevisiae* and *Escherichia coli* have been widely used to produce plant-derived high-value compounds, including morphinan alkaloids due to their rapid growth and ease of handling, (Facchini et al. 2012; Fossati et al. 2014; Diamond and Desgagné-Penix 2016). Unicellular photosynthetic organisms such as microalgae and cyanobacteria have recently emerged as alternative research platforms, owing to their versatile photosynthetic, heterotrophic, and mixotrophic metabolic lifestyles (Slattery et al. 2018). Common strategies for enhancing metabolite production in heterologous hosts include gene deletion, overexpression of endogenous metabolic genes, and replacement of endogenous enzymes with more catalytically active homologues (Mora-Vasquez et al. 2022). Following host optimization, a candidate biosynthetic pathway is designed by mapping stepwise chemical intermediates from host metabolism to the target compound and selecting the enzymes needed to catalyze each reaction (Kitney and Freemont 2012). Recently, green microalgae have been the subject of interest for the production of natural bioactive molecules by heterologous expression (Bolanos-Martinez et al. 2022). Microalgae are favoured by scientists for synthetic biology because of their ability to offer post-translational modifications and appropriate maturation for a variety of proteins and ease of growth and cultivation under autotrophic, heterotrophic, and mixotrophic conditions in a cost-effective manner (Bolanos-Martinez et al. 2022). Furthermore, many microalgae have been approved as edible microorganisms or Generally Recognized as Safe (GRAS) by the Food and Drug Administration (FDA), which makes them much more favourable than organisms such as *E. coli* for genetic engineering (Torres-Tiji, Fields, and Mayfield 2020). As a result, *Chlamydomonas reinhardtii* has attracted increasing attention in recent years, both on the scientific and commercial planes, for its exploitation as a means to produce valuable natural compounds. These include polysaccharides, carotenoids, and fatty

acids, long-chain polyunsaturated fats, which are prized for their diverse applications in industrial, pharmaceutical, and cosmetic products (Masi et al. 2023; Sproles et al. 2021).

## 1.5. *Chlamydomonas reinhardtii*

Many studies took place in the nineteenth century with the goal of understanding the life cycle of the *Chlamydomonas* genus. J.N. Goroschankin, L. Reinhardt, P.A. Dangeard, W. Schmidle, O. Dill, and G. Klebs were the most prominent scientists who worked on this genus between 1876 and 1900. The species *C. reinhardtii* was described in 1888 by Dangeard. He named it after Ludwig Reinhard(t), a Ukrainian botanist who published a description of copulation in a species he identified as *C. pulvisculus*. Dangeard described Reinhardt's isolate as a new species, *C. reinhardti*, because its sexual reproduction differed in several ways from that of *C. pulvisculus* as described by Goroschankin (Ettl 1976). Even though Reinhardt did not spell his own name with a "t" at the end, he was referred to as Reinhardt in the literature, and therefore the presence of the "t" in the original species description is required for taxonomic purposes. The use of two “i”s rather than one is dictated by botanical Latin nomenclature rules: when the name of the discoverer of a species ends in a consonant, the letters "ii" are added. Thus, the correct spelling is Reinhardtii (Stern and Witman 2009; Ettl 1976). *C. reinhardtii* is a eukaryotic, unicellular, green microalgae. It is a facultative autotrophic microorganism that has both a sexual and asexual life cycle. It can mostly be found in freshwater and even damp soil (Salome and Merchant 2019; Stern and Witman 2009). *C. reinhardtii* alternates between sexual and asexual reproduction, and development depends on the conditions of the growing environment (Stern and Witman 2009). Although *C. reinhardtii* is part of the plant subkingdom (Viridiplantae), its lineage (Chlorophyta) diverged from terrestrial plants (Embryophyta) around one billion years ago. Often considered a micro-plant, the anatomical study of *C.*

*reinhardtii* shows that the structural organization of its organelles is similar to that of a plant cell. Its cell has an oval shape, measures about 10 μm in diameter, and is surrounded by a cell wall composed of glycoproteins and carbohydrates arranged in seven layers. (Goodenough and Heuser 1985; Stern and Witman 2009). It is mainly composed of a nucleus, a large chloroplast that occupies half the cell volume, several mitochondria, and two flagella (also called cilia) that play important roles by optimizing the exposure of cells to light during photosynthesis and in cell recognition during sexual reproduction (Figure 10). These flagella play an important role in phototaxis by optimizing cells during sexual reproduction (Stern and Witman 2009). Compared to other microorganisms like bacteria and yeasts, *C. reinhardtii*'s cell similarity to those of land plants and its photoautotrophic nature are advantageous when considering heterologous synthesis of plant metabolites (Scaife et al. 2015).

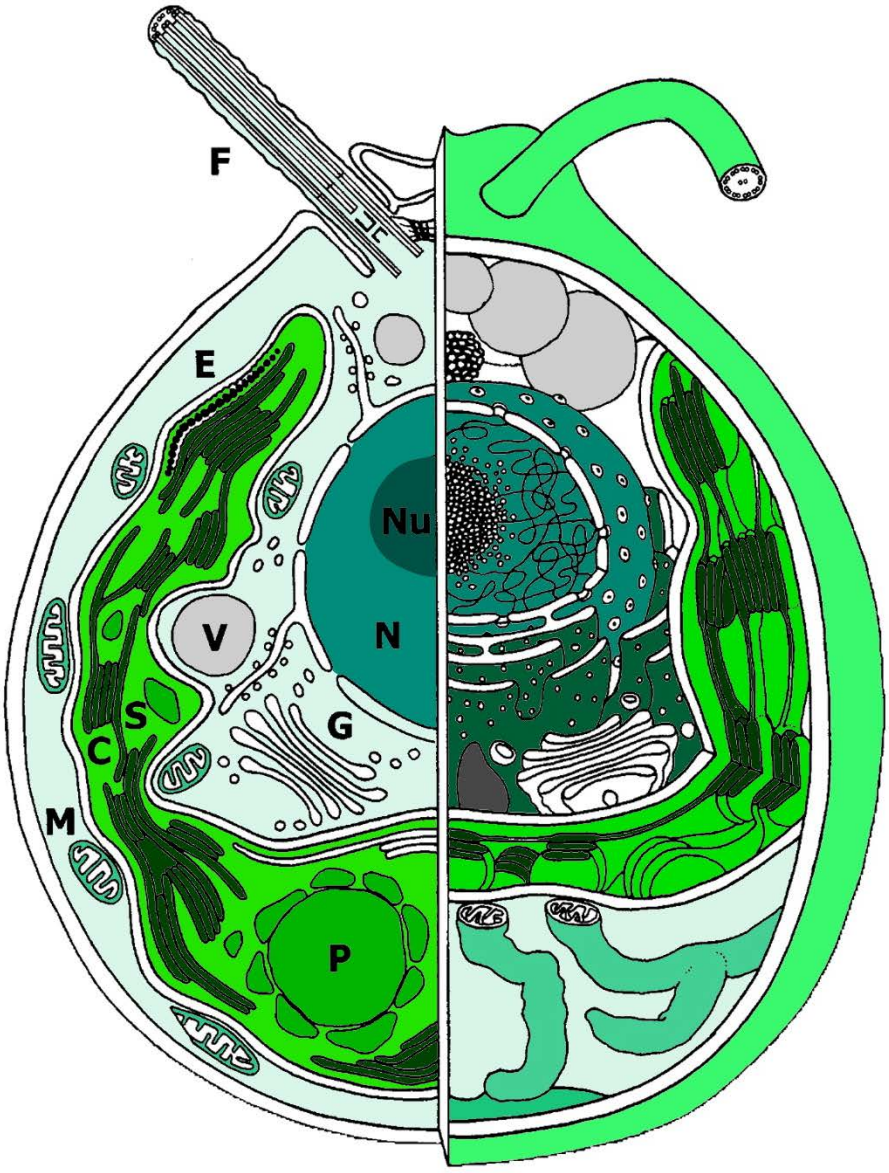



Figure 10. Cell structure of *Chlamydomonas reinhardtii*, showing the central nucleus (N) with the nucleolus (Nu), the two isoform flagella (F), the cup-shaped chloroplast (C) with the eyespot (E) and the starch-containing pyrenoid (P), and the mitochondria (M). In addition, one may distinguish the Golgi vesicle (G), starch grains (S), and vacuoles (V). From (Nickelsen and Kück 2000) license number: 6257910404464

In recent years, *C. reinhardtii* has become one of the model organisms widely used in genetic engineering (Salome and Merchant 2019; Sproles et al. 2021). Its three genomes (nuclear, chloroplastic, and mitochondrial) can be exploited for heterologous gene expression, thus

offering flexibility in its operation as a production platform for recombinant proteins (Merchant et al. 2007; Salome and Merchant 2019). The sequencing of the *C. reinhardtii* genomes reveals that it has a nuclear genome of a size of around 120 million base pairs (Mbp), organized into 17 chromosomes, and contains approximately 15143 genes with a high GC content, representing approximately 64% of the entire genome and 68% for coding sequences (Merchant et al. 2007). The chloroplast genome is 205 kbp, organized into large protein-DNA complexes, called nucleoids, with a low GC content of about 34.6% (Gallaher et al. 2015; Gallaher et al. 2018). Finally, in each cell of *C. reinhardtii*, there are approximately 130 mitochondria, whose genome is a linear molecule of 15.8 kbp encoding 8 proteins (Gallaher et al. 2018; Salome and Merchant 2019). This microalga has been used as a model for studying chloroplast biology, photosynthesis, the structure and function of plant flagella, and the control of the cellular cycle and certain genomic characteristics that it shares with animals, like tyrosine kinases and scavenger receptor cysteine-rich (SRCR) domains (Merchant et al. 2007; Stern and Witman 2009). It has been used as a host for elucidating the metabolic pathway of keto-carotenoid biosynthesis in several plant species (Perozeni et al. 2020). Also, *C. reinhardtii* can be used as a platform for the production of recombinant proteins, metabolites of industrial interest, or drugs (Tran and Kaldenhoff 2020; Scranton et al. 2016; Sproles et al. 2021).

### 1.5.1. Gene expression in *C. reinhardtii*

Nuclear transformation, the most extensively studied expression route in this organism, is based on the random integration of transgenes into the nuclear genome, which is mostly accomplished through electroporation, agitation with glass beads, or biolistic delivery (Shimogawara et al. 1998; Kindle 1990; Rasala and Mayfield 2015; Sproles et al. 2021). Nuclear expression in *C. reinhardtii* is frequently hampered by pronounced transgene silencing. This is a phenomenon

driven by epigenetic mechanisms such as cytosine methylation and chromatin compaction at randomly inserted loci. Silencing in transgenes leads to highly variable and often negligible recombinant protein yields, rarely exceeding 0.1% of total soluble protein (TSP) under standard conditions (Neupert, Karcher, and Bock 2009; Rasala and Mayfield 2015). These yields are much lower than those achieved in established microbial hosts. In *E. coli*, for example, strong promoters can drive recombinant protein accumulation to 10–30% or more of total cellular protein (Overton 2014). In the same way, yeast systems such as *Pichia pastoris* can reach gram-per-liter scales under optimized growth conditions, which is far higher than what is typically obtained from nuclear expression in *C. reinhardtii* (Baghban et al. 2018). The chloroplast genome has a high copy number per cell, which naturally amplifies transgene dosage and contributes to increased transcript abundance (Harris 2001). Furthermore, the plastid compartment can tolerate polycistronic transcript architectures and does not require the codon optimization strategies necessary for nuclear expression (Rasala and Mayfield 2015). On the other hand, chloroplastic expression is associated with several inherent limitations. For example, the chloroplast lacks the N-glycosylation machinery present in the endomembrane system, which means that proteins requiring complex glycan modifications cannot be produced properly in this compartment. Additionally, the accumulation of the protein reduces the available space within the stroma, which may interfere with the correct formation of disulfide bonds (Lauersen et al. 2013; Rasala and Mayfield 2015). As a result, the choice between nuclear and chloroplastic expression in *C. reinhardtii* is context-dependent, determined by the target protein's biochemical requirements, the intended application, and the acceptable trade-offs between yield, post-translational fidelity, and downstream processing complexity (Rasala and Mayfield 2015).

#### 1.5.1.1.1. UV-mutagenized strains, specifically UVM4 and UVM11.

Neupert et al. (2009) developed the UV-mutagenized strains UVM4 and UVM11 by exposing wild-type *C. reinhardtii* cells to ultraviolet irradiation and screening progeny for improved transgene expression, which was one of the most significant advances. These strains have a significantly lower susceptibility towards epigenetic silencing at randomly integrated loci, and they consistently produce recombinant protein accumulation levels several times higher than those obtained in parental wild-type backgrounds (Neupert, Karcher, and Bock 2009). The molecular basis of this phenotype was subsequently identified by (Neupert et al. 2020), who showed that both strains carry distinct non-synonymous point mutations in the same gene, which encodes a Sir2-type sirtuin histone deacetylase (SRTA). In UVM4, a Gly-to-Ser substitution at position 55 of the catalytic domain (the *srta-2* allele) appears to disrupt binding of the cofactor $NAD^+$. In UVM11, on the other hand, a Pro-to-Leu substitution at position 222 (the *srta-1* allele) seems to affect protein structure and its interaction with other proteins. Consequently, loss of SRTA function in both strains prevents the assembly of a repressive chromatin structure on transgenic DNA, thereby allowing sustained, high-level transgene expression (Neupert et al. 2020). UVM4 has since become one of the most widely used nuclear expression hosts in the *C. reinhardtii* research community, and the causative mutation was later mapped to a locus encoding a Sir2-type histone deacetylase, providing a mechanistic explanation for the reduced silencing phenotype (Rasala and Mayfield 2015; Neupert, Karcher, and Bock 2009).

#### 1.5.1.1.2. Codon optimization

*C. reinhardtii*'s nuclear codon usage is strongly biased toward GC-rich codons, and transgenes derived from heterologous organisms with different codon preferences are translated with significantly lower efficiency (Barahimipour et al. 2015; Fuhrmann, Oertel, and Hegemann

1999). Codon optimization, which involves completely redesigning the transgene sequence to match the preferred codon usage of the *C. reinhardtii* nuclear genome, has been shown to significantly increase mRNA translation rates and thus recombinant protein yield (Rasala and Mayfield 2015; Fuhrmann, Oertel, and Hegemann 1999). For instance, (Fuhrmann, Oertel, and Hegemann 1999) demonstrated that a codon-optimized synthetic GFP gene, redesigned to match the *C. reinhardtii* nuclear codon bias, produced detectable fluorescent protein in transgenic cells. In contrast, the native jellyfish GFP sequence yielded no detectable expression under the same conditions. These findings established codon optimization as an essential prerequisite for nuclear transgene expression in this organism.

#### 1.5.1.1.3. Inclusion of endogenous introns

Lumbreras, Stevens, and Purton (2002) demonstrated that inserting endogenous *C. reinhardtii* introns, most commonly the first intron of the *Ribulose-1,5-Bisphosphate Carboxylase/Oxygenase Small Subunit 2 (RBCS2)* gene, into the transgene coding sequence significantly increased recombinant gene expression at the mRNA level. Lauersen et al. (2018) went on to systematically characterize the insertion site dependence of this effect, demonstrating that the position of *RBCS2* within the coding sequence critically determines the magnitude of expression enhancement and that the effect is additive when multiple introns are inserted in their physiological order.

#### 1.5.1.1.4. Promoter engineering: *HSP70A* and *PsaD* promoters.

The discovery of strong, constitutive promoters capable of driving high-level transcription in the *C. reinhardtii* nucleus has been a critical goal. Schroda, Blocker, and Beck (2000) found that placing the heat shock protein Heat Shock Protein 70A *(HSP70A)* promoter upstream of

the *RBCS2* promoter significantly increased transgene transcript levels compared to using either promoter alone, which they attributed to the transactivating properties of *HSP70A* regulatory elements on the adjacent *RBCS2* promoter.

This *HSP70A-RBCS2* tandem configuration became one of the most commonly used transcriptional drives for nuclear transgene expression in *C. reinhardtii*. Fischer and Rochaix (2001) discovered a second major promoter system by analyzing the flanking regions of the *PsaD* gene, which encodes a Photosystem I stromal subunit and is one of the most highly and constitutively expressed nuclear genes in *C. reinhardtii*. Because the *PsaD* open reading frame lacks introns, the flanking promoter and untranslated regions contain all of the regulatory information that drives its abundant transcript accumulation. Fischer and Rochaix (2001) demonstrated that these elements could drive high-level expression of both endogenous genes and heterologous cDNAs that had previously failed to be expressed from existing vectors. Kumar, Falcao, and Sayre (2013) conducted a systematic comparison of seven nuclear promoters using luciferase as a reporter and found that the pairing of the promoter and terminator of the *PsaD* gene was the best-performing combination among all configurations tested. The *PsaD* promoter has since been incorporated into widely used modular expression vectors for *C. reinhardtii* and is now considered, along with the *HSP70A-RBCS2* tandem, one of the two standard strong promoter systems for nuclear expression in this organism (Heitzer and Zschoernig 2007; Rasala et al. 2014; Rasala and Mayfield 2015).

## 1.6. Problematic, Hypothesis and Objectives

### 1.6.1. Problematic

*N. pseudonarcissus* produces a large number of pharmacologically important AmAs, including galanthamine, lycorine, and cherylline (Eichhorn et al. 1998; Suhadolnik, Fischer, and Zulalia

1963). So far, direct extraction from native plants remains the primary source for supplying these compounds, notably galanthamine for clinical use (Takos and Rook 2013). However, this approach presents significant challenges. The production rate of AmAs in native plants is naturally low. Furthermore, meeting growing pharmacological demand would lead to the over-exploitation of natural plant populations, endangering their existence (Santos et al. 2020). Seasonal and environmental factors also affect metabolite yields in natural habitats, making supply less reliable (Demir et al. 2022). Although commercial cultivation of Amaryllidaceae plants is possible, it requires large areas of agricultural land and does not scale easily to meet expected therapeutic demand (Desgagné-Penix 2021). Consequently, these limitations highlight the need for more sustainable and cost-effective approaches to produce AmAs.

Instead of relying on plant agriculture, heterologous biological systems offer a distinct and innovative method to produce molecules of interest. For instance, the development of photosynthetic microbial platforms capable of producing pathway precursors might offer a viable route toward reducing the ecological burden placed on these plant populations. Expressing plant-derived biosynthetic enzymes in such hosts would provide a renewable and scalable production system that does not depend on natural plant resources.

The key to reconstructing AmA biosynthesis in a microbial host is to first characterize the enzymes involved in each pathway step, particularly those that produce the earliest precursor molecules. In recent years, AmAs biosynthetic enzymes have been identified, including NBS, NR, and N4'OMT (Lamichhane et al. 2025; Majhi et al. 2023; Liyanage et al. 2025; Kilgore, Augustin, Starks, O'Neil-Johnson, et al. 2014; Kilgore et al. 2016; Singh et al. 2018). However, the enzyme responsible for one of the precursor steps, the decarboxylation of L-tyrosine to tyramine, remains poorly characterized in *N. pseudonarcissus*.

In parallel, the choice of a suitable microbial chassis for AmA precursor production remains an open question. *C. reinhardtii* is an attractive candidate, as it is a eukaryotic photosynthetic microorganism with a fully sequenced genome, well-developed genetic tools, and the capacity to grow rapidly under controlled conditions.

## 1.6.2. Research hypotheses

We propose two hypotheses in this work. First, we hypothesize that of the two TyDC isoforms identified in *N. pseudonarcissus* 'King Alfred', are functionally specialized rather than redundant, and that only one of them is catalytically dedicated to supplying tyramine for AmA biosynthesis. We further hypothesize that this isoform acts as a regulated, low-flux gatekeeper consistent with the kinetic properties of characterized TyDC homologs in related Amaryllidaceae. Second, we hypothesize that *C. reinhardtii* does not possess a functional endogenous TyDC and therefore provides a metabolically suitable host for the heterologous expression of *NpTyDC1*.

## 1.6.3. Objectives

The general objective of this thesis is to characterize the TyDC enzyme responsible for tyramine biosynthesis in *N. pseudonarcissus* 'King Alfred' and to evaluate *C. reinhardtii* as a photosynthetic chassis for the heterologous expression of this enzyme. This general objective was addressed through the following specific aims.

### 1.6.3.1. Objective 1: Biochemical characterization of TyDCs from *N. pseudonarcissus* 'King Alfred'

First, we conducted *in silico* analysis of the full-length open reading frame sequences of *Np*TyDC1 and *Np*TyDC2, including conserved domain searches, phylogenetic reconstruction,

homology modelling, and molecular docking, to predict their structural features and substrate preferences. Next, we cloned both isoforms and heterologously expressed in *E. coli* as maltose-binding protein fusions. Then, we performed enzymatic assays coupled with High-Performance Liquid Chromatography-Tandem Mass Spectrometry (HPLC-MS/MS) to determine substrate preferences using L-tyrosine, L-phenylalanine, L-tryptophan, and L-DOPA as substrates. Lastly, we compared kinetic parameters ($K_m$, *kcat*, and $V_{max}$) of the enzyme (or enzymes) that accept L-tyrosine as a substrate to those reported for TyDC homologs from related Amaryllidaceae species.

#### 1.6.3.2. Objective 2: Evaluation of *C. reinhardtii* as a chassis for *Np*TyDC1 expression and tyramine production.

First, we searched for possible endogenous Aromatic Amino Acid Decarboxylase-like (AAAD) proteins in *C. reinhardtii* and characterize their sequences through bioinformatic analysis and metabolite screening to determine whether the algae produce tyramine on its own. Next, we assessed the growth response of *C. reinhardtii* to exogenous L-tyrosine and tyramine supplementation to evaluate substrate and product compatibility, followed by different assays to assure that the pre-chosen strain (*C. reinhardtii* UVM4) was a good candidate for transformation. Then, we transformed this strain with a codon-optimized, *mVenus-tagged NpTyDC1* construct under the *PsaD* promoter, using both intron-free and intron-containing designs. Lastly, we screened transformants for fluorescence to detect cells that expressed the construct.

# Chapter 2

**Preface**

This chapter consists of a research article that has been peer-reviewed and accepted for publication in the journal *Phytochemistry*. The article is entitled *"Molecular cloning and functional characterization of tyrosine decarboxylase genes from galanthamine-producing Narcissus pseudonarcissus 'King Alfred'"* and is reproduced here in its accepted form. Figure numbers and table numbers have been updated to match the thesis.

The work presented in this chapter addresses the first hypothesis of this thesis: that of the two TyDC isoforms identified in *N. pseudonarcissus* 'King Alfred', one isoform serves as the principal enzyme directing L-tyrosine into the Amaryllidaceae alkaloid biosynthetic pathway. To test this, the two candidate genes, *NpTyDC1* and *NpTyDC2*, were cloned from *N. pseudonarcissus* 'King Alfred' bulb tissue and expressed in *E. coli* for *in vitro* enzymatic characterization. The recombinant enzymes were assayed against L-tyrosine and related substrates, and the kinetic parameters of *Np*TyDC1 were determined.

The results show that *Np*TyDC1 is a functional tyrosine decarboxylase with measurable activity on L-tyrosine, with a $K_m$ of 109 μM, a *kcat* of 0.02337 $s^{-1}$, and a Vmax of 0.23 nkat $mg^{-1}$. In contrast, *Np*TyDC2 showed no detectable activity under the assay conditions tested, despite sharing significant sequence identity with *Np*TyDC1. These findings identify *Np*TyDC1 as the principal isoform supplying tyramine for AmA biosynthesis in *N. pseudonarcissus* 'King Alfred'.

The research presented in this chapter was carried out collaboratively, under the supervision of Isabel Desgagné-Penix. Starting from the ligation step, the candidate performed the cloning and

expression workflow for *Np*TyDC1 and *Np*TyDC2, comprising ligation, cloning via *E. coli* DH5α, transformation of *E. coli* Rosetta, IPTG-induced protein expression, protein extraction, purification, together with the subsequent enzymatic assays. The molecular docking was performed by Natacha Mérindol and the candidate. The bioinformatic analyses (multiple sequence alignment, conserved domain identification, and phylogenetic tree construction), together with the data analysis, statistical analysis, and figure preparation, were carried out by the candidate, with Karen Cristine Goncalves dos Santos providing training in R and support in troubleshooting the analyses. The manuscript was drafted by the candidate and revised by Natacha Mérindol, Karen Cristine Goncalves dos Santos, and Isabel Desgagné-Penix. The earlier cloning steps, including primer design and amplification, and the subcellular localization experiments, were performed by Bharat Bhusan Majhi and interns Yasmin Moreto Guaitolini and Isabella Burgos-Holguin. HPLC-MS/MS analysis was performed by Sarah-Eve Gélinas.

# Molecular cloning and functional characterization of tyrosine decarboxylase genes from galanthamine-producing *Narcissus pseudonarcissus* 'King Alfred.'

Arghavan Arjmandi[1], Bharat Bhusan Majhi[1], Natacha Mérindol[1], Sarah-Eve Gélinas[1], Karen Cristine Goncalves dos Santos[1], Isabella Burgos-Holguin[1], Yasmin Moreto Guaitolini[1], Patrick Lagüe[2], and Isabel Desgagné-Penix[1, *]

[1]Department of Biochemistry, Chemistry, Physics and Forensic Science, Université du Québec à Trois-Rivières, Trois-Rivières, Québec, Canada

[2]Department of Biochemistry, Microbiology and Bioinformatics, Université Laval, Québec, Québec, Canada

*Correspondence: Isabel.Desgagne-Penix@uqtr.ca ; Tel.: 1-819-376-5011

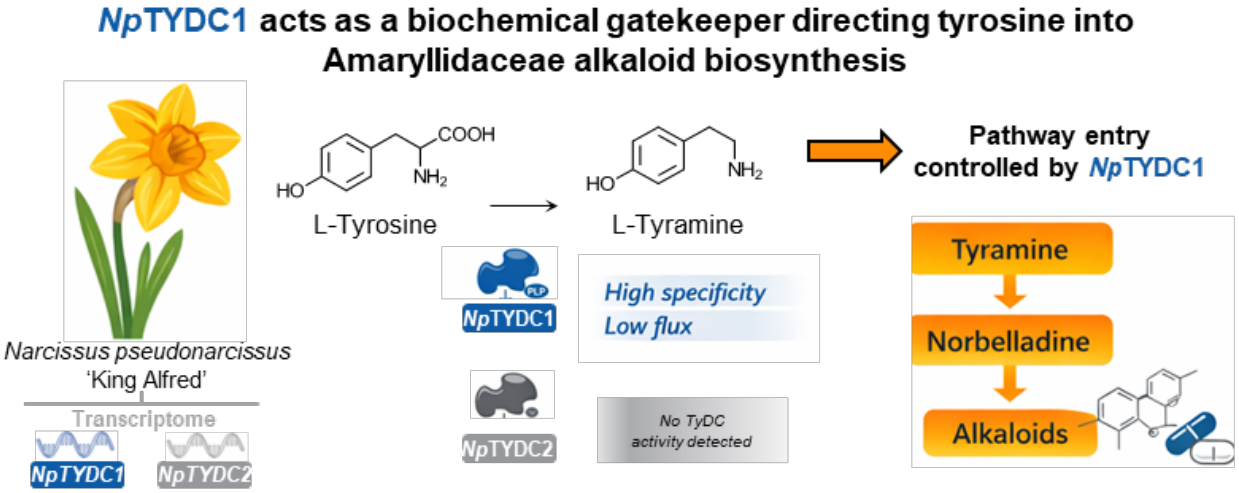
## 2.1. Highlights

- TyDC isoforms from *Narcissus pseudonarcissus* belong to distinct phylogenetic clades.
- *Np*TyDC1 decarboxylates L-tyrosine to tyramine.
- *Np*TyDC2 does not catalyze tyrosine decarboxylation under tested conditions.
- Kinetic properties identify *Np*TyDC1 as a low-flux gatekeeper enzyme.
- A standardized workflow enabled quantitative comparison of TyDC kinetics.

## 2.2. Keywords

Amaryllidaceae alkaloids; Aromatic amino acid decarboxylase; Tyramine biosynthesis; Pyridoxal 5′-phosphate–dependent enzyme; Molecular docking; Gatekeeper enzyme; Specialized metabolism; Amaryllidoideae

## 2.3. Graphical abstract



# 2.4. Abstract

Tyrosine decarboxylases (TyDCs) are pyridoxal 5′-phosphate–dependent enzymes that catalyze the conversion of L-tyrosine into tyramine, a key entry point for Amaryllidaceae alkaloid biosynthesis. From transcriptome data of *Narcissus pseudonarcissus* 'King Alfred', two full-length TyDC isoforms, *NpTyDC1* and *NpTyDC2*, were identified. In this study, both genes were cloned, heterologously expressed in *Escherichia coli*, and purified for functional characterization. Fluorescent protein tagging indicated nucleocytoplasmic localization of both isoforms. Enzymatic assays coupled with HPLC-MS/MS demonstrated that *Np*TyDC1 exhibits decarboxylase activity with a strong preference for L-tyrosine, producing tyramine as the predominant product. In contrast, *Np*TYDC2 showed no detectable tyrosine decarboxylase activity under the conditions tested, and no tryptophan decarboxylation despite structural features associated with indole decarboxylases but displayed minor activity toward L-phenylalanine. Collectively, these findings establish *Np*TyDC1 as a strong candidate for directing tyrosine into the Amaryllidaceae alkaloid biosynthesis. By integrating computational predictions with biochemical validation, this study provides new insight into the TyDC functional diversity in *Narcissus*.

## 2.4. Introduction

The daffodil (*Narcissus spp.*) is the symbol of the Canadian Cancer Society, a noteworthy coincidence given that *Narcissus* species produce a wide array of bioactive alkaloids with documented anticancer activity. As members of the Amaryllidaceae family, *Narcissus* species produce a remarkably diverse group of specialized metabolites, most of which are derived from amino acids such as L-tyrosine and L-phenylalanine. To date, more than 650 Amaryllidaceae alkaloids have been identified, exhibiting a broad spectrum of pharmacological activities. For instance, galanthamine is an acetylcholinesterase inhibitor used to treat mild symptoms of Alzheimer's disease, lycorine displays anticancer properties, and cherylline has antiviral activity (Cortes et al. 2015; Georgiev, Ivanov, and Pavlov 2020; Ka et al. 2021). Despite the pharmaceutical importance of these compounds, the biochemical mechanisms governing entry into the Amaryllidaceae alkaloid biosynthetic pathway remain incompletely defined, underscoring the need for detailed functional characterization of the enzymes involved.

All Amaryllidaceae alkaloids can be traced back to a common precursor molecule, 4'-O-methylnorbelladine, formed through the condensation of tyramine and 3,4-dihydroxybenzaldehyde followed by its reduction and 4'-O-methylation (Singh et al. 2018; Kilgore et al. 2016; Tousignant, Diaz-Garza, Majhi, Gélinas, Singh, and Desgagne-Penix 2022; Majhi et al. 2023; Kilgore, Augustin, Starks, O'Neil-Johnson, et al. 2014; Koirala et al. 2024). In several Amaryllidaceae species, including *Lycoris aurea* and *Lycoris radiata*, tyramine is produced by a pyridoxal 5'-phosphate (PLP)-dependent non-oxidative tyrosine decarboxylase (TyDC) (Wang et al. 2019; Hu et al. 2021). TyDC belongs to the group II family of aromatic amino acid decarboxylases (AAADs), which also includes tryptophan decarboxylases (TDC), phenylacetaldehyde synthases (PAAS) and DOPA decarboxylases (DDC) (Sandmeier, Hale, and

Christen 1994). Despite high sequence similarity, individual TyDCs often differ in substrate preference and catalytic behaviour (Li et al. 2022; Luaces et al. 2024). Such differences typically arise from subtle variations in the PLP-binding pocket and active-site architecture, which influence substrate positioning and reaction outcome (Torrens-Spence et al. 2020a).

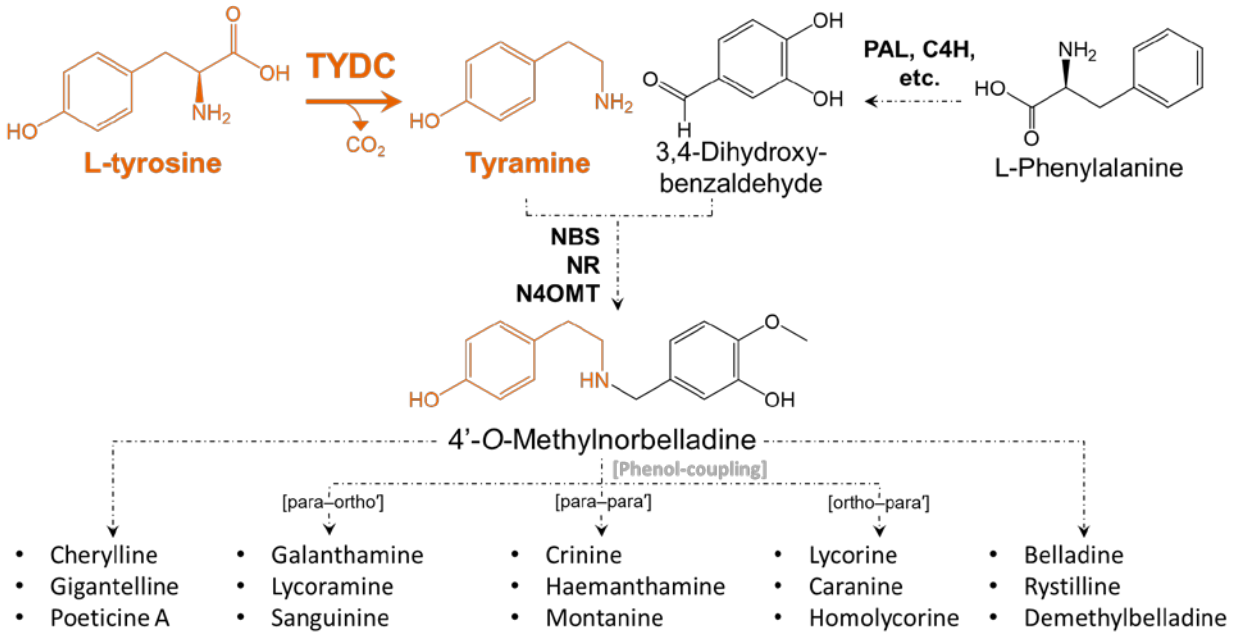



**Figure 11**. **Simplified overview of Amaryllidaceae alkaloid biosynthesis highlighting the tyrosine decarboxylase (TyDC)–dependent entry step.** L-Tyrosine is decarboxylated to tyramine by TyDC with the release of $CO_2$. In parallel, L-phenylalanine is converted through the phenylpropanoid pathway (PAL, C4H, and downstream enzymes) to yield 3,4-dihydroxybenzaldehyde. Tyramine and 3,4-dihydroxybenzaldehyde condense to form norbelladine via norbelladine synthase (NBS), followed by reduction via norcrausodine/noroxomaritidine reductase (NR) and O-methylation by norbelladine 4′-O-methyltransferase (N4OMT) to produce 4′-O-methylnorbelladine. Subsequent reactions, including phenol-coupling (para–ortho′, para–para′, or ortho–para′), give rise to the major structural classes of Amaryllidaceae alkaloids, including cherylline-, galanthamine-, crinine-, lycorine-, and belladine-type compounds, with representative alkaloids indicated. A solid arrow represents one enzymatic reaction whereas a dashed arrow represents multiple enzymatic steps.

Across biological kingdoms, TyDCs carry out distinct roles. In plants, they are often involved in the production of important specialized metabolites. Examples include benzylisoquinoline

alkaloids in *Papaver somniferum*, phenylethanoids in *Rehmannia glutinosa*, and health-promoting phenolics in *Olea europaea* (Facchini et al. 1994; Li et al. 2022; Luaces et al. 2024). TyDC activity also contributes to inducible defence responses. In these cases, tyramine is incorporated into the cell wall, where it may help reinforce the tissue during pathogen attack (Kawalleck et al. 1993). Although TyDCs have been characterized in several plant systems, individual isoforms within a given species often exhibit divergent substrate specificities and physiological roles despite high sequence similarity. In many plants, TyDCs are encoded by small multigene families, yet the functional differentiation among isoforms remains poorly resolved, particularly in Amaryllidaceae species where TyDC represents a potential regulatory entry point into alkaloid biosynthesis.

Earlier studies have researched TyDCs in other Amaryllidaceae species by employing transcriptomic analyses, gene cloning, and expression profiling, which uncovered that TyDC is encoded not by a single gene but by a multi-gene family (Hotchandani, de Villers, and Desgagne-Penix 2019; Singh and Desgagné-Penix 2017; Wang et al. 2019; Li et al. 2025). In *Narcissus papyraceus,* multiple isoforms were identified. Each display distinct spatial and temporal expression patterns across organs like bulbs, leaves, and roots. (Hotchandani, de Villers, and Desgagne-Penix 2019). However, the biochemical properties, substrate preferences, and structural determinants of individual TyDC isoforms in *Narcissus pseudonarcissus* have not yet been experimentally validated.

In the present study, we addressed this gap by cloning and functionally characterizing two TyDC isoforms from *N. pseudonarcissus* ‘King Alfred’ (trumpet daffodil). Conserved domain searches, phylogenetic analysis, homology modelling, and molecular docking were combined to predict structural and functional features and identify essential residues within the PLP-binding pocket. Next, these results were experimentally validated using enzymatic assays and kinetic calculations

under varying conditions to identify optimal activity parameters. While the *Np*TyDC2 substrate could not be identified, our results revealed that *Np*TyDC1 exhibited activity toward L-tyrosine and L-phenylalanine, consistent with a primary role in directing flux into Amaryllidaceae alkaloid biosynthesis, whereas *Np*TyDC2 does not display detectable tyrosine decarboxylase activity under the conditions tested. Together, these findings establish a biochemical framework for understanding TyDC functional diversification in Amaryllidaceae and provide a foundation for future physiological and metabolic engineering studies.

## 2.5. Results and Discussion

### 2.5.1. Phylogenetic analysis supports that *Np*TyDC1 is evolutionarily close to other alkaloid-producing plants.

The *de novo* transcriptome assembly of *N. pseudonarcissus* cultivar 'King Alfred' yielded 14 TyDC-related transcripts, with two full-length isoforms identified and deposited in GenBank as TyDC-1 (*Np*TyDC1, MF405171) and TyDC-2 (*Np*TyDC2, MF405172) (Singh and Desgagné-Penix 2017). Protein sequences of TyDC isoforms *Np*TyDC1 and *Np*TyDC2 from *N. pseudonarcissus* were retrieved from public data (UniProt: A0A2H5AIY0 and A0A2H5AIY2, respectively). *Np*TyDC1 comprises 515 amino acids, whereas *Np*TyDC2 is 500 amino acids in length, and the two isoforms share 57% sequence identity. The domain search analysis of these sequences revealed that they belong to the AAT_1 superfamily. Both enzymes shared a PLP binding pocket, and the catalytic residues are, respectively, Lys321 and Lys305 (**Figure S3).**

The phylogenetic analysis revealed that *Np*TyDC1 and *Np*TyDC2 cluster into two distinct clades. *Np*TyDC1 grouped with TyDC sequences from Amaryllidaceae species including *Lycoris*, *Leucojum*, *Narcissus*, and *Crinum*, whereas *Np*TyDC2 clustered with TyDCs from a broader range of monocot species, including sequences from *Acorus*, *Musa* (banana), *Phoenix* (date palm), *Curcuma* (turmeric), *Asparagus*, and *Dendrobium*, and other uncharacterized TyDC2 sequences from Amaryllidaceae species, such as *Leucojum* and *Crinum*. This indicates a potential lineage-specific adaptation for specialized metabolite production, such as in the alkaloid pathway. This clustering is consistent with previous phylogenetic studies on Amaryllidaceae TyDCs, where TyDC1-like isoforms form a distinct group associated with galanthamine production (Desgagné-Penix 2021). For instance, *Lau*TYDC1 from *L. aurea*, which decarboxylates tyrosine to tyramine (Wang et al. 2019), shares high sequence identity and phylogenetic proximity with *Np*TyDC1. By contrast, this clustering implies broader AAAD functions. This divergence mirrors patterns in other

alkaloid-producing plants, such as *P. somniferum*, where TyDC isoforms separate into clades for primary versus specialized metabolism (Facchini et al. 1994). Several of the 12 remaining partial TyDC-like sequences from the *N. pseudonarcissus* grouped within the Amaryllidaceae TyDC1 clade alongside *Np*TyDC1 and characterized *Lycoris* enzymes, while others clustered with *Np*TyDC2 in the broader monocot clade. This distribution suggests that the TyDC gene family in *N. pseudonarcissus* comprises isoforms potentially associated with both specialized and general metabolic functions. Because these sequences are incomplete, their functional contribution could not be further assessed.

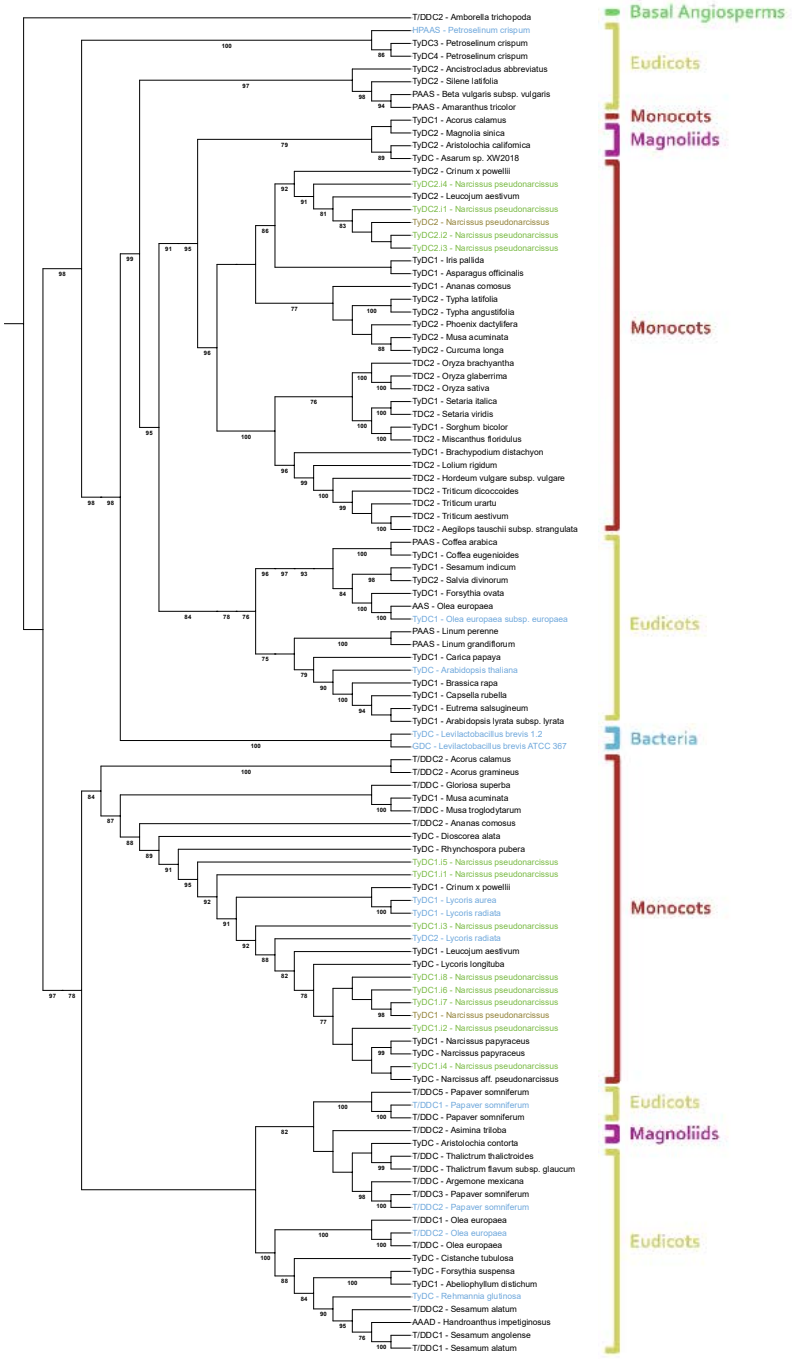



**Figure 12. *Np*TyDC1 clusters with other Amaryllidaceae TyDCs, and *Np*TyDC2 clusters with TyDCs from Amaryllidaceae and other plants.** *Np*TyDC1 and *Np*TyDC2 are highlighted with orange. The 12 additional partial TyDC-like sequences from the *N. pseudonarcissus* are shown in light orange. The blue-coloured entries are characterized enzymes. Bootstrap numbers are shown below the branches.

### 2.5.2. Docking analysis suggests that *Np*TyDC1 and *Np*TyDC2 could bind multiple substrates.

*Np*TyDC isoforms were modelled as homodimers, with the active site located at the dimer interface and formed by residues from both chain A and B, as in previous structural studies (Torrens-Spence et al. 2020a). The models adopted a canonical type II PLP-dependent decarboxylase fold and superposed closely with *Ps*TyDC with an RMSD of 0.363 Å (**Figure 13**, B, C, and D.). Multiple sequence alignment (**Figure 13**, A.) showed that residues predicted to constitute the *Np*TyDC1 and 2 active sites are largely conserved across characterized plant TyDCs. LLP consistently interacted with Thr169, Cys170, and Asp289, as in *Cr*TDC, stabilized by pi-stacking with His205 in a closed loop conformation, as in *Ps*TYDC (*e.g.*, **Figure S4**). *Np*TyDC1 active-site residues predicted with MOE encompassed conserved aromatic and hydrophobic residues, including Trp94, Phe103, Pro104, Phe126, and His320, consistent with active-site architectures described for other plant AAADs such as *Cr*TyDCs, as well as Tyr350 and Ser372, as reported for *Ps*TyDCs (**Table S7**). In chain A, all predicted active-site residues are conserved except for the position corresponding to Phe103, which is replaced by Tyr103 in *Np*TyDC2, while phenylalanine is retained at this position in all other present proteins (**Figure S4**). Tyr350 is replaced by a Phe in parsley HPAAS, an enzyme previously thought to be a TyDC (Torrens-Spence et al. 2012). The presence of Ser372 at the active site of most TyDCs, which is associated with phenolic amino acid recognition, is replaced by Gly356 in *Np*TyDC2, which is linked instead to indolic substrate recognition in a previous study (Torrens-Spence et al. 2020a).

The four ligands, L-tryptophan (-6.9 kCal/mol), L-tyrosine (-6.4 kCal/mol), L-Dopa (-7.0 kCal/mol), and L-phenylalanine (-5.9 kCal/mol) (**Table S7**), docked in a similar orientation in the active site of *Np*TyDC1, presenting their Cα-carboxyl bond in proximity to the pyridine ring of LLP aldimine (Figure S4). The predicted *Np*TyDC1 folding exhibited the least affinity towards L-phenylalanine

and the most towards L-DOPA and tryptophan (**Table S7, A**). Direct interaction with the putative catalytic Tyr350 was detected for L-DOPA, while it was positioned in proximity to the Cα of all ligands. The latter formed a salt bridge with His205 for all ligands, as in *Ps*TyDC. The model is consistent with the catalytic mechanism proposed for *Cr*TDC and *Ps*TyDC. Similar orientation and docking scores were predicted in the *Np*TyDC2 active site (**Figure S4**). The latter displayed predicted higher affinities for L-DOPA and L-tryptophan (-7.5 and -7.4 kcal/mol, respectively) and the lowest score for L-phenylalanine (-6.4 kcal/mol) (**Table S7, B**). A conserved salt-bridge interaction between the ligands' carboxylate and His189 was observed. Tyr334B (corresponding to Tyr350 in *Np*TyDC1) was located in the vicinity of the ligand tail as well. Although *Np*TyDC2 Gly356B superposed sharply with *Np*TYDC1 Ser372, it induced a conformational change of Leu355B (371B), diving into the active site close to the carboxyl group of the ligand in *Np*TyDC2 (a distance of 3.3 Å in *Np*TyDC2 vs 7.6 Å in *Np*TyDC1), possibly obstructing access to the active site (**Figure S4**). Although docking suggests that *Np*TyDC1 and *Np*TyDC2 could both accommodate the substrates in orientations consistent with their decarboxylation, the difference in the orientation of Leu371/Leu355 could cause steric hindrance to the ligand in *Np*TyDC2 (**Figure S5**). The Ser372 to Gly356 substitution in *Np*TyDC2 resulted in Leu355 encumbrance of the active site, possibly reducing efficient binding of phenolic substrates. Although docking predicted that both *Np*TyDC1 and *Np*TyDC2 could accommodate several aromatic amino acids with comparable binding energies, this approach primarily reflects static binding compatibility rather than catalytic competence. In PLP-dependent decarboxylases, small changes in active-site geometry, loop dynamics, or transition-state stabilization can strongly impact reaction outcome without substantially altering predicted binding scores. Our results therefore underscore the limitation of

docking alone to infer substrate specificity in AAADs and highlight the necessity of biochemical validation (Torrens-Spence et al. 2013).

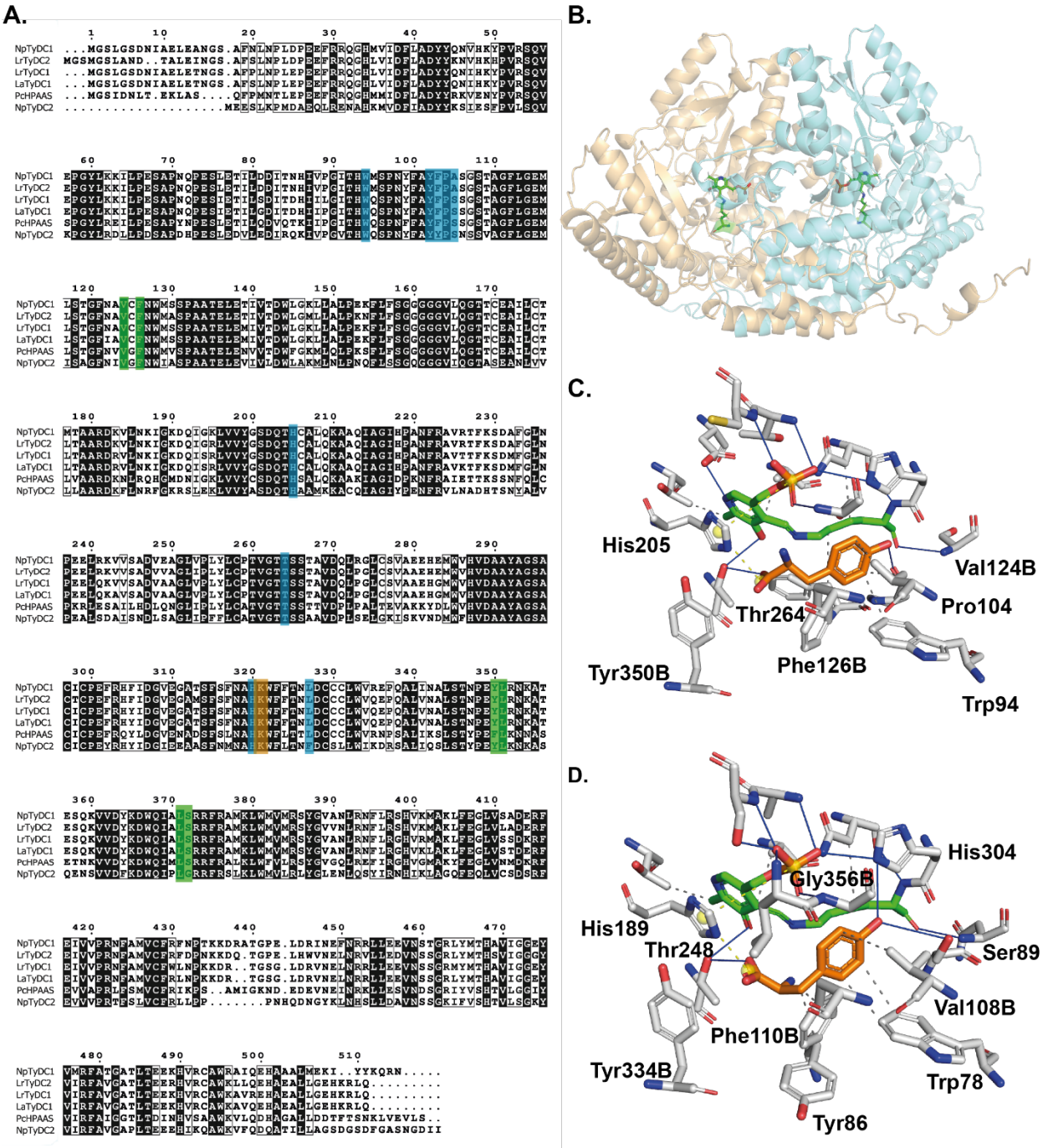



**Figure 13. Conserved active-site architecture of *Np*TyDC1 and *Np*TyDC2 candidates despite key residue differences. A.** Multiple sequence alignment of plant TyDCs (and HPAAS from parsley) highlights the conservation of residues that form the *Np*TyDC1 active site. Shaded positions correspond to equivalent amino acids involved in substrate binding and catalysis, as identified by MOE-based pocket detection. Blue positions are from chain A, green positions are from chain B, and the LLP binding site is highlighted in orange. **B.** *Np*TyDC1 dimer predicted folding

represented as a cartoon. Chain A is beige, and chain B is turquoise. N'-pyridoxyl-lysine-5'-monophosphate (Lys321-bound PLP) is shown as green sticks. **C.** L-Tyrosine docked inside *Np*TyDC1 active site. Leu355B (not annotated) is displayed bound to Gly356B. **D.** L-Tyrosine docked inside *Np*TyDC2 active site. Interacting residues are shown as grey sticks, LLP is shown as green sticks, and the ligand as orange sticks. H-bonds are shown as blue lines, hydrophobic bonds as dotted grey lines, and salt bridges as dotted yellow lines with yellow spheres. Amino acids from chain B are identified with "B".

### 2.5.3. Both *Np*TyDC1 and *Np*TyDC2 localize to the cytoplasm and nucleus

To investigate the subcellular localization of *Np*TyDC1 and *Np*TyDC2, their coding sequences from *N. pseudonarcissus* 'King Alfred' were fused in-frame upstream of the *YFP* gene. The resulting *NpTyDC1-YFP* and *NpTyDC2-YFP* constructs were transiently expressed in *Nicotiana benthamiana* leaves via *Agrobacterium tumefaciens*-mediated infiltration, and fluorescence signals were examined by confocal laser scanning microscopy. The cyan fluorescent protein (CFP), which localizes to both the cytoplasm and nucleus (Kruse et al., 2010) was used as a reference marker. As shown in Figure 14, both *Np*TyDC1-YFP and *Np*TyDC2-YFP fusion proteins were detected in the cytoplasm and nucleus, displaying a localization pattern similar to that of CFP. These findings indicate that *Np*TyDC1 and *Np*TyDC2, which lack predicted signal peptides, are localized to the same nucleocytoplasmic compartment of the cell. This pattern matches what we expected for soluble aromatic amino acid decarboxylases. As a result, neither protein is sent to the secretory pathway or to a membrane-bound compartment. Our finding is consistent with the cytoplasmic localization reported for the *Arabidopsis* tyrosine decarboxylase *At*TyrDC (Lehmann and Pollmann 2009). Demostrating that a nucleocytoplasmic location is a shared feature of plant TyDCs. Furthermore, our result agrees with the localization of the downstream enzymes of the pathway. Norbelladine synthase (NBS) and noroxomaritidine/norcraugsodine reductase (NR) both localize to the cytoplasm and the nucleus (Majhi et al. 2023). These two enzymes use the tyramine that TyDC produces. Their shared location with *Np*TyDC1 seems to place the start of the pathway and its first committed steps in the same soluble compartment.

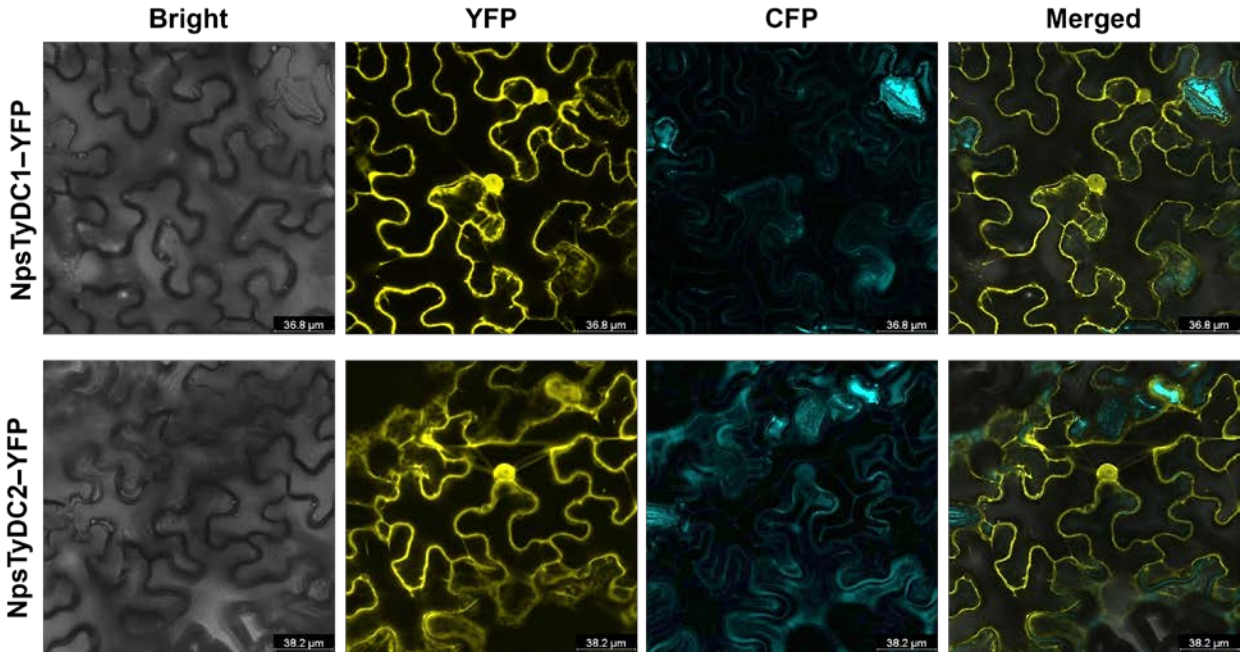



Figure 14.Subcellular localization of *Np*TyDC1 and *Np*TyDC2 in *Nicotiana benthamiana* epidermal cells. Both *Np*TyDC1 and *Np*TyDC2 localize to the cytoplasm and nucleus. The indicated YFP fusion proteins were co-expressed with cyan fluorescent protein (CFP) in *N. benthamiana* leaves via *Agrobacterium tumefaciens*-mediated transient transformation. Forty-eight hours post-infiltration, fluorescence was observed in epidermal cells using confocal laser scanning microscopy. Bright-field, chlorophyll autofluorescence, yellow fluorescent protein (YFP), cyan fluorescent protein (CFP), and merged fluorescence images are shown. Scale bars are indicated in the images. CFP was used as a nucleocytosolic marker.

### *2.5.4. Np*TyDC1 exhibits high substrate specificity for L-tyrosine compared to *Np*TyDC2

To compare the catalytic efficiencies of *Np*TyDC1 and *Np*TyDC2, we expressed the enzymes in *E. coli* (The SDS-PAGE results are shown in **Figure S6**) and measured the standard area ratio of products (tyramine, phenylethylamine, tryptamine, and dopamine) generated from their respective substrates (L-tyrosine, L-phenylalanine, L-tryptophan, and L-DOPA) in enzymatic assays. Product formation was significantly impacted by the combined influence of enzyme isoform, substrate identity, and assay condition. (**Table S8**).

**Table 1**. Comparison of product formation by *Np*TYDC1 and *Np*TYDC2 based on standard area ratios relative to the internal standard papaverine.

| Substrate | Enzyme | Product | Average ± Std. Deviation* |
|---|---|---|---|
| L-Tyrosine | *Np*TyDC1 | Tyramine | 0.15 ± 0.02 |
| | *Np*TyDC2 | | 0.00053 ± 0.00001 |
| L-Tryptophan | *Np*TyDC1 | Tryptamine | 0.004 ± 0.001 |
| | *Np*TyDC2 | | 0.0036 ± 0.0003 |
| L-DOPA | *Np*TyDC1 | Dopamine | 0.024 ± 0.002 |
| | *Np*TyDC2 | | 0.045 ± 0.004 |
| L-Phenylalanine | *Np*TyDC1 | Phenylethylamine | 0.25 ± 0.03 |
| | *Np*TyDC2 | | 0.10 ± 0.02 |

*****Values represent HPLC–DAD peak area ratios normalized to the internal standard (papaverine) and are provided for qualitative comparison of substrate conversion. Due to differences in UV absorption and detector response factors between products, area ratios are not directly comparable across different substrates.

For L-tryptophan and L-DOPA, neither isoform produced detectable tryptamine or dopamine, respectively. However, both enzymes generated phenylethylamine above background when phenylalanine was used as a substrate ($p < 0.001$), although to different extents. There was a 2.4-fold increase in L-phenylalanine conversion for *Np*TyDC1 compared to *Np*TYDC2 ($p < 0.001$). Because tyramine and phenylethylamine differ in their UV detector response factors relative to the internal standard, the ISTD-normalized area ratios for these two products cannot be directly compared within the same enzyme; only comparisons of the same product across the two isoforms are valid. Interestingly, *Np*TyDC1 produced tyramine, the direct precursor of Amaryllidaceae alkaloid biosynthesis, at levels well above those of both controls, with an average product formation of 0.15 based on standard area ratio ($p < 0.001$), confirming strong enzymatic activity. *Np*TyDC2 showed no detectable conversion of substrate with a standard ratio of 0.00053 for the product. In conclusion, *Np*TyDC1 catalyzes the decarboxylation of L-tyrosine under the assay conditions. In contrast, *Np*TyDC2 shows detectable activity toward phenylalanine and no detectable tyrosine decarboxylation. Neither isoform converts tryptophan or L-DOPA *in vitro*. Together, these results show clear functional divergence between the two TyDC isoforms, with

NpTyDC1 uniquely positioned to channel L-tyrosine toward the alkaloid pathway. This selectivity aligns partially with Amaryllidaceae TyDCs like *Lau*TYDC1 from *L. aurea*, which prefers L-tyrosine over L-DOPA, but the latter shows no L-phenylalanine activity (Wang et al. 2019). Similarly, *Lr*TyDC from *L. radiata* exhibits high tyrosine specificity, correlating with galanthamine levels (Hu et al. 2021). TyDCs from other plants decarboxylate both tyrosine and L-DOPA but not L-phenylalanine. For example, olive (*O. europaea) Oe*TDCs and *R. glutinosa Rg*TyDC2 both prefer tyrosine but also accept L-DOPA (Luaces et al. 2024; Li et al. 2022). In *N. pseudonarcissus* 'King Alfred', *Np*TyDC1 carries the expected structural signatures of phenolic substrate recognition (Torrens-Spence et al. 2020a), and is the only characterized isoform catalyzing L-tyrosine decarboxylation. Although the enzyme also accepts L-phenylalanine, the biological significance of this activity remains unclear, as phenylethylamine is not a known intermediate in Amaryllidaceae alkaloid biosynthesis. No L-tryptophan decarboxylation was detected in enzymatic assays under the tested conditions, but we cannot rule out that *Np*TyDC2 may instead recognize a different indole substrate, not included in the present assays. The lack of tryptophan decarboxylation differentiates *Np*TyDC2 from *Cr*TDC in *Catharanthus roseus*, which produces tryptamine for indole alkaloids (Torrens-Spence et al. 2020a). *Np*TyDC2 is a divergent AAAD-like isoform, consistent with its phylogenetic clustering, suggesting a role in primary metabolism instead. *Np*TyDC2 retains all canonical features of PLP-dependent AAADs, including conserved catalytic residues and a well-defined active site, and is broadly conserved across monocots. This suggests that *Np*TyDC2 likely acts on alternative substrates or operates under physiological contexts not captured in the present *in vitro* assays, such as stress-related or developmental regulation, rather than contributing directly to Amaryllidaceae alkaloid biosynthesis. Future studies using broader substrate libraries or *in planta* perturbations will be

required to clarify its physiological role. In addition, longer read transcriptome or genome analyses (or RACE) will help resolve the functional contributions of the remaining 12 incomplete TyDC sequences to tyramine biosynthesis.

### 2.5.5. Optimization of enzymatic assay conditions for *Np*TyDC1

Since only *Np*TyDC1 exhibited tyramine production, we continued the subsequent optimization assay focusing exclusively on this enzyme. For temperature Figure 15, A), kinetic characterization revealed an optimal temperature of approximately 37 °C, with activity rising from low levels at 20 °C and declining slowly at higher temperatures. For enzyme quantity (**Figure S7**), tyramine production increased until maximum activity was observed at 30 ng (**Table S9**).

We next evaluated the impact of reaction duration (**Figure S8**). Tyramine production by *Np*TyDC1 increased progressively with reaction duration, with significant overall differences (**Table S10**). Substrate conversion increased at short assay durations, reached a maximum at intermediate times (around the 80-minute mark), and then reached a plateau. In conclusion, these findings show that *Np*TyDC1 activity is time-dependent, increasing during the early phase of the reaction and peaking at intermediate durations. After measuring product formation in different concentrations of substrate available, tyramine production by *Np*TyDC1 increased in a concentration-dependent manner, with highly significant overall differences ($p < 0.001$). *Np*TyDC1 optimal temperature was 37 °C, similarly to *Oe*TDCs (40 °C) but lower than *Lau*TYDC1 in Wang et al., which was 50 °C. (Luaces et al. 2024; Wang et al. 2019). Enzyme concentration assays showed saturation at 30-60 ng. Increasing enzyme abundance beyond this range did not increase product formation because substrate availability was fixed under the assay conditions. Reaction duration indicated

accumulation peaking at 80-160 min, suggesting turnover limits or product inhibition, consistent with *Lb*TDC assays (Zhu et al. 2016).

We propose that TyDC functional divergence within Amaryllidaceae is consistent with adaptation to temperatures. Ptak et al. showed that cold stress (15 °C) causes TyDC expression and the buildup of specialized metabolites in *Leucojum aestivum* cultures grown *in vitro* (Ptak et al. 2026). Together, these observations are consistent with a role for TyDC isoforms in responding to temperature-associated physiological constraints, although this hypothesis remains speculative.

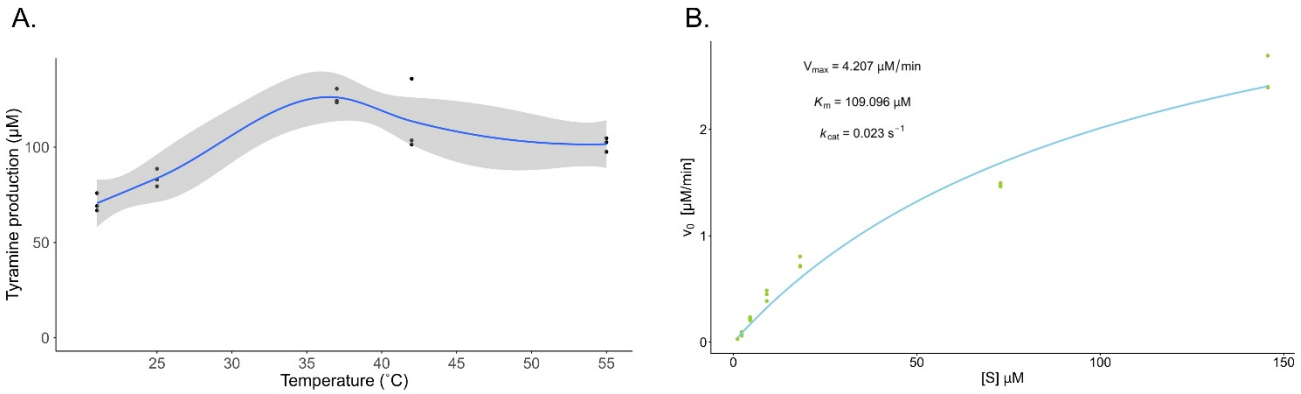



Figure 15.Kinetic characteristics of *Np*TyDC1. **A. Tyramine production (mM) by *Np*TyDC1 varied with temperature (°C).** 95% Confidence level calculated using 3 replicates. **B. Michaelis-Menten kinetics of *Np*TyDC1**, plotting initial velocity ($v_0$, µM/min) against L-tyrosine concentration ([S]µM), with fitted curve and annotated parameters. Kinetic analysis was performed at 37 °C with 30 ng of enzyme and a reaction duration of 80 minutes. $V_{max}$ was projected but not achieved under these conditions.

Initial velocity values ($v_0$) were calculated and used as input for nonlinear regression analysis, resulting in a $K_m$ of 109.1 µM for *Np*TyDC1 (Figure 15, B). The reaction is projected to reach a maximal rate of 4.207 µM/min (0.23 nkat/mg), as $V_{max}$ was not achieved under the tested conditions. This projected value was then used to derive a turnover number of 0.023 $s^{-1}$ based on the enzyme concentration in the assay. *Np*TyDC1 functions as a tyrosine decarboxylase that converts L-tyrosine to tyramine. The enzyme shows specificity for L-tyrosine and displays

consistent kinetic behaviour under the assay conditions, supporting its role as an aromatic amino acid decarboxylase.

Comparison of kinetic parameters with the phylogenetic reconstruction shows that evolutionary relatedness often aligns with enzyme behaviour, but not in a strictly linear manner (**Table 2**). *Np*TyDC1, characterized in this study, exhibits substrate affinity values that fall within the small range defined by closely related *Lycoris* enzymes as in the phylogenetic tree. Its $K_m$ of 109 µM lies between that of *Lr*TyDC2 at 60 µM and *Lr*TyDC1 at 390 µM, while *Lau*TyDC1 displays a higher $K_m$ of 602 µM, consistent with its slightly more distant placement in the phylogeny. Catalytic turnover among these enzymes remains uniformly low. *Np*TyDC1 shows a calculated *kcat* of 0.02337 $s^{-1}$, closely matching *Lr*TyDC2 at 0.03199 $s^{-1}$ and *Lr*TyDC1 at 0.03817 $s^{-1}$, whereas *Lau*TyDC1 exhibits a moderate increase to 0.2664 $s^{-1}$. Maximal velocities follow the same constrained pattern, ranging from 0.23 nkat $mg^{-1}$ for *Np*TyDC1 to 0.44–0.53 nkat $mg^{-1}$ for *L. radiata* enzymes, with *Lau*TyDC1 reaching 3.19 nkat $mg^{-1}$ (Hu et al. 2021; Wang et al. 2019).

**Table 2.** Comparison of different aromatic amino acid decarboxylases that have been characterized using L-tyrosine as a substrate. The values in blue have been determined by either a unit conversion or have been calculated based on the data available in each corresponding article. The detailed table with all the calculations is in **Table S11.** All values have been converted to identical units to facilitate the comparisons. Only the entries for which all values were present or could be calculated were kept in the table.

| Organism | Enzyme / Isoform | $K_m$ (µM) | calculated *kcat* ($s^{-1}$) | *kcat* ($s^{-1}$)/$K_m$ (µM) | $V_{max}$ (nkat/mg) | Molecular weight (kDa) | Reaction volume (µL) | Reference |
|---|---|---|---|---|---|---|---|---|
| *Lycoris radiata* | *Lr*TyDC2 | 60 | 0.03199 | 0.00053317 | 0.44 | 72.7 | 100 | (Hu et al. 2021) |
| ***Narcissus pseudonarcissus*** | ***Np*TyDC1** | **109** | **0.02337** | **0.0002144** | **0.23** | **100*** | **100** | **This study** |
| *Rehmannia glutinosa* | *Rg*TyDC2 | 250 | 0.15 | 0.0006 | 2.68 | 56.05 | 250 | (Li et al. 2022) |
| *Lycoris radiata* | *Lr*TyDC1 | 390 | 0.03817 | 9.7872E-05 | 0.53 | 72.7 | 100 | (Hu et al. 2021) |
| *Petroselinum crispum* | *Pc*AAS | 460 | 1.06 | 0.00230435 | 18.62 | 57 | 100 | (Torrens-Spence et al. 2012) |
| *Lactobacillus brevis IOEB 9809* | TDC | 580 | 0.134 | 0.00023103 | 1.92 | 70 | 2000 | (Moreno-Arribas and Lonvaud-Funel 1999) |
| *Lactobacillus brevis CGMCC 1.2028* | *Lb*TDC | 590 | 343.1 | 0.58152542 | 2452 | 70 | 1000 | (Zhang and Ni 2014) |
| *Lycoris aurea* | *Lau*TyDC1 | 602 | 0.2664 | 0.00044252 | 3.19 | 83.5 | 150 | (Wang et al. 2019) |
| *Lactobacillus brevis* (Sci Rep 2016) | *Lb*TDC | 630 | 124.8 | 0.19809524 | 1783 | 70 | 1000 | (Zhu et al. 2016) |
| *Lactobacillus brevis ATCC 367* | TDC | 670 | 0.077 | 0.00011493 | 1.1 | 70 | 2000 | (Moreno-Arribas and Lonvaud-Funel 1999) |
| *Arabidopsis thaliana* | *At*TyrDC | 745 | 3.99 | 0.0053557 | 61.35 | 65 | 300 | (Lehmann and Pollmann 2009) |
| *Papaver somniferum* | *Ps*TyDC1 | 1000 | 3.36E-08 | 3.36E-11 | 0 | 57 | 1000 | (Facchini and De Luca 1994) |
| *Papaver somniferum* | *Ps*TyDC2 | 1002 | 7.08E-09 | 7.0659E-12 | 0 | 59 | 1000 | (Facchini and De Luca 1994) |

| | | | | | | | | |
|---|---|---|---|---|---|---|---|---|
| *Olea europaea* | *Oe*TDC2 | 1290 | 23.98 | 0.01858915 | 161.5 | 56.4 | 200 | (Luaces et al. 2024) |
| *Olea europaea* | *Oe*TDC1 | 1900 | 12.79 | 0.00673158 | 187.7 | 56.3 | 200 | (Luaces et al. 2024) |

*The molecular weight for *Np*TYDC1 of 100 kDa includes the MBP-tag which is of approximately 40-42 kDa.

Rather than reflecting inefficiency, the low catalytic turnover of *Np*TyDC1 is consistent with a gatekeeping role at the entry point of Amaryllidaceae alkaloid biosynthesis, where tight regulation of tyramine availability may be critical to downstream pathway control. Enzymes catalyzing committed steps in specialized metabolism often operate under constrained kinetic regimes, with pathway flux regulated primarily through enzyme abundance, localization, or activation rather than maximal catalytic capacity. In this context, the kinetic properties of *Np*TyDC1 align with its proposed role in regulating access to the alkaloid biosynthetic network rather than sustaining high-flux primary metabolism.

We calculated catalytic efficiencies (*kcat*/$K_m$) for the enzymes in Table 2. These values support our interpretation. They also place *Np*TyDC1 within the wider kinetic range of characterized AAADs. *Np*TyDC1 shows a low catalytic efficiency of about $2.1 \times 10^{-4}$ $\mu M^{-1}$ $s^{-1}$. This value is close to that of its nearest phylogenetic relatives. The *Lycoris* enzymes cluster in the same low range (*Lr*TyDC2, ~$5.3 \times 10^{-4}$; *Lau*TyDC1, ~$4.4 \times 10^{-4}$; *Lr*TyDC1, ~$9.8 \times 10^{-5}$ $\mu M^{-1}$ $s^{-1}$). This narrow range indicates that *Np*TyDC1 is kinetically typical of tyrosine decarboxylases linked to specialized metabolism in this lineage, once we consider affinity and turnover together. On the other hand, enzymes tied to higher-flux or primary metabolism appear far more efficient. Their catalytic efficiencies are greater by one to several orders of magnitude. These include the plant decarboxylases of *O. europaea* (~$6.7 \times 10^{-3}$ to $1.9 \times 10^{-2}$ $\mu M^{-1}$ $s^{-1}$) and *A. thaliana* (~$5.4 \times 10^{-3}$ $\mu M^{-1}$ $s^{-1}$). The bacterial *L. brevis* enzymes are higher still (~$2.0 \times 10^{-1}$ to $5.8 \times 10^{-1}$ $\mu M^{-1}$ $s^{-1}$), consistent with sustained tyramine production in primary metabolism. The *P. somniferum* TyDCs fall at the opposite extreme (~$10^{-11}$ to $10^{-12}$ $\mu M^{-1}$ $s^{-1}$), in line with their negligible activity on L-tyrosine. As a result, the low catalytic efficiency of *Np*TyDC1 mirrors its low turnover. This pattern seems consistent with a

gatekeeping role at the entry point of Amaryllidaceae alkaloid biosynthesis, where tyramine supply might be controlled through tight kinetic regulation rather than high catalytic throughput.

TyDC1 activity in *N. pseudonarcissus* 'King Alfred' differs fundamentally from that observed in plant systems that are estimated to operate at higher flux, such as *O. europaea*, based on their kinetic characteristics. Comparison with enzymes from *O. europaea* indicates that *Np*TyDC1 operates under kinetic constraints that restrict catalytic activity. These constraints could prevent high-flux tyramine biosynthesis even when substrate affinity is preserved. So, *Np*TyDC1 functions as a tightly regulated, low-output enzyme rather than a bulk metabolic TyDC like in *O. europaea* TyDC1 and TyDC2, where the *kcat* values reach 23.98 $s^{-1}$ and 12.79 $s^{-1}$, respectively. This increase is also mirrored by their $V_{max}$ (Li et al. 2022; Luaces et al. 2024). TyDCs from *P. somniferum* display the most constrained catalytic profiles in the dataset. Both *Ps*TyDC1 and *Ps*TyDC2 exhibit high $K_m$ values of 1000 and 1002 µM, placing them among the lowest-affinity enzymes examined. Their catalytic turnover is several orders of magnitude lower than all other entries, with *kcat* values of $3.36 \times 10^{-8}$ $s^{-1}$ and $7.08 \times 10^{-9}$ $s^{-1}$, and $V_{max}$ values of $5.90 \times 10^{-7}$ and $1.20 \times 10^{-7}$ nkat $mg^{-1}$, respectively (Facchini and De Luca 1994).

Bacterial TyDCs define a distinct kinetic regime. Although their $K_m$ values overlap with those of plant enzymes, ranging from 580 to 670 µM, their catalytic turnover exceeds all plant values by orders of magnitude. *Lactobacillus brevis* CGMCC 1.2028 r*Lb*TDC reaches a *kcat* of 343.1 $s^{-1}$, while the TyDC from a subspecies of *L. brevis* reaches 124.8 $s^{-1}$, consistent with sustained high-flux activity typical of primary metabolic pathways. Correspondingly, $V_{max}$ values of 2451.67 and 1783 nkat $mg^{-1}$ dwarf those observed in plant systems, including the highly active *O. europaea* enzymes. Other *L. brevis* strains show lower but still elevated $V_{max}$ values of 1.92 and 1.1 nkat $mg^{-1}$, underscoring strain-level variability within a broadly conserved metabolic function (Zhang

and Ni 2014; Zhu et al. 2016; Moreno-Arribas and Lonvaud-Funel 1999). This suggests that these bacteria may require tyramine to a greater extent than plants do. Plants such as *N. pseudonarcissus* have evolved to tightly regulate the amount of tyramine they produce.

Although the contribution of the remaining partial TyrDC-like sequences awaits further investigation, these results suggest that *Np*TyDC1 is a biochemically defined gatekeeper enzyme that directs L-tyrosine into Amaryllidaceae alkaloid biosynthesis, while providing functional evidence for the divergence of TyDC isoforms in *Narcissus pseudonarcissus* 'King Alfred'.

# 2.6. Materials and Methods

## 2.6.1. Conserved domain search

Two full-length TyDC isoforms from *N. pseudonarcissus* cultivar 'King Alfred' (*Np*TyDC1, GenBank: MF405171; *Np*TyDC2, GenBank: MF405172) were analyzed with the NCBI Conserved Domain Database, with the e-value threshold set to 0.0001 and otherwise default settings. The search focused on verifying the presence of the PLP-dependent decarboxylase domain and identifying the conserved lysine residue required for Schiff base formation. In addition, multiple sequence alignment was carried out using *Np*TyDC1 and *Np*TyDC2 sequences (**Table S1**) via ClustalW in MEGA (Molecular Evolutionary Genetics Analysis, version 11.0.13) with default parameters.

## 2.6.2. Phylogenetic analysis

To evaluate evolutionary relationships, the R 4.4.1 (R Core Team 2024) and MEGA software were employed to construct a phylogenetic tree. Sequences for the tree were selected by searching all known and characterized decarboxylases that matched *Np*TyDC1 and *Np*TyDC2 in the non-

redundant protein sequence database using BlastP, with the parameters max_target_sequence=500 and e-value=0.0001. All the hypothetical, unnamed, etc. proteins were excluded, and isoform annotations were consolidated into a single sequence per enzyme per organism (**Table S2).** The remaining twelve isoforms, which were partial, were also included in the tree to provide a fuller representation of the *Np*TyDC family. *Amborella*, the most basal extant angiosperm, was used as the outgroup in the phylogenetic reconstruction (James W. Byng 2016). The sequences were aligned with ClustalW. Following alignment, a phylogenetic tree was inferred using the BIONJ method from a maximum-likelihood distance matrix under the JTT model. Node support was assessed using 999 bootstrap replicates. The tree was then edited using the Interactive Tree of Life (ITOL interface) (Letunic and Bork 2024).

### 2.6.3. Structural modelling and docking

*Np*TyDC1 and *Np*TyDC2 were modelled as a dimer with the AlphaFold3 server. PLP was covalently linked to Lys321 using MOE2024.09 software's builder (Chemical Computing Group, Québec, Canada) following superimposition with the X-ray crystal structures of *Catharanthus roseus* TDC (*Cr*TDC) in complex with L-tryptophan (PDB:6EEW), *P. somniferum* TyDC (*Ps*TyDC, PDB:6EEM) in complex with L-tyrosine, and *Arabidopsis thaliana* PAAS (*At*PAAS, PDB:6EEI) in complex with L-phenylalanine (Torrens-Spence et al. 2020a). MOE software was used to prepare receptors for docking, as outlined by (Lamichhane et al. 2025). Ligand SMILES codes (L-tyrosine, L-tryptophan, L-DOPA, and L-phenylalanine) were obtained from PubChem and cross-referenced with the ZINC20 database (Irwin et al. 2020) to obtained 3D structures for docking. The docking site was predicted using the MOE Site Finder tool, and N(6)-(pyridoxal phosphate)-L-lysine (LLP, lysine covalently linked to PLP) was added by homology. Docking was performed with the AMBER10:EHT force field using Triangle Matcher as the placement method

for 200 poses. Flexible and rigid receptor dockings were performed, and the 10 best poses were analyzed. The pose with the best docking score, consistent with the catalytic reaction and closely superimposing with the orthologous crystallized enzyme ligand position, is presented for each ligand. PDB files of docked structures were subsequently submitted to PLIP to identify interactions between ligands and receptor residues (Adasme et al. 2021). Models were then visualized using PyMOL 3.0.0 (Schrödinger, New York, USA).

### 2.6.4. Bacterial strains and growth conditions

The bacterial strains used in this study were *Escherichia coli* DH5α (Invitrogen, Thermo Fisher Scientific, ON, Canada), *E. coli* Rosetta (DE3) pLysS (Novagen, MilliporeSigma Canada Ltd., ON, Canada), and *Agrobacterium tumefaciens* GV3101 (Holsters and Silva 1980). The bacteria were cultured in Luria–Bertani (LB) medium supplemented with the appropriate antibiotics under standard growth conditions: *E. coli* strains at 37 °C and *A. tumefaciens* at 28 °C. Antibiotics were used at the following final concentrations (μg $mL^{-1}$): ampicillin, 100; chloramphenicol, 34; kanamycin, 50; rifampicin, 50; and gentamicin, 30 (all from Fisher Scientific Canada, ON, Canada).

### 2.6.5. RNA extraction, cDNA synthesis, and cloning of *Np*TyDC isoforms

A classical restriction enzyme-based cloning approach was used to construct all desired vectors. Total RNA was extracted from *N. pseudonarcissus* 'King Alfred' (*Np*) bulbs using the cetyltrimethylammonium bromide (CTAB) method as described by Singh and Desgagné-Penix (2017). First-strand cDNA was synthesized from 1 μg of total RNA using the SensiFAST™ cDNA Synthesis Kit (Bioline, Meridian BioScience, Froggabio Inc, ON, Canada) according to the manufacturer's protocol. The open reading frames (ORFs) of *NpTyDC1* and *NpTyDC2* were

amplified from bulb cDNA using PrimeSTAR® GXL Premix (TaKaRa Bio, CA, USA) in 50 µL reactions containing 0.2 µM of each forward and reverse primer (**Table S3;** Integrated DNA Technologies, IO, USA). The PCR cycling conditions were as follows: 98 °C for 2 min (initial denaturation), followed by 35 cycles of 98 °C for 10 s, 55 °C for 20 s, and 72 °C for 1 min, with a final extension at 72 °C for 5 min and an infinite hold at 4 °C. PCR products were analyzed on agarose gels and purified using the GenepHlow™ Gel/PCR Kit (Geneaid, Froggabio). For recombinant protein expression in *Escherichia coli, NpTyDC1* and *NpTyDC2* ORFs were fused in-frame to the C-terminus of the maltose-binding protein (MBP) in the pMAL-c2x vector (New England Biolabs, NEB, ON, Canada). digested with the appropriate enzymes, EcoRI and HindIII for *NpTyDC1*, and BamHI and SalI for *NpTyDC2*, and ligated into the pMAL-c2x vector digested with the same enzyme pairs, using T4 DNA ligase (NEB).

The recombinant plasmids were transformed into chemically competent *E. coli* DH5α cells by heat-shock transformation and plated on LB agar containing ampicillin. Positive clones were screened by colony PCR in 20 µL reactions using Taq DNA polymerase with ThermoPol buffer (NEB) under the following conditions: 95 °C for 5 min, 30 cycles of 95 °C for 30 s, 55 °C for 40 s, and 68 °C for 1 min, followed by a final extension at 68 °C for 5 min. All constructs were confirmed by Sanger sequencing to verify the correct insert orientation and sequence integrity (Génome Québec, QC, Canada).

For subcellular localization studies, *NpTyDC1* and *NpTyDC2* coding sequences were amplified and fused upstream of the yellow fluorescent protein (YFP) gene in the pBTEX binary vector under the control of the CaMV 35S promoter (Majhi et al. 2023). *NpTyDC1* fragments were digested with KpnI and XbaI, while *NpTyDC2* fragments were digested with KpnI and BamHI. Recombinant plasmids were transformed into chemically competent *E. coli* DH5α cells and

selected on LB agar plates containing kanamycin. Positive clones were confirmed by colony PCR, and all binary vectors were verified by DNA sequencing prior to further analyses.

### *2.6.6. Agrobacterium* transformation and transient expression for subcellular localization in *Nicotiana benthamiana*

The YFP-fusion binary vectors were introduced into *A. tumefaciens* strain GV3101 by electroporation, and transformants were selected on LB agar plates supplemented with rifampicin, kanamycin, and gentamicin at 28 °C. Positive colonies were confirmed by colony PCR. For transient expression assays, *A. tumefaciens* cultures were grown overnight in 5 mL of LB broth containing the same antibiotics at 28 °C with shaking. Cells were harvested by centrifugation at 7,900 rcf for 5 min at room temperature, washed three times with 10 mM $MgCl_2$, and resuspended in 5 mL of induction medium (10 mM $MgCl_2$, 10 mM MES [pH 5.6], and 200 µM acetosyringone, Cayman Chemical Co, Cedarlane, ON, Canada). The bacterial suspension was incubated at 28 °C with shaking (200 rpm) for 3–4 h. The *A. tumefaciens* suspension was then adjusted to an optical density of $OD_{600}$ = 0.25 with induction medium and infiltrated into the abaxial side of young, fully expanded leaves of five-week-old *Nicotiana benthamiana* plants using a 1 mL needleless syringe. Following agroinfiltration, plants were maintained in a controlled-environment growth chamber under long-day conditions (16 h light/8 h dark) at 22 °C for 48 h.

To visualize the subcellular localization of *Np*TyDC1 and *Np*TyDC2, 48 hours post-infiltration, the abaxial epidermis of leaf discs was mounted on microscope slides in a drop of distilled water, covered with a coverslip, and immediately imaged. Protein localization was observed using a confocal laser scanning microscope (Leica TCS SP8; Leica Microsystems, ON, Canada) equipped with a 40×/1.30 oil-immersion objective. Images were initially processed using LAS AF Lite software (Leica Microsystems). CFP was used as a marker control of nucleus and cytoplasmic

localization (Kruse et al. 2010). YFP was excited with an argon laser at 488 nm, and fluorescence emission was collected between 500 and 525 nm. CFP was excited with a diode laser at 405 nm, and emission was detected between 420 and 490 nm. Composite images were generated using LAS X software (Leica Microsystems).

### 2.6.7. Expression of MBP fusion proteins in *E. coli*

*NpTyDC1* and *NpTyDC2* cloned into the pMAL-c2x vector were transformed using heat shock transformation into chemically competent *E. coli* Rosetta (DE3) pLysS strain for protein expression. Transformed cells were selected on LB plates with ampicillin and chloramphenicol overnight at 37 °C. The positive colonies were screened by colony PCR. A PCR-positive single colony was picked and grown overnight at 37 °C at 220 rpm in 12.5 mL LB broth containing ampicillin and chloramphenicol. The bacteria were then scaled up to flasks containing 200 mL of LB with antibiotics. At an OD of 0.3-0.8, IPTG (Isopropyl β-D-1-thiogalactopyranoside) was added to a final concentration of 0.5 mM (Donovan, N., and Glick 1996). A negative control was also present without any IPTG. After 16 hours in the shaker at 18 °C at 150 rpm, cultures were centrifuged at 12,300 rcf at 4 °C for 10 minutes. The supernatant was discarded and resuspended in a total of 25 mL of binding buffer (1 mM EDTA at pH 8, 150 mM NaCl, 10% glycerol, and 25 mM Tris-HCl at pH 7.5). Each sample was then sonicated for 14 seconds on and 35 seconds off at 41 A for 8 minutes after the addition of 250 µl of phenylmethylsulfonyl fluoride (PMSF, MilliporeSigma), a serine protease inhibitor, and 2 µL of protease inhibitor cocktail (Lively and Powers 1978). The samples were then centrifuged at 24,100 rcf for 30 minutes at 4 °C.

### 2.6.8. Protein quantification

Protein concentration was determined using the DC Protein Assay (Bio-Rad Laboratories, Inc., ON, Canada). Quantification was performed by measuring absorbance and calculating protein concentration from a standard curve generated using known concentrations of bovine serum albumin (BSA). In each well, 25 µl of reagent A and 5 µl of either the standards or the 1/10-1/20 diluted protein samples were added. After adding 200 µl of reagent B, the plate was covered with foil and incubated at room temperature for 30 minutes. The $OD_{750}$ was measured using a Synergy H1 Biotek plate reader (VT, USA), and the concentration was calculated using the concentration curve of the BSA samples in Microsoft Excel with the formula $x = \frac{y-b}{a}$. The final concentration was then calculated by multiplying the result by the dilution factor.

### 2.6.9. SDS-PAGE

Considering the predicted molecular weight of the tagged recombinant protein (~100 kDa), an 8% sodium dodecyl sulfate (SDS)–polyacrylamide gel was prepared. Each sample had 50 µg of protein in a final volume of 30 µl, to which 7.5 µl of Laemmli 4x buffer (Bio-Rad Laboratories, Inc.) was added. Electrophoresis was first conducted at 80 V until the samples exited the stacking gel; thereafter, the voltage was increased to 120 V and maintained for two hours. Protein bands were visualized using Coomassie Blue staining. Following staining, excess dye was removed by incubating the gel in water overnight prior to imaging.

### 2.6.10. Protein purification and desalination

Following cell lysis by sonication, the lysates were clarified twice at 4 °C to remove cell debris, and the soluble fraction was gently mixed with amylose resin beads (NEB). The target proteins were retained on the column matrix, while non-binding proteins were washed away with column buffer. Bound MBP–*Np*TyDC1 and MBP–*Np*TyDC2 were then released using 10 mM maltose,

and the flow-through, wash, and elution fractions were examined by SDS-PAGE to confirm the expected ~100 kDa bands. For the enzymatic assay, the maltose-containing eluates were desalted and exchanged into 150 mM Tris-HCl (pH 8.0) using MilliporeSigma Amicon Ultra centrifugal filter tubes. Several rounds of dilution and reconcentration ensured efficient removal of small molecules and salts. The final protein preparations were quantified by BSA assay as described earlier, divided into aliquots, flash-frozen in liquid nitrogen, and stored at −80 °C until further use.

### 2.6.11. Enzymatic assays

Enzymatic assays were performed in 100 µL reaction volumes containing purified recombinant protein, substrate, PLP, and Tris–HCl buffer (pH 8.0). For each assay, two negative controls were included, one lacking enzyme and one lacking substrate. Experiments were performed in triplicate and analyzed using high-performance liquid chromatography (HPLC) coupled with tandem mass spectrometry (MS/MS). Substrate specificity of *Np*TyDC1 and *Np*TyDC2 was first analyzed to identify products formed from individual aromatic amino acids. Optimization experiments were conducted only for *Np*TyDC1, as this isoform was selected for further characterization based on the outcome of substrate specificity assays. Enzymatic assays were optimized in a stepwise manner. A common set of baseline conditions was used at the start, and each experimental parameter was then examined individually. After each experiment, the conditions identified as optimal were carried forward and used as fixed settings for the next assay. At each step, only the parameter being studied was changed. Reaction duration was set to 80 minutes, and the enzyme amount was 30 ng per 100 µL reaction in the final experiment assessing substrate concentration. Before the optimization, a substrate specificity assay was performed using L-tyrosine, L-phenylalanine, L-tryptophan, and L-DOPA as individual substrates. The reaction temperature was varied at five levels in triplicate. Purified *Np*TyDC1 was tested beginning at 120 ng per 100 µL

reaction, followed by serial dilutions down to 0.234 ng. L-tyrosine concentrations ranged from 0.046 mM to 0.15 mM in triplicate. The reaction duration was optimized by repeating the enzymatic assay under identical conditions and stopping each reaction at specified time points, ranging from 10 to 720 minutes.

Statistical analyses were performed using R 4.4.1. The effects of temperature, enzyme concentration, reaction time, and substrate concentration on tyramine formation were then examined in sequence. Dilution factors were incorporated, and the molecular weight of each molecule was used to convert concentrations from ng/mL to μM across all analyses. Statistical significance was assessed using either three-way or one-way ANOVA, followed by Tukey's test. Trends in tyramine production were analyzed using local weighted smoothing (loess) fit to identify optimal ranges, linear response regions, and saturation behaviour.

Initial velocities were calculated from tyramine formation over the 80-minute incubation. Results were summarized using the *get* package version 1.0.0 (Iannone et al. 2025), and dose–response relationships were visualized by plotting tyramine formation against tyrosine concentration. We integrated the time course and substrate range data to determine Michaelis–Menten parameters. For the time-course, we focused on the 0-40-minute window, added a t = 0 point with zero product for each replicate, and fit linear regressions of tyramine concentration versus time to obtain $v_0$ values. We combined these points with the $v_0$ values from the substrate series and fit the Michaelis–Menten equation by nonlinear regression, estimating $V_{max}$ and $K_m$ for both the substrate-only and combined datasets. We calculated *kcat* by converting $V_{max}$ to micromolar per second and normalizing them by enzyme concentration.

### 2.6.12 HPLC-MS/MS analysis

An HPLC-MS/MS system equipped with an Agilent Jet Stream ionization source, a binary pump, an autosampler, and a column compartment (Agilent Technologies, Santa Clara, California, USA) was used for the analysis. Compound separation was achieved using a Kinetex EVO C18 column (150 × 4.6 mm, 5 μm, 100 Å; Phenomenex, Torrance, USA). Five microliters of each sample were injected onto the column that was set at 30 °C. A gradient method made of (A) formic acid 0.1% v/v in milli-Q water and (B) formic acid 0.1% v/v in methanol with a flow rate of 0.4 mL/min was used to achieve chromatographic separation. The HPLC elution program is described as follows: 0 min, 10% B; 10.0 min, 10% B; 20.0 min, 100% B; 25.0 min, 100% B; 26.0 min, 10% B. The total run time was 30 min per sample to allow the reconditioning of the column prior to the next injection. The parameters used in the MS/MS source were set as follows: gas flow rate 10 $L \cdot min^{-1}$, gas temperature 300°C, nebulizer 45 psi, sheath gas flow 11 $L \cdot min^{-1}$, sheath gas temperature 300°C, capillary voltage 4000 V in ESI+ and 3500 V in ESI- and nozzle voltage 500 V. Agilent MassHunter Data Acquisition (version 1.2) software was used to control the HPLC-MS/MS. MassHunter Qualitative Analysis (version 10.0) and MassHunter Quantitative QQQ Analysis (version 10.0) software were used for data processing. Compound identifications were made using authentic reference standards in MRM mode for kinetic study and enzyme assay optimization or by using Single Ion Monitoring (SIM) mode and Product Ion (PI) mode to generate collision-induced dissociation (CID) mass spectra for substrate specificity assays. MRM transitions and instrument parameters used for identifications in kinetic study and enzyme assays optimization (*i.e.,* temperature, substrate concentration, time, and enzyme concentration) experiments are included in Table S4. Instrument parameters used in SIM and in PI modes to obtain the full CID mass spectrum of signals detected are presented in Table S5 and Table S6, respectively. Standard calibration curves were prepared as follows: Two working solutions were prepared containing L-

tyrosine (L-TYR) and tyramine (TYR) at 10 mg/L in mobile phase solution (*i.e.,* milli-Q water and methanol (90:10), both containing 0.1% formic acid). These solutions were further diluted to prepare calibration solutions with the following concentrations in triplicate: 0, 12.5, 25, 50, 100, 200, 1000, and 5000 ng/mL. Internal standard papaverine was added at a constant concentration of 1000 ng/mL in each calibration solution. These standard solutions were injected into the HPLC-MS/MS system and used to generate calibration curve regressions. Figure S1 and Figure S2 show the calibration curves obtained by plotting the area ratio (*i.e.,* analyte's peak area divided by internal standard's peak area) obtained as a function of the analyte's concentration, which allowed L-TYR and TYR quantification for all enzymatic assays. Following analysis, reported values represent HPLC-DAD peak area ratios normalized to the internal standard papaverine. Because substrates like tyramine and phenylethylamine have different UV absorption coefficients, their detector response factors relative to the internal standard differ; consequently, area ratios cannot be compared across different products within the same enzyme.

## 2.7. Conclusion

This study defines the biochemical properties of tyrosine decarboxylase isoforms from *Narcissus pseudonarcissus* 'King Alfred', a genus renowned for producing pharmacologically important Amaryllidaceae alkaloids. *Np*TyDC1 functions as a gatekeeping enzyme that converts L-tyrosine to tyramine and exhibits constrained catalytic turnover, consistent with regulatory control at the entry point of alkaloid biosynthesis rather than sustained high metabolic flux.

The phylogenetic separation of *Np*TyDC1 and *Np*TyDC2 is mirrored by their distinct biochemical behaviours. *Np*TyDC1 displays strong specificity for L-tyrosine in enzymatic assays, whereas *Np*TyDC2 lacks detectable tyrosine decarboxylase activity under the same conditions, providing functional evidence that these isoforms have diverged rather than retained redundant roles.

Together, these findings suggest that *Np*TyDC1 is a biochemically defined gatekeeper of Amaryllidaceae alkaloid biosynthesis, among the characterized isoforms, and provide a framework for understanding the functional diversification of aromatic amino acid decarboxylases in this family. Full-length sequencing and functional characterization of the remaining partial TyDC-like transcripts will be necessary to fully delineate the enzymatic network directing carbon flux into Amaryllidaceae alkaloid biosynthesis in *N. pseudonarcissus*.

## 2.8. Funding

This research was financially supported by the Canada Research Chair on plant specialized metabolism Award No CRC-2023-00353 to I.D-P. Thanks are extended to the Canadian taxpayers and to the Canadian government for supporting the Canada Research Chairs Program.

## 2.9. Acknowledgement

We thank all members of our research team, as well as Professor Hugo Germain and his team, for insightful discussions and for their scientific, technical, and collegial support.

## 2.10. Authors Contribution

Arghavan Arjmandi: Conceptualization, Data Curation, Formal analysis, Investigation, Validation, Visualization, Writing - Original Draft, Writing - Review & Editing. Bharat Bhusan Majhi: Conceptualization, Formal analysis, Investigation, Methodology, Resources, Writing - Review & Editing. Natacha Mérindol: Conceptualization, Project administration, Resources, Visualization, Validation, Writing - Review & Editing. Sarah-Eve Gélinas: Investigation, Methodology,

Validation, Writing - Review & Editing. Karen Cristine Goncalves dos Santos: Data Curation, Formal analysis, Software, Visualization, Writing - Review & Editing. Isabella Burgos-Holguin: Investigation, Methodology, Writing - Review & Editing. Yasmin Moreto Guaitolini: Investigation, Methodology, Writing - Review & Editing. Patrick Lagüe: Resources, Software, Writing - Review & Editing. Isabel Desgagné-Penix: Conceptualization, Funding acquisition, Project administration, Resources, Supervision, Validation, Visualization, Writing - Review & Editing.

## 2.11. Declaration of Interest

The authors declare that there is no situation real, potential, or apparent conflict of interest.

# Chapter 3

**Preface**

This chapter presents the evaluation of *Chlamydomonas reinhardtii* as a platform for tyramine biosynthesis through the heterologous expression of *NpTyDC1*. This article addresses the second hypothesis of this thesis: that *C. reinhardtii* does not possess a functional endogenous TyDC and therefore provides a metabolically suitable host for the heterologous expression of *NpTyDC1*. The AAAD-like protein encoded in the *C. reinhardtii* genome was researched through bioinformatic, conserved-domain, and phylogenetic analyses to determine whether it functions as a tyrosine decarboxylase. The growth response of *C. reinhardtii* strains to L-tyrosine and tyramine supplementation was measured. Substrate availability was assessed by endogenous metabolite screening and supplementation-uptake assays and pathway compatibility. A codon-optimized *NpTyDC1* expression construct was assembled in the pSL18 backbone with the *PsaD* promoter and terminator and an *mVenus* reporter and was introduced into *C. reinhardtii* by glass-bead and electroporation methods. Transformants were screened by colony imaging, quantitative 96-well fluorescence assays, and flow cytometry. The results show that the AAAD-like protein in *C. reinhardtii* is not a functional tyrosine decarboxylase, and no tyramine or alkaloid intermediates were detected in wild-type cultures. Externally supplied L-tyrosine was taken up by the cells. Nuclear transformation of *NpTyDC1* produced colonies with detectable mVenus fluorescence on solid medium, but no stable fluorescent population was recovered in liquid culture.

The research presented in this chapter was carried out by the candidate under the supervision of Isabel Desgagné-Penix. The candidate performed the bioinformatic, conserved-domain, and

phylogenetic analyses; the culture and growth work; the toxicity, endogenous metabolite, time-course, and permeability assays; the assembly of the codon-optimized *Np*TyDC1 expression construct in the pSL18 backbone, including Gibson assembly, amplification in *E. coli*, and validation; and the nuclear transformation of *C. reinhardtii* and subsequent screening by colony imaging, quantitative 96-well fluorescence assays, and flow cytometry. Data analysis, statistical analysis, and figure preparation were also carried out by the candidate, with Karen Cristine Goncalves dos Santos providing training in R and support in troubleshooting the analyses. HPLC analysis was performed by Sarah-Eve Gélinas. The manuscript was drafted by the candidate and revised by Natacha Mérindol, Karen Cristine Goncalves dos Santos, and Isabel Desgagné-Penix.

# Evaluation of *Chlamydomonas reinhardtii* as a Platform for Tyramine Biosynthesis

Arghavan Arjmandi[1,2], Natacha Mérindol[1,2], Sarah-Eve Gélinas[1,2], Karen Cristine Gonçalves dos Santos[1,2], Fatma Meddeb-Mouelhi[1,2], and Isabel Desgagné-Penix[1,2,*]

[1]Department of Chemistry, Biochemistry, and Physics, Université du Québec à Trois-Rivières, Trois-Rivières, QC, Canada.

[2]Plant Biology Research Group, Trois-Rivières, Québec, Canada.

*****Correspondence: Isabel.Desgagne-Penix@uqtr.ca; Tel.: 1-819-376-5011

## 3.1. Highlights

- A single AAAD-like enzyme was identified in *C. reinhardtii,* but it lacks support for tyrosine decarboxylase (TyDC) specificity.
- Phylogenetic analysis places the algal enzyme closer to HPAAS (4-hydroxyphenylacetaldehyde synthase) than to Amaryllidaceae TyDCs.
- No endogenous tyramine or alkaloid intermediates were detected in algal extracts.
- Supplemented tyrosine is efficiently taken up and retained intracellularly.
- Nuclear TyDC transformation produced colony-level fluorescence but no stable liquid-culture expression.

## 3.2. Keywords

Tyrosine decarboxylase, heterologous expression, nuclear transgene silencing, microalgal biotechnology, *Narcissus pseudonarcissus*.

## 3.3. Abstract

In this study, we investigated whether *Chlamydomonas reinhardtii* can serve as a chassis to express a plant tyrosine decarboxylase and convert endogenous or supplemented L-tyrosine into tyramine. Tyramine is a key precursor of pharmacologically important plant alkaloids, including the Amaryllidaceae alkaloids that yield the Alzheimer's drug galanthamine. In plants, tyramine is produced from L-tyrosine by tyrosine decarboxylase (TyDC). We assessed the alga's growth capacity in media supplemented with either tyrosine or tyramine. While L-tyrosine supplementation did not alter the growth of *C. reinhardtii*, tyramine was tolerated at lower concentrations, but growth inhibition was observed at higher levels (16–32 mM). We analyzed a *C. reinhardtii* gene *in silico* annotated as TyDC, showing that *C. reinhardtii*'s putative TyDC had Gly335 at the substrate selectivity position instead of the serine found in decarboxylases that use L-tyrosine as a substrate. The candidate included a residue linked to HPAAS-type aldehyde synthase activity. In the absence of an endogenous functional TyDC, we transformed *C. reinhardtii* with mVenus-tagged *Np*TyDC. Colony imaging after transformation on solid media suggested mVenus fluorescence; however, quantitative 96-well assays and flow cytometry did not detect a stable fluorescent population in liquid culture. Growth kinetics remained largely unchanged under these conditions. In conclusion, the microalgae show no detectable endogenous activity for tyrosine decarboxylation. The cells can take up and accept the substrate (L-tyrosine). The substrate is not toxic until it reaches its solubility limit in the culture medium. Similarly, the algae tolerated low concentrations of the product tyramine. The introduced *Np*TyDC construct shows that heterologous expression is possible, but further optimization is needed to obtain consistent functional output. The main barrier to establishing tyramine biosynthesis in this host is the instability of nuclear transgene expression (Schroda 2019). Future work should therefore focus on

improving transgene stability, for example by targeting expression to alternative compartments such as the chloroplast.

## 3.4. Introduction

### 3.4.1. Tyramine as a precursor of pharmacologically important plant alkaloids

Plants produce specialized metabolites of considerable pharmaceutical value, including alkaloids used to treat cancer, neurological disorders, and viral infections (Aniszewski 2007; Dey et al. 2019; Ka et al. 2021). However, direct extraction from plants is often limited by low yields, lengthy growth cycles, and the demands of large-scale cultivation, which has motivated the development of alternative production platforms (Desgagné-Penix 2021; Pyne, Narcross, and Martin 2019).

Tyramine is a central entry metabolite for some specialized metabolic pathways, including the Amaryllidaceae alkaloids (Facchini, Huber-Allanach, and Tari 2000; Singh 2018). TyDC catalyzes the decarboxylation of tyrosine to tyramine (Singh and Desgagné-Penix 2017). Reconstructing tyramine biosynthesis in a tractable host would provide a defined entry point into this pathway and a starting platform on which downstream alkaloid biosynthetic enzymes could subsequently be added (Pyne, Narcross, and Martin 2019; Diamond and Desgagné-Penix 2016).

An efficient platform for the synthesis of plant metabolites is therefore highly desirable. *C. reinhardtii* is an established model organism in biological research. This unicellular green alga is a eukaryote with a fully sequenced genome and developed genetic tools (Tran and Kaldenhoff 2020). *C. reinhardtii* is easy to culture, grows rapidly, and can be scaled under controlled conditions, which makes it a suitable host for reconstructing specialized metabolite pathways (Marshall 2024). It has already been used to produce a range of recombinant products through nuclear expression (Sproles et al. 2021). Early work by Lauersen et al. (2016) established phototrophic patchoulol production through nuclear expression of a *Pogostemon cablin* patchoulol synthase (Lauersen et al. 2016). The same group subsequently achieved 13R(+)-manoyl oxide by combining plant diterpene synthases with plastid targeting and MEP-pathway enhancement

(Lauersen et al. 2018). Wichmann et al. (2018) reported ~11 mg $L^{-1}$ of (E)-α-bisabolene using a plant-derived synthase under both mixotrophic and phototrophic regimes, while Einhaus et al. (2022) engineered scalable sclareol production from *Salvia sclarea* and markedly improved overall diterpene yields (Wichmann et al. 2018; Einhaus et al. 2022). Beyond terpenoids, phenylpropanoids have also been explored: Xiang et al. (2020) successfully introduced 4CL and STS to produce resveratrol, although yields remained lower than those obtained for terpenoids (Xiang et al. 2020).

We aimed to engineer *C. reinhardtii* to produce tyramine. To address this, we mined the microalgae transcriptome and used bioinformatic analysis to study the *C. reinhardtii* protein that was annotated as a TyDC in the PhycoCosm *C. reinhardtii* genome database (JGI) (Grigoriev et al. 2021). Growth and supplementation assays were also used to assess the microalgae as a suitable platform to produce tyramine. We also transformed *C. reinhardtii* to express *Np*TyDC1. *In silico* analysis of the protein in *C. reinhardtii* revealed the presence of a glycine at the active site, which suggests a substrate specificity different from other TyDCs, and no tyramine was detected in liquid cultures upon feeding tyrosine. Tyrosine was efficiently taken up and remained non-toxic up to its solubility limit, while tyramine showed toxicity only at very high concentrations; however, no measurable tyramine production was detected. Meanwhile, fluorescence of mVenus-*Np*TyDC in *C. reinhardtii* was detected in solid cultures but not in liquid ones.

## 3.5. Materials and methods

### 3.5.1. Bioinformatic Identification of AAAD-Like Proteins

To determine whether *C. reinhardtii* encodes a protein related to tyrosine decarboxylase, the term "TyDC" was searched against the *C. reinhardtii* CC-503 v5.6 predicted proteome available through PhycoCosm using the BLASTP algorithm (version 2.12.0+) with default settings (Grigoriev et al. 2021), except for the substitution matrix, which was set to BLOSUM62, and the expect threshold, set to $1^{e-4}$ (Henikoff and Henikoff 1992).

The protein with high similarity to both *N. pseudonarcissus* queries was selected for further characterization. The amino acid sequence of this candidate was retrieved and used as a query in a second BLASTP search against the NCBI non-redundant protein (NR) database (Sayers et al. 2025). In this search, the maximum number of target sequences was set to 500 and the expect threshold to $1^{e-4}$. Compositional adjustments were disabled, and low-complexity filtering was enabled. All other parameters were kept at default values.

The list of sequences was filtered using R (version 4.4.1) (R Core Team 2024). Partial and truncated sequences were removed, as were hypothetical or unnamed proteins lacking functional annotation. Redundant isoforms from the same organism were consolidated to retain a single representative per enzyme when appropriate. Multiple sequence alignment was performed using Clustal Omega (Sievers and Higgins 2018). The gap opening penalty was set to 10, and the gap extension penalty to 0.2. The negative matrix option was disabled, and a 30% identity cutoff was applied. The resulting alignment was inspected to confirm the correct positioning of conserved pyridoxal phosphate-dependent (PLP-dependent) enzyme motifs. For visualization of conserved residues, alignment figures were generated using ESPript 3.2 and coloured according to the BLOSUM62 matrix (Robert, Guillon, and Gouet 2025).

### 3.5.2. Conserve Domain and Phylogenetic Analysis

To confirm domain architecture, conserved domain analysis was performed using the NCBI Conserved Domain Database with default settings and expect threshold of $1^{e-4}$. The analysis focused on verifying the presence of the PLP-dependent decarboxylase domain and identifying the conserved lysine residue required for Schiff base formation. Phylogenetic reconstruction was conducted using both R and MEGA (version 11.0.13). The curated protein alignment was used to compute a maximum likelihood distance matrix under the JTT substitution model. A tree was inferred using the BIONJ algorithm, and node support was assessed by 999 bootstrap replicates. Final tree visualization and annotation were performed using the Interactive Tree of Life (iTOL) interface (Letunic and Bork 2024).

### 3.5.3. *C. reinhardtii* Culture Conditions

Experiments were performed using *C. reinhardtii* ultraviolet modified 4 (UVM4) and UVM11 strains initially (Neupert, Karcher, and Bock 2009), and then UVM4 was chosen for the transformation. Cultures were maintained in tris acetate phosphate (TAP) medium at 21 °C in flasks on a shaker or at 25 °C on agar plates. Both were under moderate white, fluorescent light at 50 μmol photons $m^{-2}$ $s^{-1}$ and 50% relative humidity (RH). All experiments were initiated from actively growing pre-cultures in the logarithmic phase, and the starting optical density (OD) for all experiments was 0.01 to ensure comparable physiological states. The OD was recorded at defined intervals and used as a proxy for biomass throughout growth, supplementation, and transformation workflows.

### 3.5.4. Toxicity Assays

Because the strategy was to introduce a TYDC pathway, the first step was to determine whether higher aromatic amino acid levels influence algal growth. For this, TAP medium was supplemented with L-tyrosine (0 to 2 mM) or tyramine (0 to 32 mM). Supplemented media were freshly prepared and sterilized by vacuum filtration using a 0.22 μm PES membrane filter unit (Corning) before inoculation. Cultures were initiated at equal starting densities and grown in parallel under identical conditions. OD was measured daily across the experimental time course, and each condition was analyzed in biological triplicates. Growth data were analyzed in R using ANOVA-based models, and Tukey's HSD was applied for post hoc comparisons when appropriate, with a p-value threshold of 0.05.

### 3.5.5. Endogenous Metabolite Production

After establishing growth tolerance to supplementation, endogenous metabolite production was evaluated. Targeted metabolite screening was conducted to determine whether *C. reinhardtii* produces tyramine or related alkaloid intermediates under standard growth conditions. First, the OD of each culture was measured. Next, the cultures were harvested by centrifugation at 4000 rpm for 10 min. The pellets were then extracted in ethanol. The extraction ratio was 1 mL of ethanol per 100 mg of wet biomass. The samples were incubated at −20 °C overnight. After that, the extracts were clarified by centrifugation at 4000 rpm for 10 min. The supernatants were then filtered and transferred to autosampler vials. Papaverine was included as an internal standard where indicated. Chromatographic analyses were performed using HPLC.

### 3.5.6. Metabolite Production Over a Course of Time

Because intracellular metabolite levels may vary with growth stage, tyrosine and tyramine concentrations were quantified across a defined time course. Cultures were sampled between days

3 and 9, and OD was recorded at each time point. A defined culture volume was harvested and processed using the same extraction workflow described above. Metabolite concentrations were determined using calibration curves when available. The relationship between intracellular metabolite levels and biomass was evaluated using linear regression models in R.

### 3.5.7. Permeability to Substrate

To determine whether externally supplied substrates could enter and persist within algal cells, supplementation-extraction assays were conducted to measure intracellular recovery of added metabolite. Cultures were supplemented at defined concentrations and sampled during exponential growth. The cells were washed with unsupplemented TAP media two times. Ethanol was used for the extraction. The extraction ratio was 1 mL of ethanol (95%) per 100 mg of wet biomass. Recovery percentages were calculated relative to supplemented controls, with blank subtraction and normalization to internal standards where applicable. All treatment and time effects were modelled in R, with ANOVA and Tukey tests to analyze the dataset.

### 3.5.8. Assembly of the Construct

Following confirmation that substrate uptake could be quantified reliably, nuclear expression constructs were generated to introduce a heterologous tyrosine decarboxylase into *C. reinhardtii*. A codon-optimized *Np*TyDC1 coding sequence, according to *C. reinhardtii* preferences, was synthesized for nuclear expression by Bio Basic Inc. The construct was assembled in a pSL18 backbone containing the Photosystem I reaction center subunit II (PsaD) promoter and terminator (Fischer and Rochaix 2001). Since intron presence can influence nuclear expression efficiency, two configurations were designed in parallel: an intron-free coding sequence and a version incorporating engineered introns at predefined positions (**Figure S1**). An mVenus fluorescent

reporter was included to enable screening of transformants, and paromomycin resistance was used for selection.

Assembly of the expression cassette was performed using a stage-by-stage Gibson strategy using the Gibson Assembly® Master Mix by New England Biolabs. Individual fragments were amplified with high-fidelity PrimeSTAR GXL DNA Polymerase and verified by agarose gel electrophoresis. When non-specific products were detected, gel extraction was performed using the NEB Monarch DNA Gel Extraction Kit. Otherwise, PCR products were purified using a Geneaid PCR purification kit according to the manufacturer's instructions. DNA concentrations were measured prior to assembly. Intermediate assemblies were screened by PCR and gel electrophoresis to confirm fragment integrity before proceeding to final plasmid construction.

The completed plasmids were introduced into chemically competent *E. coli* DH5α for amplification. Colonies were plated on Luria–Bertani (LB) agar supplemented with 100 µg/mL ampicillin for selection. Colony PCR was performed using primers specific to the insert. Positive colonies were isolated and validated by restriction digestion using enzyme combinations selected based on predicted cut sites. Sequence integrity was confirmed by whole plasmid sequencing or next-generation sequencing prior to algal transformation.

### 3.5.9. Transformation

For nuclear transformation of *C. reinhardtii*, 500 ng and 1000 ng of purified plasmid DNA were prepared for the electroporation and glass bead methods, respectively. Cultures were grown to an OD of 0.1 before DNA introduction. Cells were allowed to recover overnight and were then plated onto TAP agar supplemented with paromomycin. After 7 days, the plates were taken for imaging using the Azure Sapphire™ Biomolecular Imager (Azure Biosystems). Transformant colonies were screened using the Azure Sapphire™ Biomolecular Imager (Azure Biosystems). Chloroplast

fluorescence was recorded using a 658 nm excitation and 710 nm detection setting to confirm algal identity. Reporter fluorescence (mVenus) was detected using 488 nm excitation and 518 nm emission settings. Imaging was performed across successive generations under antibiotic selection (paromomycin 10 mg/L), with exposure parameters maintained consistently within each experiment. Colonies were streaked through successive rounds of selections each week to promote stable integration events. The image was then prepared for publication using QuPath-0.5.1 console (Bankhead et al. 2017). Each detected fluorescence was assigned to a different channel. Chloroplast was assigned to the green channel, and mVenus was assigned to the red channel. When both channels were active, a mix of both colours would be shown in yellow.

To obtain quantitative population-level data, transformants and control strains were cultivated in 96-well plates for parallel measurement of OD and fluorescence. Chlorophyll fluorescence was recorded using a 430 nm excitation and 645 nm emission setting, and reporter fluorescence was recorded using a 500 nm excitation and 540 nm emission setting. An empty vector and another control with only mVenus were included. Blank corrected relative fluorescence unit (RFU) values were exported to Excel and processed in R for normalization and statistical analysis.

Finally, single-cell fluorescence distributions were assessed by flow cytometry to distinguish reporter signal from background autofluorescence. Liquid cultures were analyzed using forward scatter (FSC), side scatter (SSC), mVenus fluorescence (excitation 488 nm, emission 530/30 nm), and chlorophyll autofluorescence (excitation 488 nm, emission 695/40 nm) channels. Gating thresholds were defined using an empty vector and mVenus-only controls. Fluorescence distributions were compared across strains at sampling days 5 and 14 using the Floreada web-based cytometry analysis platform (Mladenovic et al. 2025).

## 3.6. Results

### 3.6.1. The only AAAD-like protein from *C. reinhardtii* is likely not a tyrosine decarboxylase

We searched for a tyrosine decarboxylase in the *Chlamydomonas reinhardtii* CC-503 protein database (**Table S1**). One protein, Cre01.g028423, was a hit, which was annotated as a tyrosine decarboxylase when Cre01.g028423 was used as bait for BLASTP against the NR database, *Np*TyDC2 was included in the hit list, but not *Np*TyDC1. We then searched for conserved domains in the protein identified, revealing a complete aromatic amino acid transferase superfamily domain, with folding type I (AAT_I, **Figure S2**). As a result, we will refer to this protein as *C. reinhardtii* amino acid transferase or *Cr*AAT. The reason this enzyme is presented as an AAT instead of the original TyDC annotation is that the multiple sequence alignment (MSA) showed that there are two other active residues present in *Cr*AAT (**Figure 16**). One is the serine versus glycine at the 335 amino acid position in *Cr*AAT that has been associated with indolic rather than phenolic substrate preferences in plant aromatic amino acid decarboxylases, respectively (Torrens-Spence et al. 2014; Torrens-Spence et al. 2020b). In addition, a second relevant residue, which was first described in parsley, 4-hydroxyphenylacetaldehyde synthase (HPAAS), a bifunctional aromatic aldehyde synthase that catalyzes decarboxylation followed by oxidative deamination (Torrens-Spence et al. 2013). The corresponding residue associated with aldehyde synthase activity is also present in *Cr*AAT Phe317, suggesting structural compatibility with alternative catalytic outcomes beyond strict decarboxylation.

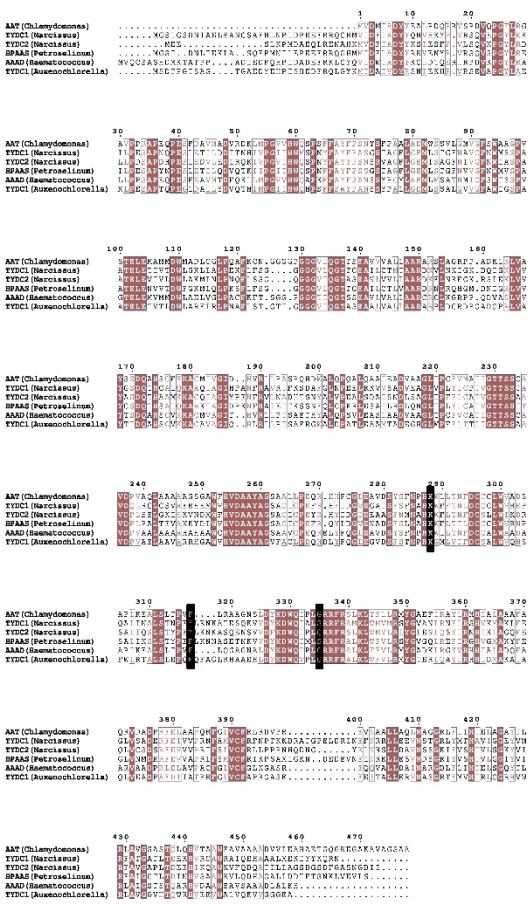


**Figure 16. Multiple sequence alignment by Clustal Omega shows conserved PLP-dependent catalytic residues, while active-site features suggest a preference for indolic substrates and possible alternative catalytic activity.** Coloured according to the BLOSUM62 matrix. The proteins are *Cr*AAT (TyDC) (Accession: XP_042928513), *Np*TyDC1 (Accession: AUG71933) and *Np*TyDC2 (Accession: AUG71932), HPAAS from parsley (Accession: AAA33860), and two other algae proteins with the highest percentage identity with the *C. reinhardtii* unknown protein (Accessions: KAL6764535 and XP_011401077). The active residues are highlighted in black.

We constructed a phylogenetic tree using BLASTP results obtained by querying the unknown *C. reinhardtii* protein against the NR database (**Figure 17**). Multiple plant and algal AAAD sequences were retrieved as hits. The *C. reinhardtii* amino acid decarboxylase clustered within an algal cluster together with sequences from *Haematococcus lacustris, Auxenochlorella protothecoides, Coccomyxa subellipsoidea,* and other red and green algae. *Np*TyDC2 formed a separate plant cluster distinct from the *C. reinhardtii* sequence. Although both the *C. reinhardtii* protein and *Np*TyDC2 share the glycine residue associated with indolic substrate preference, they did not group together phylogenetically. The shared glycine residue between the *C. reinhardtii* decarboxylase and *Np*TyDC2 appears to reflect convergent conservation rather than shared ancestry, as their distinct phylogenetic positions suggest independent evolutionary origins despite similar active site features.

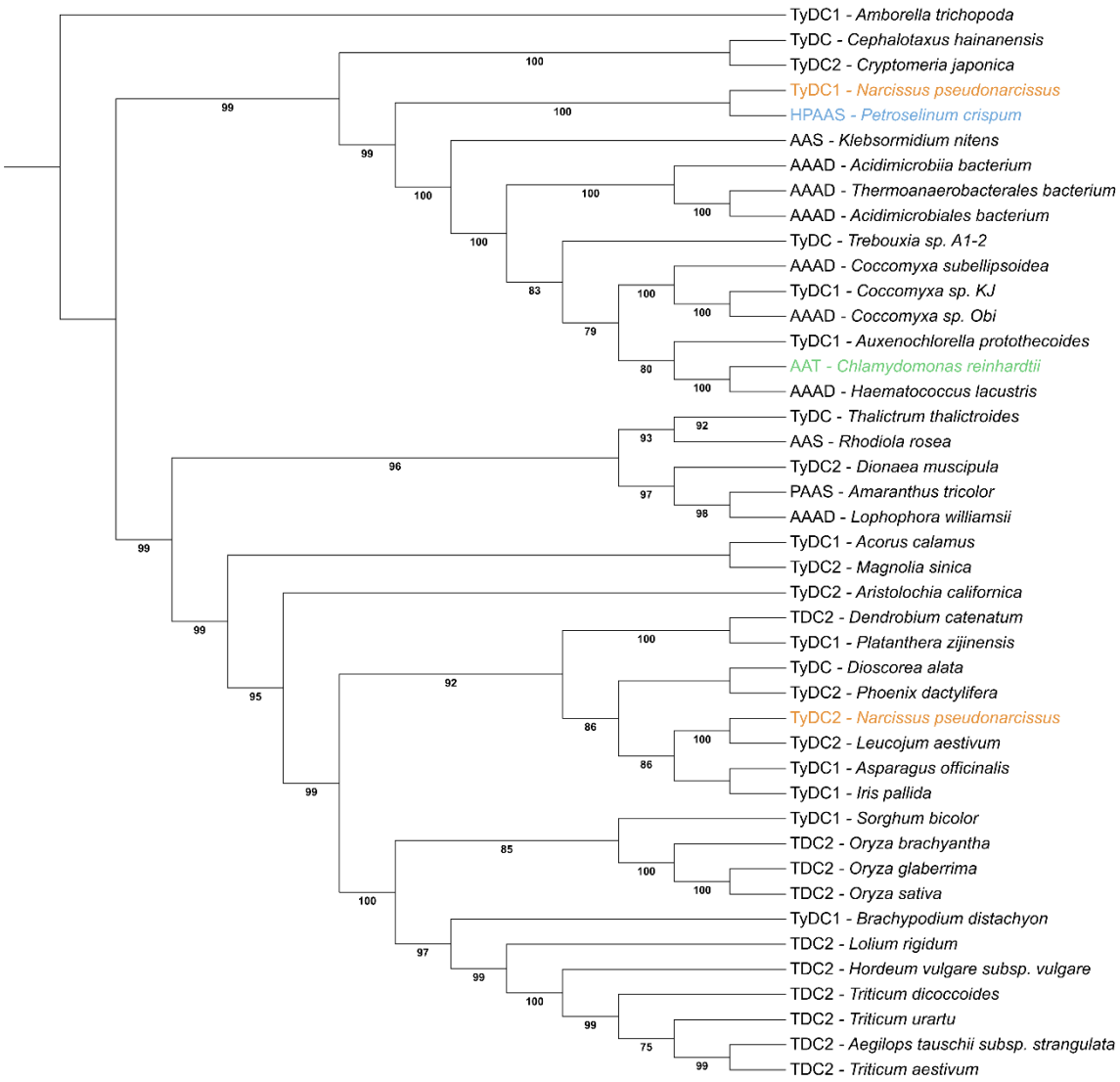
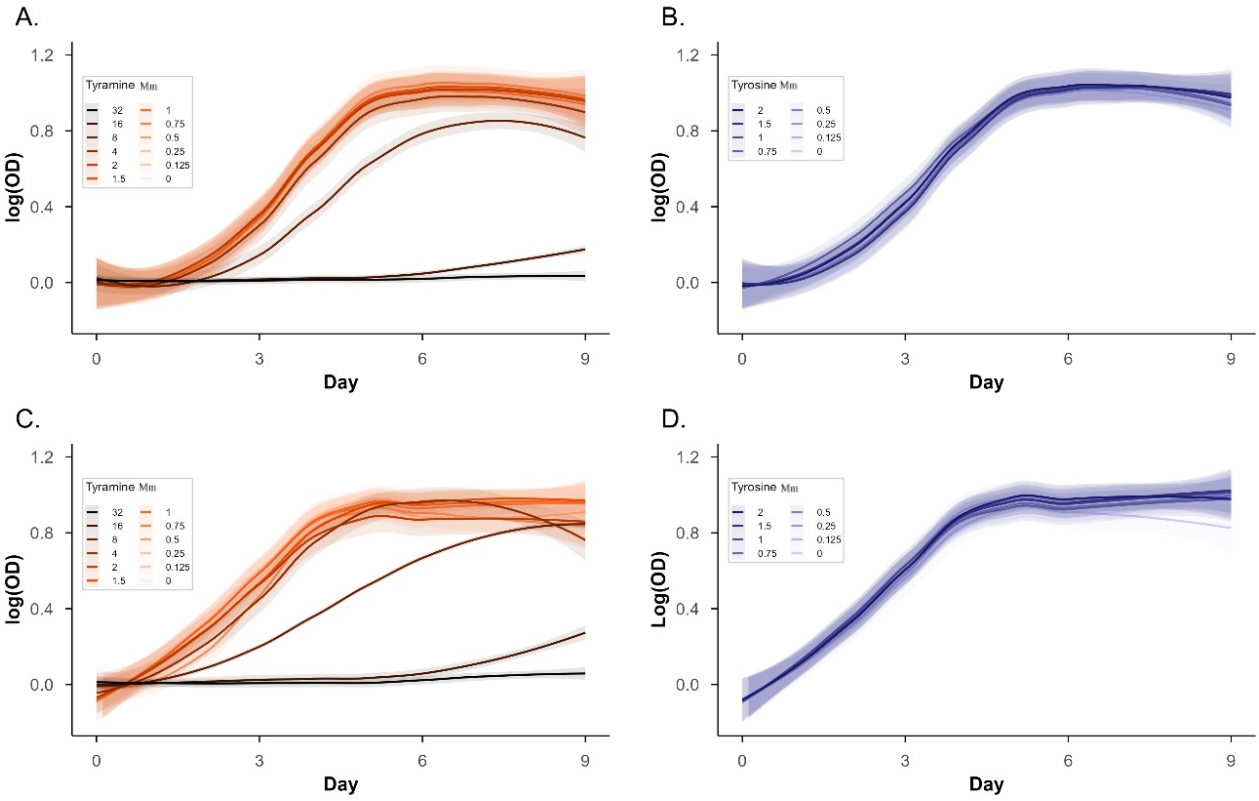



**Figure 17. *C. reinhardtii*'s AAT clusters with algal homologs and is positioned closer to parsley HPAAS than to *Np*TyDC2.** Accession numbers can be found in **Table S1**. The protein from *C. reinhardtii* is shown in green, the *N. pseudonarcissus* proteins are in orange, and blue indicates the HPAAS from parsley. *Amborella*, the most basal extant angiosperm, was used as the outgroup in the phylogenetic reconstruction (James W. Byng 2016). The BIONJ method was used from a maximum-likelihood distance matrix under the JTT model. Node support was assessed using 999 bootstrap replicates.

## 3.6.2. Tyramine and tyrosine supplementation do not affect the growth of *C. reinhardtii* UVM strains

*C. reinhardtii* UVM4 and UVM11 cultures were grown in TAP medium supplemented with 0 to 2 mM tyramine or 0 to 32 mM tyrosine, and OD was recorded daily for 9 days (**Figure 18**). No significant differences were observed between the growth trajectories of both UVM4 and UVM11

cultures across all concentrations of L-tyrosine ($p > 0.05$), indicating that this amino acid does not have an effect on the growth of these strains in the tested concentrations. It was not possible to test higher concentrations of tyrosine without adding more HCl solvent to the media, which proved lethal to the algae. Under tyramine supplementation, low concentrations of this metabolite did not significantly impact the growth of either strain; however, both UVM4 and UVM11 cultures displayed limited to no growth at 16 mM and 32 mM ($p < 0.05$, **Table S2, and S3**). Rather than any intrinsic cellular toxicity, the solubility of L-tyrosine in aqueous media seems to be the practical upper limit for supplementation in *C. reinhardtii* experiments.




To test whether higher cell density leads to more intracellular tyrosine and possible tyramine production by the putative AAAD-like enzyme and also to check if *C. reinhardtii* is a good chassis for tyramine production. We measured tyrosine and tyramine over time alongside OD. Intracellular tyrosine and tyramine were sent for HPLC to be detected during a growth time course by extracting

*C. reinhardtii* cells from day 3 to day 9 while measuring OD daily (**Figure 5A**), which allowed us to determine whether tyrosine production follows cell growth or occurs independently. Tyrosine was not detected on day 3 but became detectable from day 4 onward. Intracellular concentration increased with culture growth and declined toward day 9. Tyramine was not detected at any time point. Linear regression analysis revealed a strong positive correlation between intracellular tyrosine concentration and OD, with a coefficient of determination ($R^2$) value of 0.93 (**Figure 5B**). The strong correlation between intracellular tyrosine and OD suggests that substrate availability for heterologous TyDC activity would scale predictably with biomass, supporting the use of *C. reinhardtii* as a host.

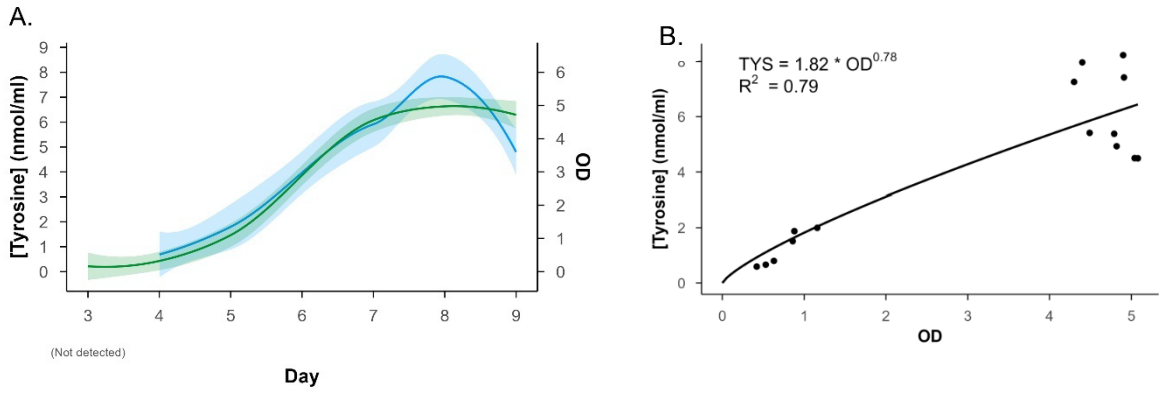



**Figure 19.** A. Growth time course of OD and intracellular tyrosine concentration in *C. reinhardtii* from day 3 to day 9. B. Linear regression analysis showing the relationship between intracellular tyrosine concentration and OD, with an $R^2$ value of 0.93.

## 3.6.4. Supplemented tyrosine is taken up and retained by *C. reinhardtii* cells

To test whether the cells are permeable to L-tyrosine in the medium, we supplemented tyrosine and then performed metabolite extraction. Intracellular tyrosine was measured after external supplementation by extracting *C. reinhardtii* cells during the exponential growth phase (**Figure 20**). Tyrosine was detected in cell pellets, with approximately 10% recovery at all sampled time points. Supplemented samples differed significantly from negative controls ($p \leq 0.0001$), whereas differences between sampling days were not significant ($p > 0.05$, **Table S4**). Recovery

percentages indicated stable intracellular retention rather than rapid depletion. Tyramine was not detected in the extracts and did not differ from negative controls ($p > 0.05$). The recovery of around 10 percent likely reflects the limited intracellular volume of *C. reinhardtii* relative to the large extracellular tyrosine pool, as two rounds of TAP washing removed surface-adsorbed metabolites and retained only internalized fractions. This suggests that tyrosine uptake is real but appears to be capacity-limited rather than concentration-driven.

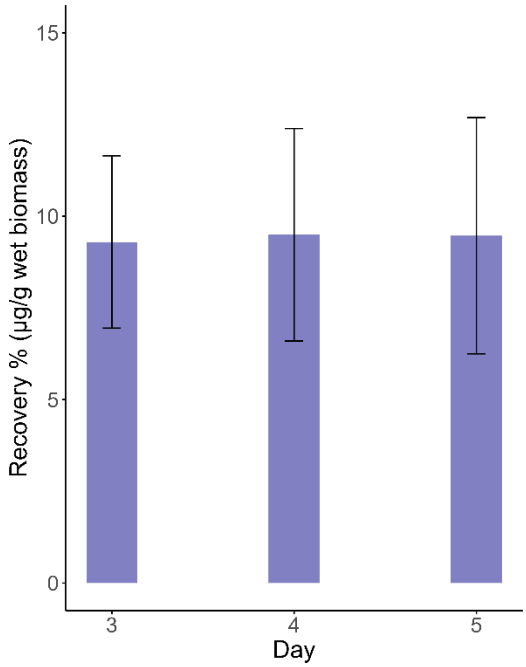



**Figure 20.** Intracellular tyrosine levels detected following supplementation during exponential growth.

**Gibson assembly and sequence validation of a stable TyDC construct for *C. reinhardtii* transformation**

Two codon-optimized TyDC constructs, with and without introns, from *N. pseudonarcissus* (*Np*TyDC1) were assembled for expression in *C. reinhardtii* using a stepwise Gibson strategy (**Figure S2**). All intermediate assemblies produced bands at the expected sizes (**Figure S2**), indicating correct fragment joining at each step. Independent assembly reactions produced

identical size profiles, and no additional bands suggestive of rearrangements were observed. Colony PCR identified multiple positive clones for both designs (**Figure S3**). Cloned assemblies were evaluated for sequence integrity prior to transformation (**Figure S4**). Sequence analysis revealed a point mutation in the backbone within the *aminoglycoside 3'-phosphotransferase type VIII* (*APHVIII*) gene, which is responsible for antibiotic resistance. This mutation was present in both constructs and consisted of a single base pair substitution that did not alter the reading frame. Because no frameshift or disruptive mutation was identified in *APHVIII*, the construct was retained for subsequent experiments. Furthermore, a deletion was detected in the intron-containing construct located within an exon of the TyDC coding sequence, resulting in a frameshift mutation that would disrupt protein function. As a result, this construct was excluded from further analysis. For the construct without introns, no mutations were detected in the coding region; however, an insertion was identified in the terminator sequence downstream of the stop codon, which does not affect the coding sequence or reading frame. As a result, the construct without introns was selected for further work because it showed no mutations in the coding region and only a minor change in the terminator sequence (**Figure S4**). The stepwise Gibson assembly strategy successfully yielded an intron-free *Np*TyDC1 construct ready for nuclear transformation of *C. reinhardtii*.

**Glass bead transformation yields higher viability but does not result in stable mVenus detection in *C. reinhardtii***

We compared transformation outcomes between electroporation and glass bead treatment by measuring colony recovery after transformation (**Figure 21**). Electroporation caused substantial cell damage and produced markedly fewer viable antibiotic-resistant colonies, resulting in a transformation efficiency of 26.7 CFU/µg, compared to a glass bead transformation efficiency of 128 CFU/µg. This corresponds to a 4.8-fold increase in transformation efficiency compared to

electroporation. In summary, glass bead transformation is a more cell-friendly method than electroporation for *C. reinhardtii*, yielding a 4.8-fold higher recovery of viable antibiotic-resistant colonies.

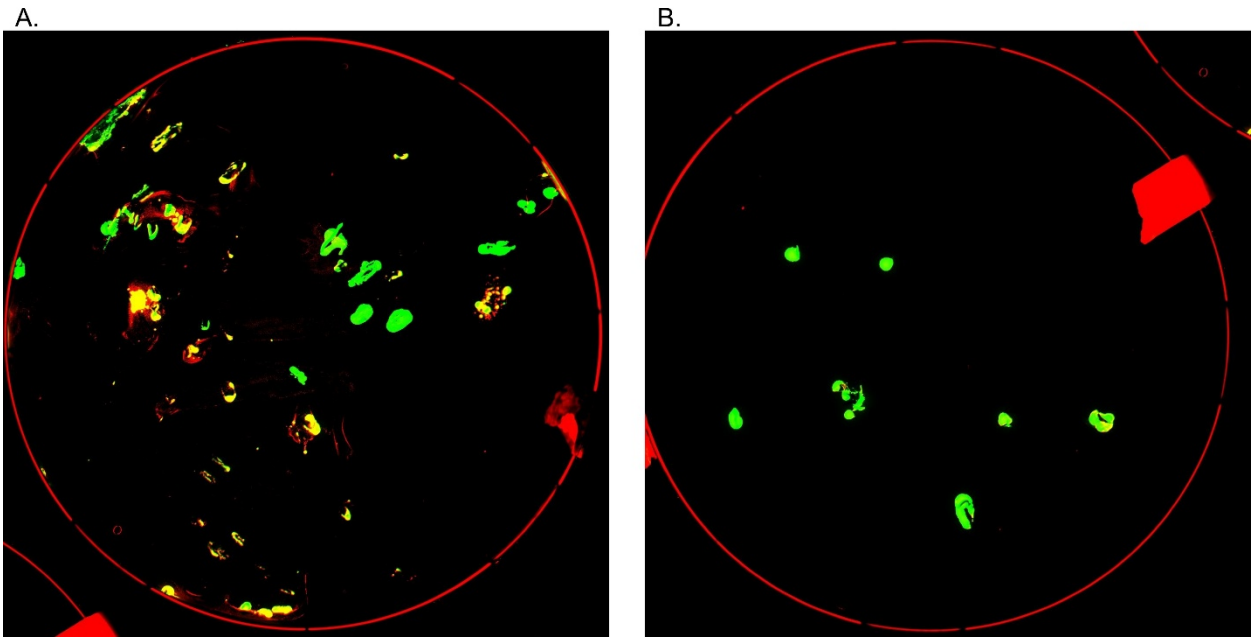



Figure 21. *C. reinhardtii* transformation by the glass bead method (A) and electroporation (B). Plates were imaged a week after transformation and selection. Chlorophyll autofluorescence (green) and mVenus reporter fluorescence (red) were overlaid; yellow indicates colocalization of both signals.

Colonies obtained after glass bead transformation were screened for chlorophyll and mVenus fluorescence using a colony imaging system (**Figure 22A-D**). Several colonies showed detectable mVenus fluorescence. Chlorophyll fluorescence was also detected in the colonies, confirming that the observed colonies consisted of viable algal cells. These signals were visible on solid medium during the initial screening phase. After rounds of subculturing and selection, colony imaging continued to show detectable fluorescence, although mVenus signal intensity appeared to decrease over time in some colonies starting at the second round of screening (three weeks after the transformation).

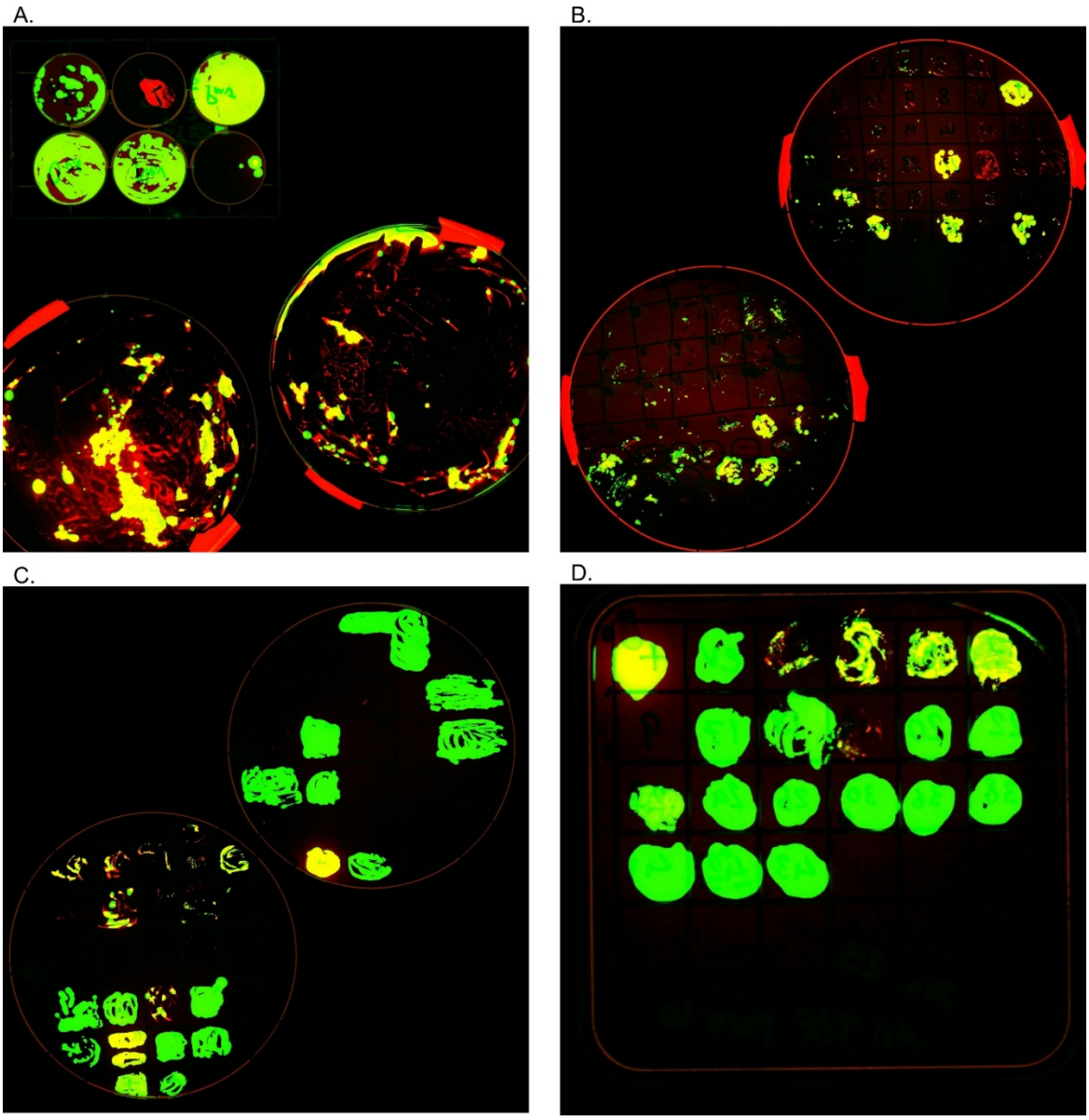



**Figure 22.** Colony fluorescence images of *C. reinhardtii* from a second transformation performed using only the glass bead method, showing mVenus signal (red) and chlorophyll autofluorescence (green) under colony imaging conditions. Yellow indicates overlap of both signals. **A.** Right after transformation, negative and positive controls are the two wells on top (solid media) **B.** Generation 1 **C.** Generation 2 **D.** Generation 3

Wanting to determine whether the observed reduction in fluorescence was due to an alteration in *C. reinhardtii* growth dynamics or to transgene silencing while growth remained unaffected, we performed quantitative fluorescence measurements in 96-well plates to assess chlorophyll RFU and mVenus RFU (

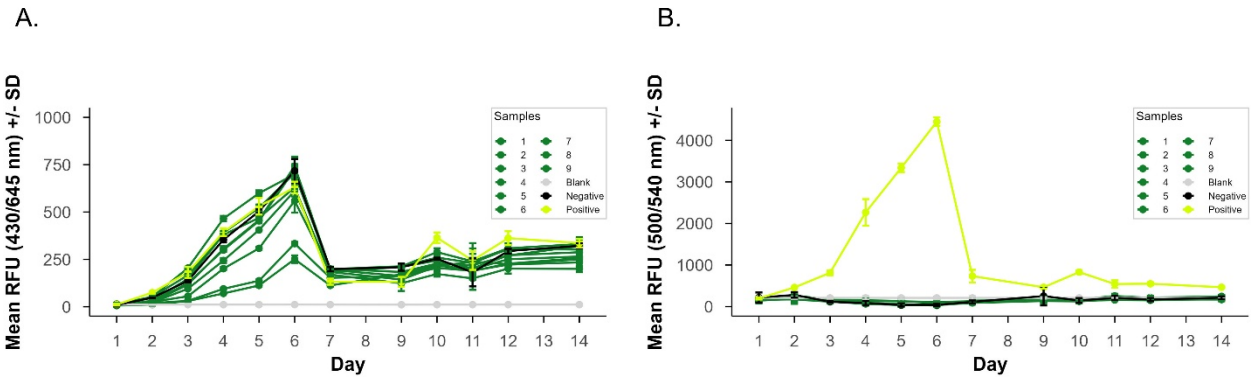



**Figure 23A,B**) after two rounds of screening and on week 3 after transformation. The growth curves were normal for all samples ($p > 0.05$) except for sample 6 ($p = 0.01$) when compared to the negative control **(Table S6)**. However, under these conditions in the liquid cultures, based on mVenus RFU, no mVenus signal could be detected ($p < 0.001$) when compared to the positive control expressing mVenus alone.

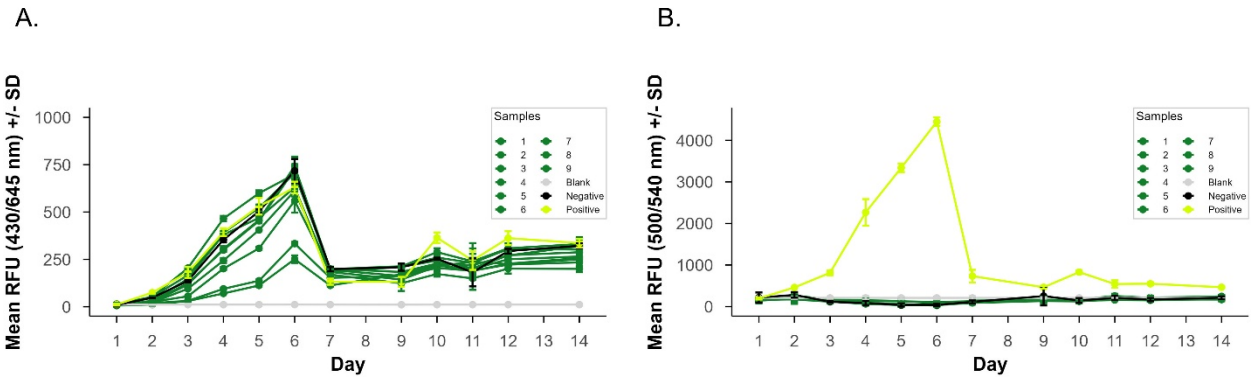



**Figure 23.** Quantitative 96-well fluorescence measurements displaying A. chlorophyll RFU and B. mVenus RFU across transformants and controls.

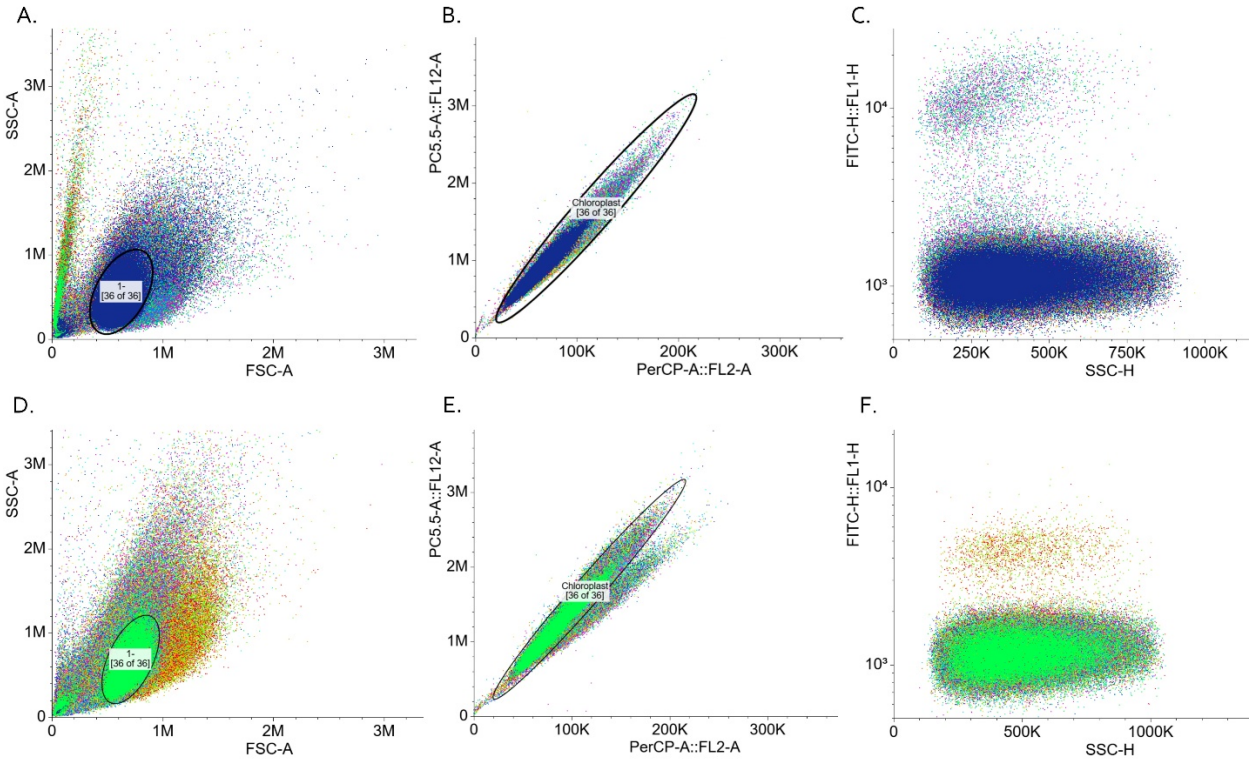



**Figure 24.** Flow cytometry plots across multiple channels on **day 5 (A, B, C) and day 14 (D, E, F)**, demonstrating the absence of a distinct mVenus-positive population in transformants and clear separation in the positive control.

Flow cytometry analysis across multiple fluorescence channels further confirmed that only the positive control population showed a distinct mVenus-positive signal for both day 5 **(Figure 24A-C)** and day 14 **(Figure 24D-F)**. Putative transformants overlapped with background autofluorescence and did not form a distinct fluorescent population. Normal growth dynamics combined with the absence of mVenus signal indicate that the construct is not cytotoxic to *C. reinhardtii*; however, our data do not allow us to identify the underlying cause of the lost signal. Possible explanations include nuclear transgene silencing, low expression below the detection threshold, and translational interference under selection.

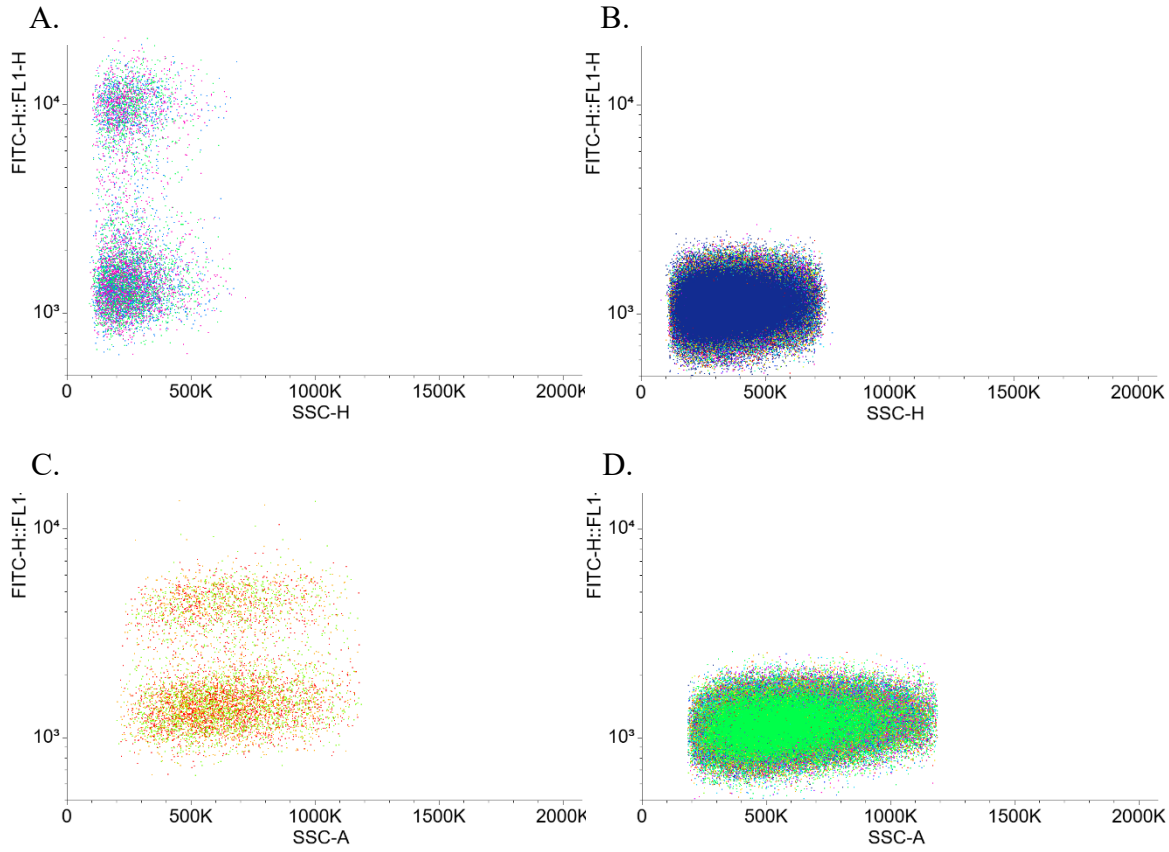



Figure 25. Flow cytometry analysis of mVenus fluorescence in *C. reinhardtii* transformants at Day 5 (top) and Day 14 (bottom). Positive controls (A and C) are shown alongside all other samples (B and D).

## 3.7. Discussion

To evaluate *C. reinhardtii* as a platform for tyramine production, we first assessed whether this organism maintains detectable endogenous tyrosine levels and can internalize exogenous L-tyrosine. L-tyrosine was detected in untreated cultures at low levels, and its concentration in the cell pellet of supplemented cultures differed significantly from that of untreated ones ($p < 0.05$). As a result, it can be concluded that L-tyrosine was taken up by the cells successfully. Furthermore, *in silico* analysis of the *C. reinhardtii* genome revealed a candidate gene annotated as TyDC, though its active site residues suggest it likely does not function as one, a conclusion supported by the absence of tyramine in wild-type cultures. These findings suggest that this alga represents a suitable metabolic entry point for the pathway, as it accepts the substrate required for tyramine formation but lacks the enzymatic capacity to convert L-tyrosine into this essential alkaloid precursor. Consequently, we introduced *Np*TyDC1 to supply this missing decarboxylation step.

BLASTP, conserved domain, and MSA analyses indicate that *C. reinhardtii* encodes an AAT_I family member. As a result, *in silico* data suggests that this sequence does not function as a TyDC. Although the catalytic lysine and PLP-binding architecture are conserved, overall sequence identity with *Np*TyDC1 is moderate, and the active residue necessary for the acceptance of phenolic compounds, like tyrosine, is absent. The presence of a glycine residue at the substrate-selectivity position aligns more closely with indole-preferring decarboxylases, similar to those found in *Papaver somniferum* and *Catharanthus roseus* (Torrens-Spence et al. 2014). The functional identity of a parsley AAAD was initially misassigned, as it was first annotated as a TyDC but later shown to function as a HPAAS, producing an aldehyde instead of tyramine (Torrens-Spence et al. 2012). The *C. reinhardtii* sequence contains the same amino acid at the position associated with this HPAAS-type activity, which suggests a similar functional shift away

from simple decarboxylation. The phylogenetic separation of the algal enzyme from plant TyDC clusters further supports the theory of this functional divergence. This enzyme clusters with other algal sequences. It is also close to parsley HPAAS, suggesting a broader role rather than a TyDC. Collectively, these features could mean that the *C. reinhardtii* protein is best interpreted as a general AAT-like enzyme rather than a dedicated decarboxylase.

This hypothesis is in line with the alkaloid screening results, in which no alkaloids were detected under the tested conditions. The extraction analyses conducted from days 3 to 9 also add up to this because tyramine was not detected in any of the samples analyzed at any time point, while L-tyrosine was detected throughout the time points 4 to 9. This indicates that substrate availability was probably not what was limiting, and the absence of detectable tyramine may reflect insufficient enzymatic conversion. However, in metabolic pathways, increased synthesis can be masked by simultaneous downstream flux, resulting in low steady-state levels despite active production (Matsuda et al. 2005). Consequently, the absence of detectable tyramine could also result from rapid turnover and downstream utilization that prevented its accumulation to measurable levels, although sequence-based evidence suggests this is less likely.

Cells usually contain enough intracellular tyrosine to support their normal metabolic needs, and in *C. reinhardtii*, tyrosine has been detected and shown to increase through de novo synthesis under changing conditions (Matthew et al. 2009). However, when an introduced enzyme uses this tyrosine, the cellular demand may increase, and competition with endogenous metabolism can limit precursor availability, as metabolic resources are shared between growth and product formation (Liu and Lu 2015). Therefore, it is important to determine whether tyrosine added to the growth medium can enter the cells and be used both for routine metabolism and as a substrate for the introduced enzyme. Our results demonstrate that externally supplied tyrosine is efficiently

transported into *C. reinhardtii* and remains intracellularly stable over time. This observation confirms that substrate accessibility across the cell wall and plasma membrane is not limiting under the tested conditions.

L-tyrosine supplementation does not affect the growth of *C. reinhardtii* UVM4 or UVM11 within the tested concentration range, showing that external L-tyrosine is neither beneficial nor harmful under standard TAP conditions. In marine microalgae, L-tyrosine used as the only nitrogen source leads to different outcomes depending on the species, even at similar concentrations (0.025–2.0 mM). It supports strong growth in the diatom *Navicula incerta*, where it can perform better than nitrate at higher levels, but it reduces growth or becomes toxic in *Isochrysis galbana* under similar conditions (Landymore and Antia 2008). These results show that the effect of external L-tyrosine depends on the species and growth conditions. Under nutrient-rich TAP medium, where inorganic nitrogen is already available, *C. reinhardtii* shows stable growth in the presence of L-tyrosine, indicating that supplementation does not create growth limitations in this freshwater green microalga. On the other hand, tyramine supplementation at 16 mM and 32 mM significantly reduced growth in both strains, while lower tyramine concentrations had no measurable effect. This suggests a threshold-dependent toxicity response of *C. reinhardtii* to tyramine, as was previously seen in *Corynebacterium glutamicum* (Poethe et al. 2024). However, in the transformation of eukaryotes, the highest aromatic amine titers reported in engineered eukaryotic hosts remain in the low millimolar range, with tyramine reaching 1.46 mM in *Saccharomyces cerevisiae* (Noda et al. 2015), serotonin reaching 1.31 mM in the same host (Planells-Carcel et al. 2025), and the tryptamine derivative psilocybin reaching 2.21 mM under fed-batch conditions (Milne et al. 2020). These values fall well below the toxicity threshold observed here for *C. reinhardtii*, suggesting that the amine concentrations expected from heterologous *Np*TyDC1

expression are unlikely to impair algal growth.

Although colony imaging showed reporter expression after transformation, quantitative fluorescence assays and flow cytometry did not detect a stable fluorescent population after two rounds of screening. We do not have direct evidence to identify a single cause for the loss of signal, and several explanations remain consistent with the data. Nuclear transgenes in *C. reinhardtii* are known to show variable and often unstable expression, owing to position effects from non-homologous end-joining integration, clone-to-clone heterogeneity, and epigenetic silencing that can develop over successive rounds of propagation (Shahar et al. 2019; Neupert et al. 2020). It has also been shown that silencing might be reversed under certain conditions (Beauchemin et al. 2024). However, the well-known instability of *C. reinhardtii* transgenes does not, on its own, prove that silencing is the cause. As a result, other explanations should be considered. The mVenus signal observed at the colony level suggests that transcription was not fully blocked, as some transcript and protein appear to have been produced. Translation also seems less likely to be the limiting step, since mVenus is small, expresses well in many heterologous systems, and could be detected in early colonies. Other explanations might be more plausible. The kinetic parameters of *Np*TyDC1 also have implications for the detection of tyramine in this system. With a $K_m$ of approximately 109 µM and a relatively low *kcat* (Arjmandi et al., in preparation - chapter 1), the catalytic output of *Np*TyDC1 is modest in absolute terms. The mVenus-*Np*TyDC1 fusion might have been misfolded or unstable in the algal cytosol. Alternatively, the *Np*TyDC1 portion might have been toxic to the highest-expressing cells, which could have led to their loss during liquid propagation. Limited availability of the pyridoxal 5′-phosphate cofactor, or restricted intracellular L-tyrosine pools, could also reduce catalytic output. The difference between colony-level and liquid-culture fluorescence is a striking observation, and we cannot fully account for it. One possibility is that

cells in colonies share a cooperative microenvironment, in which local detoxification of paromomycin and shared metabolic load might reduce stress for each cell, whereas liquid culture imposes uniform conditions on every cell. The resistance gene and the *mVenus-NpTyDC1* cassette are also driven by separate promoters and could be silenced or downregulated independently, which means that cells might keep paromomycin resistance while losing reporter expression. This decoupling could explain the observed pattern, but it does not, on its own, identify the level at which the system is failing. Community-wide reviews note that unstable or inefficient nuclear transgene expression remains a central limitation in *C. reinhardtii* engineering, even when initial screening suggests reporter positivity (Schroda 2019). Several strategies have been shown to improve reliability. Intron-containing transgene designs appear to enhance nuclear expression in *C. reinhardtii*, which suggests that intron-poor or intron-free constructs such as ours might produce weak and heterogeneous expression that falls below liquid-assay detection thresholds (Baier et al. 2018). Promoter and terminator selection also matters. The *PsaD* promoter and terminator combination used here was reported to outperform the chimeric *Ribulose-1,5-bisphosphate Carboxylase/Oxygenase Small Subunit 2/Heat Shock Protein 70A (HSP70A/RBCS2)* fusion promoter and the *RBCS2* promoter alone in a comparison of seven promoters (Fischer and Rochaix 2001; Kumar, Falcao, and Sayre 2013). Furthermore, recent promoter-testing studies emphasize that many constructs still appear to generate only background signal in bulk measurements (Niemeyer et al. 2023). Consequently, our results are consistent with a construct-specific limitation as well as with broader chassis-level constraints, and we cannot determine which dominates at this stage. Distinguishing between these possibilities will require constructs with different design choices, including intron-containing versions, alternative promoter and terminator combinations, codon-optimization variants, and chloroplast-targeted versions of *NpTyDC1*. The demonstration

of stable, detectable tyramine production from any such construct would establish *C. reinhardtii* as a viable chassis for tyramine biosynthesis. On the other hand, persistent failure across diverse construct designs would more strongly indicate *C. reinhardtii*-specific limitations rather than the design choices in this study.

Apart from expression-level constraints, the metabolic context in which *Np*TyDC1 operates should also be considered. The transformation experiments were carried out without tyrosine supplementation, so the enzyme depended entirely on endogenous pools. These pools are normally adjusted to support protein biosynthesis and the formation of aromatic compounds, and they may not be enough to sustain the flux required for the transformed organism living without stress, and it could cause complications on a cellular level. Cofactor supply is equally unclear, as *C. reinhardtii* produces PLP mainly for its own transaminases and decarboxylases, and the addition of a high-affinity PLP-binding enzyme could draw on a pool that is not in excess. So, either there is no tyramine being produced, or the mere act of its production is causing the cells to die.

Even if tyramine is being produced, the cell may not allow it to accumulate. Hydroxylation, N-methylation, conjugation, active export, and vacuolar sequestration are all possible sinks that could lower steady-state concentrations below the detection threshold, even under productive synthesis. These processes were not assessed in the present work, and future analyses targeting tyramine catabolites or conjugates in the cell pellet and the spent medium of transgenic lines would help test this possibility. Tyrosine also sits at a branch point that feeds protein synthesis and other downstream pathways, and these competing sinks have not yet been addressed in this system. Distinguishing these systems-level constraints from expression failure defines a clear set of next experiments.

## 3.8. Conclusion

The endogenous *C. reinhardtii* protein annotated as TyDC appears to lack genuine tyrosine decarboxylase function, as its active site residues suggest preference for indolic rather than phenolic substrates, and phylogenetic analysis placed it within an algal cluster distinct from plant TyDC enzymes. Consistent with this, no tyramine or alkaloid intermediates were detected in wild-type cultures. Supplementation experiments confirmed that exogenous tyrosine was taken up but not converted. Together, these findings establish *C. reinhardtii* as a metabolically clean chassis with no competing endogenous decarboxylation activity, meaning that any tyramine detected in transgenic lines could be confidently attributed to the heterologous enzyme. Furthermore, tyrosine showed no measurable effect on growth up to the tested concentrations, and a clear inhibitory threshold was identified for tyramine, providing useful boundaries for future pathway engineering. Nuclear transformation of the *Np*TyDC1 construct yielded colonies in which fluorescent signal was detected at the colony level, though this could not be confirmed at the single-cell level and may not exclusively reflect transgene-derived protein expression. Moreover, the signal appeared to decline over successive subculturing, suggesting instability of expression over time. The incorporation of additional introns was also constrained by a frameshift that arose during cloning, limiting the evaluation of intron-mediated enhancement strategies. Consequently, future work should explore compartmentalization approaches such as chloroplast-based expression, which may offer greater stability and reduce silencing in *C. reinhardtii*.

# Chapter 4 -
## Discussion, Conclusion and Perspective

The present discussion focuses on the connections between enzyme biochemistry and chassis evaluation, on what the integration of the two reveals about the design of heterologous platforms for plant alkaloid production, and on the perspectives that follow from the limitations identified along the way.

## 4.1. Overview

There are two main discoveries in this thesis. First, *Np*TyDC1 is the principal tyrosine decarboxylase of *N. pseudonarcissus* 'King Alfred', and it operates within a constrained kinetic regime that is shared with its closest characterized homologs in *L. radiata* (Hu et al. 2021) and *L. aurea* (Wang et al. 2019). *Np*TyDC1 joins a small but growing list of characterized plant TyDCs (Facchini et al. 1994; Lehmann and Pollmann 2009; Hu et al. 2021; Wang et al. 2019; Li et al. 2022; Luaces et al. 2024). Second, *C. reinhardtii* lacks a functional endogenous tyrosine decarboxylase, takes up exogenous $_{L}$-tyrosine, and tolerates tyramine well above the titers reported in any engineered eukaryotic aromatic-amine producer but does not sustain stable nuclear expression of a codon-optimized *NpTyDC1* cassette in liquid culture. *C. reinhardtii* has joined a list of microalgal hosts that have been evaluated for plant secondary metabolite production, mostly for terpenoids and phenylpropanoids (Lauersen et al. 2016; Lauersen et al. 2018; Wichmann et al. 2018; Einhaus et al. 2022; Xiang et al. 2020)The two findings define both ends of a synthetic biology pipeline that has not previously existed for AmAs: an enzyme with measured kinetic parameters at one end and a chassis with mapped metabolic and expression boundaries at

the other. The novelty of this work is not only that either piece is unique, but also they are now connected. Three observations follow from this connection that could not have been made before. First, *Np*TyDC1 is the first functionally characterized TyDC in the *Narcissus* genus. Its kinetic profile reinforces the emerging view that Amaryllidaceae TyDCs are tightly regulated low-flux gatekeepers rather than bulk-metabolic enzymes. Second, *C. reinhardtii* is shown to be metabolically clean for tyramine production. It carries no competing endogenous decarboxylation activity, no inhibitory growth response to the substrate, and tolerance for the product well above any titer relevant to current engineered eukaryotic systems. This makes it the first photosynthetic eukaryote in which the entry step of any alkaloid pathway has been formally evaluated. Third, the failure to establish stable nuclear expression maps the practical barrier that future work must address and identifies the construct-panel experiment that would resolve it. The path from a daffodil enzyme to a sustainable photosynthetic alkaloid platform is therefore better defined now.

## 4.2. *Np*TyDC1 within the broader TyDC landscape

The catalytic profile of *Np*TyDC1 acquires meaning only when placed against the kinetic data of other characterized TyDCs. Chapter 2 collected eleven such enzymes spanning bacteria, primary-metabolic plants, and alkaloid-producing plants, and the comparison reveals a pattern that we believe is significant for the field. Amaryllidaceae TyDCs, including *Np*TyDC1 (0.023 $s^{-1}$), *Lr*TyDC1 (0.038 $s^{-1}$), *Lr*TyDC2 (0.032 $s^{-1}$), and *Lau*TyDC1 (0.27 $s^{-1}$), cluster narrowly at the lower end of the plant range (Wang et al. 2019; Hu et al. 2021). This narrow

cluster is more easily read as a conserved regulatory architecture than as a coincidence. The four characterized Amaryllidaceae TyDCs come from two different genera, have been characterized by independent laboratories using different protocols, and converge on a similar *kcat* and $K_m$ range. Tyramine is the entry metabolite for AmA biosynthesis, but L-tyrosine is also an amino acid required for protein synthesis and therefore basic cell function. An alkaloid-producing plant must therefore solve a partition problem: divert enough L-tyrosine into the alkaloid pathway to support the defensive role of these compounds, but not so much that protein synthesis is starved. A low-*kcat* gatekeeper is a possible solution.

If this hypothesis is correct, then the kinetic-class concept becomes a useful predictive tool. Any newly identified TyDC from an Amaryllidaceae transcriptome, particularly one phylogenetically clustering with *Np*TyDC1, *Lr*TyDC1/2, and *Lau*TyDC1, could be expected to operate within this low-flux regime. A second observation that emerges from the comparison concerns the two-isoform paradigm. *N. pseudonarcissus* carries at least two TyDC genes, *NpTyDC1* and *NpTyDC2*, that share 57% sequence identity but differ functionally. *Np*TyDC1 accepts L-tyrosine and produces tyramine. *Np*TyDC2 does not produce detectable tyramine under the assay conditions, and active-site analysis suggests an indolic rather than phenolic substrate preference. One caveat applies to this comparison. The recombinant enzymes were assayed as MBP fusions, and the tag was not removed before measurement. For *Np*TyDC1 this is unlikely to distort the kinetics, since its $K_m$ and *kcat* fall within the range

of characterized Amaryllidaceae TyDCs. For *Np*TyDC2, however, a tag effect cannot be excluded, and the absence of activity may reflect suppression by the fusion rather than a true lack of function. A tag-free *Np*TyDC2 construct would resolve this. The phylogenetic reconstruction in Chapter 2 places *Np*TyDC1 within an Amaryllidaceae-specific TyDC1 clade and *Np*TyDC2 within a broader monocot clade alongside non-alkaloid-producing species.

Now that NpTyDC1 is established as a low-flux gatekeeper, future engineering of AmA biosynthesis in a heterologous host must account for its constrained entry rate. This property can be targeted to increase pathway output or preserved to maintain metabolic balance, depending on the design goal. On the other hand, *Np*TyDC1's constrained *kcat* reflects an evolved partition between primary and specialized metabolism, which a heterologous host should respect to avoid metabolic imbalance. *C. reinhardtii* maintains substantial intracellular $_{L}$-tyrosine pools, as our supplementation experiments and time-course analysis demonstrated, with intracellular $_{L}$-tyrosine concentration scaling positively with biomass at an $R^2$ of 0.93. In addition, *Np*TyDC1's projected Vmax of 0.23 nkat $mg^{-1}$ converts to roughly 4.2 μM $min^{-1}$ at the assay enzyme concentration. In theory, if we scale this, the volumetric tyramine production rate would likely remain in the low micromolar per hour range. This is far below the millimolar titers reported for tyramine in engineered *S. cerevisiae* strains (1.46 mM,(Noda et al. 2015)). Reaching commercially relevant titers would therefore require either substantial increases in enzyme abundance, increases in catalytic turnover, or both.

Two engineering strategies follow from this analysis. The first is overexpression. As we already had chosen the *PsaD* promoter, which is known for its high expression level compared to other promoters (Fischer and Rochaix 2001), and we have already applied other strategies for higher expression levels like codon optimization, we could be using qPCR to select for colonies with higher expression. Another strategy would be directed mutagenesis to relax the catalytic constraint. The active-site architecture of *Np*TyDC1, particularly the residues identified in Chapter 2 by docking analysis, provides a rational starting point for mutagenesis. Comparison with high-*kcat* homologs such as *O. europaea Oe*TDCs may identify residues that, when introduced into *Np*TyDC1, raise *kcat* without compromising substrate specificity. Another complication could be the lack of enough co-factor for the enzyme to get by. TyDC is a PLP-dependent enzyme, and PLP availability in the cytosol of *C. reinhardtii* has not been experimentally measured. If cytosolic PLP is limiting under standard growth conditions, then increasing enzyme abundance alone would not increase tyramine production beyond a saturable limit. This is a testable prediction. Co-expression of pyridoxal kinase or supplementation with pyridoxine in the medium would increase PLP supply. If tyramine production scales with PLP levels, the pathway is cofactor-limited. If not, the catalytic turnover of *Np*TyDC1 itself is the limit. Either outcome would be informative. These considerations argue that the low-flux character of *Np*TyDC1 must be treated as a bottleneck in any heterologous host, not as a feature to preserve. The plant's regulatory logic does not transfer to a microbial chassis, where the partition problem is differently

structured and L-tyrosine pools are accessible by supplementation. Once the gatekeeper question is reframed in this way, the choice of chassis becomes the next decision point. Whether we continue with *C. reinhardtii* or choose other widely used hosts such as *S. cerevisiae*.

## 4.3. *C. reinhardtii* against an alternative chassis option

*S. cerevisiae* has supported the reconstitution of benzylisoquinoline and tropane alkaloid pathways (Pyne, Narcross, and Martin 2019), opioid biosynthesis (Galanie et al. 2015), and complete vinblastine and vincristine precursor pathways involving 34 plant enzymes with more than 22 genetic modifications (Zhang et al. 2022). Tyramine has been produced in engineered *S. cerevisiae* at 1.46 mM (Noda et al. 2015), a titer that is well within the tolerance range we measured for *C. reinhardtii*. The expression environment in yeast is predictable. Nuclear transgenes integrated at well-characterized loci express stably across generations, and silencing is not a recurring problem. The toolbox of yeast promoters, terminators, integration sites, and selection markers is mature, and pathway scaffolding through CRISPR-mediated integration is now routine.

The case for microalgae rests on three considerations that yeast cannot match. The first is photoautotrophy. *C. reinhardtii* can grow on $CO_2$ and light alone, which means a tyramine production process based on this host could draw its carbon directly from the atmosphere rather than from a fermentation feedstock such as glucose or glycerol. At an industrial scale, the carbon footprint difference is substantial. The second is plant-like compartmentalization. *C. reinhardtii* has a chloroplast and multiple mitochondria. For pathway enzymes that originated

in plants, the compartmental architecture in *C. reinhardtii* may support more native-like folding, post-translational modification, and substrate channelling. The third is regulatory. *C. reinhardtii* has been classified as Generally Recognized as Safe (GRAS) by the FDA, which simplifies regulatory pathways for products intended for pharmaceutical or food applications.

Our chassis evaluation in Chapter 3 establishes that *C. reinhardtii* is metabolically suitable. Even though *C. reinhardtii* does not produce alkaloids, it still metabolizes L-tyrosine through conserved primary routes. Most tyrosine is used for protein synthesis. A large part is also directed into the prenylquinone pathway. In this route, tyrosine is first converted to 4-hydroxyphenylpyruvate (4-HPP) by tyrosine aminotransferase (TAT). 4-HPP is then converted to homogentisate by 4-hydroxyphenylpyruvate dioxygenase (HPPD). *C. reinhardtii* possesses a functional HPPD, which has been biochemically characterized (Gálvez-Valdivieso, Pineda, and Aguilar 2010). These two products are essential for the alga. Tocopherol acts as a membrane antioxidant, and plastoquinone acts as an electron carrier in photosynthesis. Beyond this branch, L-tyrosine can also enter the general tyrosine degradation pathway. In this pathway, homogentisate is further broken down to fumarate and acetoacetate, which feed central carbon metabolism (Luo et al. 2020)**.** Therefore, L-tyrosine in *C. reinhardtii* is directed toward protein synthesis, prenylquinone biosynthesis, and catabolic breakdown, rather than toward specialized alkaloid production. The single endogenous AAAD-like enzyme is not a functional TyDC, the host takes up exogenous L-tyrosine, and tolerance for tyramine

extends well beyond any titer that has been reported from engineered eukaryotic aromatic-amine producers (Planells-Carcel et al. 2025; Milne et al. 2020). The absence of endogenous tyramine rests on a negative result, so detection sensitivity matters here. This screen was performed by HPLC-MS/MS in MRM mode, and tyramine was quantified against a calibration curve extending into the low ng/mL range. No tyramine peak was detected in wild-type extracts, so the non-detection is supported by a sensitive and validated method.

On the other hand, our nuclear expression construct produced colony-level mVenus fluorescence on solid medium that did not survive into liquid culture. This is consistent with the well-documented instability of nuclear transgene expression in this organism, (Schroda 2019; Neupert et al. 2020) and represents the principal practical barrier to using *C. reinhardtii* for the AmA pathway.

The chloroplast offers a potential way around this barrier. Plastid integration is homologous, achieves high transgene copy numbers per cell, and has been shown to reduce silencing relative to nuclear integration (Dyo and Purton 2018). The chloroplast also offers a concrete metabolic advantage that yeast cannot match. The full AmA pathway includes an oxidative phenol coupling step catalyzed by a cytochrome P450, CYP96T1 (Kilgore and Kutchan 2016). P450 enzymes normally depend on a membrane-bound reductase and a supply of NADPH. In a photosynthetic organelle, this dependence can be bypassed. This light-driven strategy has been demonstrated for whole P450-dependent pathways in chloroplasts (Mellor et al. 2022). Yeast has no photosynthetic apparatus, so it

cannot supply reducing power in this way. A second advantage follows from precursor supply. In plants and algae, aromatic amino acids are synthesized in the plastid. The dhurrin pathway of *S. bicolor* was engineered into chloroplasts precisely to use the tyrosine supplied by endogenous chloroplast metabolism (Gnanasekaran et al. 2016). A plastid-localized AmA pathway would therefore sit next to its endogenous L-tyrosine pool. Yeast also produces tyrosine, so this benefit is co-location rather than availability. However, the chloroplast comes with a constraint that is rarely highlighted in the literature. Chloroplast-translated proteins lack a known mechanism for export to the cytoplasm (Jarvis 2008). *Np*TyDC1 is a nucleo-cytosolic enzyme, both based on its predicted localization and on our subcellular localization studies in *N. benthamiana*. Targeting it to the chloroplast would compartmentalize the enzyme away from its substrate pool (cytosolic L-tyrosine) and from the downstream enzymes of the pathway (NBS, NR, N4OMT), which are also cytosolic (Tousignant, Diaz-Garza, Majhi, Gélinas, Singh, and Desgagné-Penix 2022; Majhi et al. 2023)**.** This concern, however, applies only to a split localization, in which part of the pathway remains in the cytosol. It does not apply when the entire pathway is relocated to the plastid. In that case, no intermediate needs to cross the chloroplast envelope, and the export limitation is avoided. The dhurrin work suggests that a complete P450-dependent pathway can operate inside the chloroplast in this manner (Gnanasekaran et al. 2016). In summary, *C. reinhardtii* has unique structural and regulatory advantages that yeast cannot match. The clearest of these is the ability to power a P450 step with photosynthetic reducing power. Yeast has expression

reliability that *C. reinhardtii* does not yet match. The decision between them depends on whether the silencing problem can be solved. If it can, the photoautotrophic and compartmental advantages of the microalga become decisive. If it cannot, yeast remains the more pragmatic choice for the near future. Our work does not resolve this question, but it provides the data needed to make the resolution.

## 4.4. *C. reinhardtii*: a metabolically clean but transcriptionally challenging chassis

Beyond the platform comparison, our evaluation of *C. reinhardtii* as a chassis has two implications that deserve discussion in their own right. The first concerns the colony-versus-liquid-culture phenomenon. The second concerns the decoupling of selection and expression cassettes.

The colony-versus-liquid culture discrepancy is, in our experience, a major complication in *C. reinhardtii* nuclear engineering. Colony-level fluorescence on solid medium is widely used as the first screening step after transformation. Our results show that this evidence is not sufficient. Multiple colonies displayed clear mVenus fluorescence on solid medium, in some cases for several rounds of subculturing under antibiotic selection, only to fail in liquid culture under the same selection pressure. Several explanations are consistent with our data, and we cannot distinguish among them without further experiments. Cells in colonies share a cooperative microenvironment in which paromomycin detoxification by neighbouring cells creates locally protected zones where transgene-positive cells

are not under uniform pressure. Liquid culture removes this cooperation, exposing every cell to uniform selection. The most likely explanation follows from the independent regulation of our two transgene cassettes. Since the mVenus reporter and the paromomycin resistance gene are driven by separate promoters, antibiotic selection acts only on the resistance gene and not on the reporter. A cell can therefore silence the mVenus cassette while it continues to express the resistance cassette. Such a cell survives selection but loses fluorescence. Liquid culture imposes greater physiological stress than growth on solid medium, and this stress may favour the silencing of transgenes that are not required for survival. The reporter is one such non-essential transgene, so it is a likely target. This model fits our observation directly, because fluorescence was retained on solid medium but lost in liquid culture under the same antibiotic selection. Liquid culture amplifies a different and broader distribution of cell types, which dilutes the rare high-expressing integrants. Another cause could be position effects from non-homologous end-joining integration that produce highly variable expression depending on the chromatin context of the integration site, and the loci that survive solid-medium selection may not survive liquid-medium propagation.

The second observation, the decoupling of selection and expression, has design implications that go beyond our specific construct. The pSL18 backbone we used carries the paromomycin resistance gene (*APHVIII*) and the *NpTyDC1-mVenus* cassette under separate promoters. Cells that lost mVenus fluorescence in liquid culture continued to grow under paromomycin selection, which means that

*APHVIII* transcription was preserved while the *NpTyDC1* transcript was lost or silenced. The two cassettes can therefore be silenced independently. A bicistronic cassette in which selection and target are translated from the same transcript, separated by a self-cleaving 2A peptide, would force coupled expression.

## 4.5. Contributions to the field

We close this discussion with an explicit statement of what this thesis contributes to the field, organized by the three areas to which it speaks. To AmA biochemistry, this work contributes the first functional characterization of any TyDC in the *Narcissus* genus. *NpTyDC1* had previously been visible only at the transcriptomic level (Singh and Desgagné-Penix 2017). We have now placed it within a measured kinetic class shared with characterized TyDCs from *L. radiata* and *L. aurea*, and we have shown that its functional divergence from *NpTyDC2* follows the TyDC1/TyDC2 paradigm observed in other Amaryllidaceae. This divergence reinforces the view that TyDC multigene families in this family encode enzymes with distinct physiological roles. We further establish *Np*TyDC1 as the principal isoform directing L-tyrosine into the Amaryllidaceae alkaloid biosynthetic network, operating as a tightly regulated gatekeeper. The kinetic-class concept and the phylogenetic predictor that follows from it offer a framework for characterizing TyDC isoforms in newly sequenced Amaryllidaceae transcriptomes without exhaustive biochemical assay.

To microalgal pathway engineering, this work contributes the first systematic evaluation of *C. reinhardtii* as a chassis for any plant alkaloid pathway enzyme.

Previous studies have established the host for terpenoids and phenylpropanoids(Lauersen et al. 2016; Lauersen et al. 2018; Wichmann et al. 2018; Einhaus et al. 2022; Xiang et al. 2020), but no plant alkaloid enzyme has been attempted before this work. We provide a metabolic baseline (clean background, substrate uptake, product tolerance), a transformation protocol that achieves colony-level expression, and a clear identification of the practical barrier (nuclear silencing in liquid culture). The colony-versus-liquid culture phenomenon and the selection-expression decoupling problem, while not unique to this study, are documented here in a form that should influence design practice for future *C. reinhardtii* projects.

These findings advance our biochemical understanding of the committed entry step in Amaryllidaceae alkaloid biosynthesis, laying an experimental foundation for reconstructing this pathway in a sustainable, photosynthetically driven microbial system. Whether full pathway reconstruction in *C. reinhardtii* is ultimately feasible remains an open question, but the properties of this organism make it the most logical starting point. As a eukaryote with a fully sequenced genome, *C. reinhardtii* is capable of the post-translational modifications required for the correct folding and activity of plant enzymes, unlike prokaryotic hosts such as *E. coli* (Zhang, Wang, and Wang 2021). The transgene silencing identified in this work is real but not intractable, and *C. reinhardtii* remains a tractable model in which these obstacles can be addressed before considering less-characterized alternative hosts such as other microalgae or yeast. The path

from a daffodil enzyme to a sustainable photosynthetic alkaloid platform is therefore better defined, even though the platform itself is not yet operational.

## 4.6. Future Direction

Several avenues of investigation emerge directly from the findings and limitations of this work. The primary setback identified in *C. reinhardtii* is the instability of nuclear transgene expression; future efforts should therefore evaluate chloroplast-targeted expression as an alternative compartment that bypasses nuclear silencing and may benefit from more uniform transgene copy numbers (Dyo and Purton 2018; Schroda 2019). A key constraint of this approach, however, is that proteins expressed from the chloroplast genome are synthesized within the organelle by prokaryotic-type ribosomes and currently have no known mechanism for export to the cytoplasm (Jarvis 2008). Since *Np*TyDC1 is expected to function in the cytoplasm, chloroplast transformation may compartmentalize the enzyme away from its substrate and from the downstream enzymes of the pathway, and this constraint would need to be resolved before this strategy can be considered viable. Systematic optimization of the nuclear expression cassette, including the incorporation of validated endogenous introns at multiple positions and the evaluation of alternative promoters such as *HSP70A-RBCS2* fusions, should also be pursued (Baier et al. 2020; Schroda, Blocker, and Beck 2000; Schroda, Beck, and Vallon 2002). Beyond expression engineering, the kinetic parameters established for *Np*TyDC1 in this study provide the reference data needed to assess whether tyramine flux, once achieved, would be sufficient to support downstream

condensation by norbelladine synthase. Expanding the reconstructed pathway to include norbelladine synthase, noroxomaritidine reductase, and *O*-methyltransferases would represent the next logical step toward a complete heterologous Amaryllidaceae alkaloid precursor production platform.

# Chapter 5
# - Annex

Supplementary Table S1. Amino acid sequences of *Np*TyDC1 and *Np*TyDC2 that were used as queries for BLAST.

| | |
|---|---|
| **NpTyDC1** | MGSLGSDNIAELEANGSAFNLNPLDPEEFRRQGHMVIDFLADYYQNVHKYPVRSQVEPGYLKKILPESAPNQPESLETIL |
| | DDITNHIVPGITHWMSPNYFAYFPASGSTAGFLGEMLSTGFNAVCFNWMSSPAATELETIVTDWLGKLLALPEKFLFSGG |
| | GGGVLQGTTCEAILCTMTAARDKVLNKIGKDQIGKLVVYGSDQTHCALQKAAQIAGIHPANFRAVRTFKSDAFGLNPEEL |
| | RKVVSADVEAGLVPLYLCPTVGTTSSTAVDQLRGLCSVAEEHEMWVHVDAAYAGSACICPEFRHFIDGVEGATSFSFNAH |
| | KWFFTNLDCCCLWVREPQALINALSTNPEYLRNKATESQKVVDYKDWQIALSRRFRAMKLWMVMRSYGVANLRNFLRSHV |
| | KMAKLFEGLVSADERFEIVVPRNFAMVCFRFNPTKKDRATGPELDRINEFNRRLLEEVNSTGRLYMTHAVIGGEYVMRFA |
| | TGATLTEEKHVRCAWRAIQEHAAALMEKIYYKQRN |
| **NpTyDC2** | MEESLKPMDAEQLRENAHKMVDFIADYYKSIESFPVLSQVKPGYLRDLLPDSAPDHPESLEDVLEDIRQKIVPGVTHMQS |
| | PNYFAYYPSNSSVAGFLGEMISAGFNIVGFNWIASPAATELEVIVLDWLAKMLNLPNQFLSSGQGGGVIQGTASEANLVV |
| | LLAARDKFLNRFGKRSLEKLVVYASDQTHAAMKKACQIAGIYPENFRVLNADHTSNYALVPEALSDAISNDLSAGLIPFF |
| | LCATVGTTSSAAVDPLSELGKISKVNDMWFHVDAAYAGSACICPEYRHYIDGIEEAASFNMNAHKWFLTNFDCSLLWIKD |
| | RSALIQSLSTYPEYLKNKASQENSVVDFKDWQIPLGRRFRSLKLWMVLRLYGLENLQSYIRNHIKLAGQFEQLVCSDSRF |
| | EVVVPRTFSLVCFRLLPPPNHQDNGYKLNHSLLDAVNSSGKIFVSHTVLSGKYVIRFAVGAPLTEEEHIKQAWKVFQDQA |
| | TILLAGSDGSDFGASNGDII |

Supplementary Table S2. ID, Enzyme name, and Organism of the hits after cleaning up the dataset to prepare for the phylogenetic tree.

| ID | Enzyme | Organism |
|---|---|---|
| A0A2H5AIY0.1 | Tyrosine decarboxylase 1 | Narcissus pseudonarcissus |
| QOQ50636.1 | Tyrosine decarboxylase | Lycoris longituba |
| ALM26449.1 | Tyrosine decarboxylase | Narcissus aff. pseudonarcissus MK-2014 |
| AXU39890.1 | Tyrosine decarboxylase 1 | Narcissus papyraceus |
| UIP35205.1 | Tyrosine decarboxylase 1 | Leucojum aestivum |
| QXF78537.1 | Tyrosine decarboxylase 1 | Lycoris radiata |
| QXF78538.1 | Tyrosine decarboxylase 2 | Lycoris radiata |
| WGU11339.1 | Tyrosine decarboxylase 1 | Crinum x powellii |
| KAJ4745160.1 | Tyrosine decarboxylase | Rhynchospora pubera |
| KAH7661155.1 | Tyrosine decarboxylase | Dioscorea alata |
| XP_009407716.2 | Tyrosine decarboxylase 1 | Musa acuminata AAA Group |
| URE15633.1 | Tyrosine DOPA decarboxylase | Musa troglodytarum |
| ACJ76782.1 | Tyrosine/DOPA decarboxylase | Argemone mexicana |
| XP_026387682.1 | Tyrosine/DOPA decarboxylase 3 | Papaver somniferum |
| WYV98056.1 | Tyrosine/DOPA decarboxylase | Olea europaea |
| KAL5977409.1 | Tyrosine/DOPA decarboxylase 2 | Asimina triloba |
| NP_001413549.1 | Tyrosine/DOPA decarboxylase 2 | Papaver somniferum |
| P54770.2 | Tyrosine/DOPA decarboxylase 3 | Papaver somniferum |
| KAF5198316.1 | Tyrosine/DOPA decarboxylase | Thalictrum thalictroides |
| ABJ16446.1 | Tyrosine decarboxylase | Aristolochia contorta |
| AAG60665.1 | Tyrosine/dopa decarboxylase | Thalictrum flavum subsp. glaucum |
| WOK24097.1 | Tyrosine decarboxylase | Forsythia suspensa |
| KAL2474972.1 | Tyrosine decarboxylase 1 | Abeliophyllum distichum |
| XP_006437249.1 | Tyrosine/DOPA decarboxylase 5 | Citrus x clementina |
| XP_026437973.1 | Tyrosine/DOPA decarboxylase 1 | Papaver somniferum |
| OAY76026.1 | Tyrosine/DOPA decarboxylase 2 | Ananas comosus |
| KAI8017572.1 | Tyrosine/DOPA decarboxylase 2 | Camellia lanceoleosa |
| ACX29990.1 | Tyrosine decarboxylase | Citrus reshni |
| XP_006434677.2 | Tyrosine/DOPA decarboxylase 1 | Citrus x clementina |
| KAH9758081.1 | Phenylacetaldehyde synthase | Citrus sinensis |
| XP_026394976.1 | Tyrosine/DOPA decarboxylase 5 | Papaver somniferum |
| PIN03085.1 | Aromatic-L-amino-acid/L-histidine decarboxylase | Handroanthus impetiginosus |
| KAK4399395.1 | Tyrosine/DOPA decarboxylase 1 | Sesamum angolense |
| P54768.1 | Tyrosine/DOPA decarboxylase 1 | Papaver somniferum |
| KAK4440206.1 | Tyrosine/DOPA decarboxylase 1 | Sesamum alatum |
| XLV31471.1 | Tyrosine decarboxylase | Cistanche tubulosa |
| XP_006836315.1 | Tyrosine/DOPA decarboxylase 2 | Amborella trichopoda |
| AOC38014.1 | Tyrosine decarboxylase | Rehmannia glutinosa |
| KAK4421057.1 | Tyrosine/DOPA decarboxylase 2 | Sesamum alatum |
| XP_023881931.2 | Phenylacetaldehyde synthase | Quercus suber |
| XP_024161133.2 | Phenylacetaldehyde synthase | Rosa chinensis |
| GMI70666.1 | Aromatic aldehyde synthase | Hibiscus trionum |
| BBE38027.1 | Aromatic amino acid decarboxylase | Eriobotrya japonica |
| PON36224.1 | Aromatic-L-amino-acid decarboxylase | Trema orientale |
| XP_006448979.1 | Tyrosine decarboxylase 1 | Citrus x clementina |
| KAJ4844726.1 | Tyrosine/DOPA decarboxylase 1 | Turnera subulata |
| KAK7819704.1 | Tyrosine/dopa decarboxylase 2 | Quercus suber |
| XP_020418863.1 | Tyrosine decarboxylase 1 | Prunus persica |
| EOX96928.1 | Tyrosine/DOPA decarboxylase | Theobroma cacao |
| KAK1281629.1 | Tyrosine/DOPA decarboxylase 2 | Acorus calamus |
| UZS00562.1 | Tyrosine/DOPA decarboxylase | Gloriosa superba |
| XP_030479600.1 | Tyrosine decarboxylase | Cannabis sativa |
| AAC61841.1 | Tyrosine/dopa decarboxylase | Papaver somniferum |
| KAK1258180.1 | Tyrosine/DOPA decarboxylase 2 | Acorus gramineus |
| P54771.1 | Tyrosine/DOPA decarboxylase 5 | Papaver somniferum |
| XP_015877506.2 | Tyrosine decarboxylase | Ziziphus jujuba |
| PON65487.1 | Aromatic-L-amino-acid decarboxylase | Parasponia andersonii |
| A0A2H5AIY2.1 | Tyrosine decarboxylase 2 | Narcissus pseudonarcissus |
| UIP35206.1 | Tyrosine decarboxylase 2 | Leucojum aestivum |
| WGU11341.1 | Tyrosine decarboxylase 2 | Crinum x powellii |
| KAJ6790792.1 | Tyrosine decarboxylase 1 | Iris pallida |
| XP_020265332.1 | Tyrosine decarboxylase 1 | Asparagus officinalis |
| XP_020681680.1 | Tryptophan decarboxylase 2 | Dendrobium catenatum |
| PKU85599.1 | Tyrosine decarboxylase 1 | Dendrobium catenatum |
| XP_074560317.1 | Tyrosine decarboxylase 2 | Curcuma longa |
| XP_068656100.1 | Tyrosine decarboxylase 2 | Aristolochia californica |
| PKA54142.1 | Tyrosine decarboxylase 1 | Apostasia shenzhenica |
| KAK1290117.1 | Tyrosine decarboxylase 1 | Acorus calamus |
| XP_008358473.2 | Phenylacetaldehyde synthase | Malus domestica |
| XP_024166413.2 | Phenylacetaldehyde synthase isoform X1 | Rosa chinensis |
| AXE73167.1 | Tryptophan decarboxylase 3 | Malus domestica |

| | | |
|---|---|---|
| XP_016743391.2 | Phenylacetaldehyde synthase | Gossypium hirsutum |
| KAJ4728348.1 | Tyrosine decarboxylase | Melia azedarach |
| WOL10650.1 | Tyrosine decarboxylase 1 | Canna indica |
| XP_050108357.1 | Tyrosine decarboxylase 2 | Malus sylvestris |
| XP_004956078.1 | Tyrosine decarboxylase 1 | Setaria italica |
| XP_044492294.1 | Tyrosine decarboxylase 2 | Mangifera indica |
| XP_012484102.1 | Phenylacetaldehyde synthase | Gossypium raimondii |
| XP_059660189.1 | Tyrosine decarboxylase 2 | Cornus florida |
| KAJ6941570.1 | Tyrosine decarboxylase 1 | Populus alba x Populus x berolinensis |
| KAJ4851343.1 | Tyrosine decarboxylase 1 | Turnera subulata |
| XP_050207042.1 | Tyrosine decarboxylase 2 | Mercurialis annua |
| XP_009335237.2 | Phenylacetaldehyde synthase | Pyrus x bretschneideri |
| XP_062148052.1 | Phenylacetaldehyde synthase | Ainus glutinosa |
| XP_002459778.2 | Tyrosine decarboxylase 1 | Sorghum bicolor |
| XP_030470685.1 | Tyrosine decarboxylase 2 | Syzygium oleosum |
| XP_010036145.2 | Tyrosine decarboxylase 2 | Eucalyptus grandis |
| XP_058005809.1 | Tyrosine decarboxylase 2 | Hevea brasiliensis |
| XP_043721998.1 | Tyrosine decarboxylase 2 | Telopea speciosissima |
| QIA07379.1 | Aromatic aldehyde synthase | Olea europaea |
| XP_068322626.1 | Tyrosine decarboxylase 2 | Pyrus communis |
| XP_020163775.1 | Tryptophan decarboxylase 2 | Aegilops tauschii subsp. strangulata |
| XP_010326342.1 | Tyrosine decarboxylase 2 | Solanum lycopersicum |
| XP_042515557.1 | Tyrosine decarboxylase 2 | Macadamia integrifolia |
| XP_052163374.1 | Tryptophan decarboxylase 2 | Oryza glaberrima |
| QBL52488.1 | Aromatic aldehyde synthase | Populus trichocarpa |
| XP_021893770.1 | Tyrosine decarboxylase 1 | Carica papaya |
| KAK8951502.1 | Tyrosine decarboxylase 1 | Platanthera zijinensis |
| XCG46241.1 | Tryptophan decarboxylase | Corchorus olitorius |
| XP_049406461.1 | Tyrosine decarboxylase 2 | Solanum stenotomum |
| NP_001409650.1 | Tryptophan decarboxylase 2 | Oryza sativa Japonica Group |
| KAF5199076.1 | Tyrosine decarboxylase | Thalictrum thalictroides |
| XP_015088582.1 | Tyrosine decarboxylase 1 | Solanum pennellii |
| XP_006657648.2 | Tryptophan decarboxylase 2 | Oryza brachyantha |
| XP_006355805.1 | Tyrosine decarboxylase 1 | Solanum tuberosum |
| OMO62804.1 | Pyridoxal phosphate-dependent decarboxylase | Corchorus capsularis |
| XP_009631403.1 | Tyrosine decarboxylase 2 | Nicotiana tomentosiformis |
| KAK1353286.1 | Tryptophan decarboxylase | Heracleum sosnowskyi |
| XP_010652425.1 | Phenylacetaldehyde synthase | Vitis vinifera |
| XP_034689683.1 | Tyrosine decarboxylase 1 | Vitis riparia |
| KAI7991487.1 | Tyrosine decarboxylase 1 | Camellia lanceoleosa |
| CAA2998143.1 | Tyrosine decarboxylase 1 | Olea europaea subsp. europaea |
| ONA02291.1 | Pyridoxal phosphate-dependent decarboxylase | Macleaya cordata |
| XAR58684.1 | Tyrosine decarboxylase | Bertholletia excelsa |
| XP_049344605.1 | Tyrosine decarboxylase 2 | Solanum verrucosum |
| XP_030888932.1 | Tyrosine decarboxylase 2 | Benincasa hispida |
| CAN1131424.1 | Phenylacetaldehyde synthase | Linum perenne |
| XP_014494710.1 | Tyrosine decarboxylase 1 | Vigna radiata var. radiata |
| XP_003521317.1 | Tyrosine decarboxylase 2 | Glycine max |
| CAN0897714.1 | Phenylacetaldehyde synthase | Linum grandiflorum |
| KAL2480032.1 | Tyrosine decarboxylase 1 | Forsythia ovata |
| XP_058207624.1 | Phenylacetaldehyde synthase | Rhododendron vialii |
| XP_027915667.1 | Tryptophan decarboxylase 2 | Vigna unguiculata |
| XP_047167178.1 | Tyrosine decarboxylase 2 | Vigna umbellata |
| XP_017411095.1 | Tyrosine decarboxylase 2 | Vigna angularis |
| KAL2900321.1 | Tyrosine decarboxylase 1 | Bienertia sinuspersici |
| PHU07527.1 | Tyrosine decarboxylase 1 | Capsicum chinense |
| KAF3634703.1 | Tyrosine decarboxylase 1 | Capsicum annuum |
| XP_011080126.1 | Tyrosine decarboxylase 1 | Sesamum indicum |
| XP_022155577.1 | Tyrosine decarboxylase 1 | Momordica charantia |
| XP_030499792.2 | Phenylacetaldehyde synthase | Cannabis sativa |
| XP_020222034.1 | Tyrosine decarboxylase 1 | Cajanus cajan |
| KAL1546636.1 | Tyrosine decarboxylase 2 | Salvia divinorum |
| KAB1208646.1 | Tyrosine decarboxylase 1 | Morella rubra |
| XP_057438483.1 | Tyrosine decarboxylase 2 | Lotus japonicus |
| XP_003625307.3 | Tyrosine decarboxylase 2 | Medicago truncatula |
| XP_006404072.2 | Tyrosine decarboxylase 1 | Eutrema salsugineum |
| XP_009102040.1 | Tyrosine decarboxylase 1 | Brassica rapa |
| XP_038692799.1 | Tyrosine decarboxylase 2 | Tripterygium wilfordii |
| XP_065865254.1 | Phenylacetaldehyde synthase | Euphorbia lathyris |
| XP_022000563.1 | Tyrosine decarboxylase 1 | Helianthus annuus |
| XP_006299006.2 | Tyrosine decarboxylase 1 | Capsella rubella |
| AES81613.1 | Tyrosine/DOPA decarboxylase | Medicago truncatula |
| EXB46033.1 | Tyrosine decarboxylase 1 | Morus notabilis |
| GAB4830111.1 | Tyrosine decarboxylase 2 | Ancistrocladus abbreviatus |
| WMX25290.1 | Aromatic amino acid decarboxylase TyDC3 | Lophophora williamsii |
| XP_002884194.2 | Tyrosine decarboxylase 1 | Arabidopsis lyrata subsp. lyrata |

Supplementary Table S3. Oligonucleotides used in this study.

| Gene | Primer name | Sequence (5'→3') |
|---|---|---|
| **Cloning into pMAL-c2x (protein expression in E. coli)** | | |
| NpsTYDC1 | TYDC1_FP_EcoRI | AACGGAATTCATGGGCAGCCTTGGCTCTGATAATATTG |
| | TYDC1_RP_HindIII | ACGCAAGCTTTTAATTCCTTTGTTTATAATATATCTTCTCCATCAAAGCCGC |
| NpsTYDC2 | TYDC2_FP_BamHI | AACGGGATCCATGGAGGAATCTTTGAAGCCCATGGATG |
| | TYDC2_RP_SalI | ACGCGTCGACTCAAATAATGTCTCCGTTGCTAGCGCCAAAATC |
| **Cloning into pBTEX-YFP (subcellular localization)** | | |
| NpsTYDC1 | NpsTYDC1_FP_KpnI | AACGGGTACCATGGGCAGCCTTGGCTCTGATAATATTG |
| | NpsTYDC1_RP_XbaI | ACGCTCTAGAATTCCTTTGTTTATAATATATCTTCTCCATCAAAGCCGC |
| NpsTYDC2 | NpsTYDC2_FP_KpnI | AACGGGTACCATGGAGGAATCTTTGAAGCCCATGGATG |
| | NpsTYDC2_RP_BamHI | ACGCGGATCCAATAATGTCTCCGTTGCTAGCGCCAAAATC |

Supplementary Table S4. MRM transitions and instrumental parameters used for HPLC-MS/MS analyses in kinetic study and enzyme assays optimization.

| Compound name | Retention time (min) | Precursor (m/z) | Product (m/z) | Fragmentor (V) | CE (V) | Polarity (ESI +/-) |
|---|---|---|---|---|---|---|
| L-Tyrosine | 4.366 | 182 | 165 | 83 | 10 | Positive |
| | | | **136** | | 10 | |
| | | | 123 | | 14 | |
| Papaverine | 18.129 | 340 | 324 | 165 | 40 | Positive |
| | | | **202** | | 27 | |
| | | | 171 | | 40 | |
| Tyramine | 3.507 | 138 | 121 | 81 | 5 | Positive |
| | | | 91 | | 20 | |
| | | | **77** | | 20 | |
| Notes: Quantifier ion for each compound is bold and qualifier ions are not. Identification criteria used (FDA GFI 118, 2003): Retention time window (tolerance on RT): 10% Signal-to-noise: noise algorithm used = RMS ; noise used = between retention time of each compound ± 0.5 min. Signals with signal-to-noise ratio ≤ 3 were not considered in the analysis. Qualifier ratio tolerance: uncertainty of 20% (relative) Number of qualifiers used (MRM transitions monitored per compound): 3 ISTD used: papaverine Softwares used for identifications: MassHunter Qualitative Analysis 10.0 and MassHunter Quantitative Analysis (for QQQ) Version 10.0 | | | | | | |

Supplementary Table S5. Instrumental parameters used in Single Ion Monitoring mode on HPLC-MS/MS for substrate specificity experiments.

| Compound name | Precursor (m/z) | Fragmentor (V) | Polarity |
|---|---|---|---|
| Dopamine | 154 | 78 | Positive |
| Levodopa | 198 | 78 | Positive |
| L-tyrosine | 182 | 83 | Positive |
| Papaverine | 340 | 165 | Positive |
| Phenethylamine | 122 | 74 | Positive |
| Phenylalanine | 166 | 74 | Positive |
| Tryptamine | 161 | 69 | Positive |
| Tryptophane | 205 | 69 | Positive |
| Tyramine | 138 | 81 | Positive |

Supplementary Table S6. Instrumental parameters used in Product Ion mode on HPLC-MS/MS for substrate specificity experiments.

| Compound name | Precursor (m/z) | Start mass (m/z) | End mass (m/z) | Fragmentor (V) | Collision energy (V) | Polarity |
|---|---|---|---|---|---|---|
| Dopamine | 154 | 50 | 156 | 78 | 20 | Positive |
| Phenethylamine | 122 | 50 | 125 | 74 | 20 | Positive |
| Tryptamine | 161 | 50 | 165 | 69 | 20 | Positive |
| Tyramine | 138 | 50 | 140 | 81 | 20 | Positive |

Supplementary Table S7 (Table S3 in paper)

**Table S3.** B. NpTyDC2 predicted interactions with L-tyrosine, L-tryptophan, L-phenylalanine, and L-DOPA following docking.

| Active Site residues | Ligand | **Score** (kCal/mol) | Interactions | | |
|---|---|---|---|---|---|
| | | | Hydrophobic | H-bonds | Other |
| A: Trp78, Tyr86, Tyr87, Pro88, Ser89, Thr152, Ala153, Ser154, Asn157, Gln187, His189, Ala191, Thr244, Val245, Gly246, Thr247, Thr248, Asp273, Ala274, Ala275, Tyr276, Ala277, Ser279, Asn302, His304, Trp306, Phe311; B: Val108, Phe110, Tyr334, Leu335, Leu355, Gly356 | PLP »LLP | N/A | Thr244A, Ala275A, Asn302A | Asn90A, Ala153A, Ser154A (n=2), Thr248A, Asn302A (n=2), His304A, Leu355B, Gly356B | π-stacking: His189A |
| | L-Tyrosine | -6.9 | Trp78A (n=2), Tyr86A, Val108B Phe110B | Ser89A, Thr248A, His304A | Salt-bridge: His189A (carboxylate) |
| | L-DOPA | -7.5 | Trp78A (n=2), Tyr86A, Phe110B | Pro88A, Thr248A, His304A | Salt-bridge: His189A (carboxylate) |
| | L-Tryptophan | -7.4 | Trp78A, Tyr86A, Val108B (n=2), Phe110B | Thr248A, | Salt-bridge: His189A (carboxylate) |
| | L-Phenylalanine | -6.4 | Trp78A, Val108B (n=2), Phe110B | n.d. | Salt-bridge: His189A (carboxylate) |

PLP: Pyridoxal 5-phosphate, LLP: N'-pyridoxyl-lysine-5'-monophosphate (lysine-bound PLP).

**Table S3.** A. *Np*TyDC1 predicted interactions with L-tyrosine, L-tryptophan, L-phenylalanine, and L-DOPA following docking.

| Active Site residues | Ligand | **Score** (kCal/mol) | Interactions | | |
|---|---|---|---|---|---|
| | | | Hydrophobic | H-bonds | Other |
| A :Trp94, Tyr102, Phe103, Pro104, Ala105, His205, Thr264, His320, LLP321, Leu327. Chain B :Val124 Phe126, Tyr350, Leu351, Leu371, Ser372 | PLP »LLP | N/A | Phe103, His205, Thr260, Ala291, Asn318 | Ser106, Thr169, Cys170, Thr264, Asp289, Asn318 (n-2), Leu317(A), Ser372 (A, n=2) | π-stacking: His205; Salt bridge: His205 |
| | L-Tyrosine | -6.4 | Trp94A, Val124B (n=2) Phe126B | Pro104A, Thr264A, LLP, His205 | Salt-bridge: His205A (carboxylate) |
| | L-DOPA | -7.0 | Trp94A, Tyr102A, Val124B (n=2), Phe126B | Pro104A, Asn318A, His320A, Tyr350B, Ser372B, | Salt-bridge: His205A (carboxylate) |
| | L-Tryptophan | -6.9 | Trp94A, Tyr102A, Val124B (n=2) | Thr264A, Ser372B, His205A, LLP(n=2) | Salt-bridge: His205A (carboxylate) |
| | L-Phenylalanine | -5.9 | Trp94A, Tyr102A, Val124B (n=2), Phe126B | Thr264A | His205A (carboxylate) |

PLP: Pyridoxal 5-phosphate, LLP: N'-pyridoxyl-lysine-5'-monophosphate (lysine-bound PLP).

Supplementary Table S8. Selected Specific Comparisons for substrate specificity.

| Comparison | Difference | Lower 95% | Upper 95% | P adjusted |
|---|---|---|---|---|
| TYDC1:Phenylalanine:Sample-TYDC1:None:NoS | 0.2469 | 0.2009 | 0.2929 | 1.1668e-13 |
| TYDC1:Phenylalanine:Sample-TYDC1:Phenylalanine:NoE | 0.247 | 0.182 | 0.312 | 7.6811e-11 |
| TYDC1:L-tyrosine:Sample-TYDC1:None:NoS | 0.1477 | 0.1047 | 0.1907 | 5.0202e-10 |
| TYDC2:Phenylalanine:Sample-TYDC1:Phenylalanine:Sample | -0.1422 | -0.1882 | -0.0962 | 3.5938e-09 |
| TYDC1:L-tyrosine:Sample-TYDC1:L-tyrosine:NoE | 0.1477 | 0.0847 | 0.2107 | 5.3332e-07 |
| TYDC2:Phenylalanine:Sample-TYDC2:None:NoS | 0.1047 | 0.0587 | 0.1507 | 8.9371e-07 |
| TYDC2:Phenylalanine:Sample-TYDC2:Phenylalanine:NoE | 0.1048 | 0.0397 | 0.1698 | 0.0002 |
| TYDC2:Levodopa:Sample-TYDC2:None:NoS | 0.0453 | -0.0007 | 0.0913 | 0.0564 |
| TYDC2:Levodopa:Sample-TYDC2:Levodopa:NoE | 0.0455 | -0.0196 | 0.1105 | 0.4494 |
| TYDC1:Levodopa:Sample-TYDC1:None:NoS | 0.0236 | -0.0224 | 0.0696 | 0.8901 |
| TYDC1:Levodopa:Sample-TYDC1:Levodopa:NoE | 0.0237 | -0.0414 | 0.0887 | 0.9969 |
| TYDC2:L-tyrosine:Sample-TYDC2:L-tyrosine:NoE | 0.0005 | -0.0645 | 0.0656 | 1 |
| TYDC1:Tryptophane:Sample-TYDC1:Tryptophane:NoE | 0.0042 | -0.0608 | 0.0693 | 1 |
| TYDC2:Tryptophane:Sample-TYDC2:Tryptophane:NoE | 0.0036 | -0.0614 | 0.0687 | 1 |
| TYDC1:Tryptophane:Sample-TYDC1:None:NoS | 0.0056 | -0.0404 | 0.0516 | 1 |
| TYDC2:L-tyrosine:Sample-TYDC2:None:NoS | 0.0005 | -0.0455 | 0.0465 | 1 |
| TYDC2:Tryptophane:Sample-TYDC2:None:NoS | 0.0041 | -0.0419 | 0.0501 | 1 |

Supplementary Table S9. Tukey's HSD post hoc pairwise comparisons with p-adjusted values > 0.05, indicating non-significant differences in tyramine production across enzyme concentrations.

| Comparison (ng of protein) | Difference | Lower | Upper | Adjusted P-Value |
|---|---|---|---|---|
| 3.75-1.875 | 0.24 | -0.1 | 0.58 | 0.3563 |
| 1.875-0 | 0.15 | -0.19 | 0.49 | 0.8832 |
| 1.875-0.234375 | 0.15 | -0.2 | 0.49 | 0.8954 |
| 1.875-0.46875 | 0.14 | -0.2 | 0.48 | 0.917 |
| 60-30 | 0.13 | -0.22 | 0.47 | 0.9529 |
| 1.875-0.9375 | 0.12 | -0.23 | 0.46 | 0.9755 |
| 120-30 | 0.07 | -0.27 | 0.41 | 0.9995 |
| 120-60 | -0.06 | -0.4 | 0.29 | 0.9999 |
| 0.234375-0 | 0 | -0.34 | 0.35 | 1 |
| 0.46875-0 | 0.01 | -0.33 | 0.35 | 1 |
| 0.9375-0 | 0.03 | -0.31 | 0.38 | 1 |
| 0.46875-0.234375 | 0.01 | -0.34 | 0.35 | 1 |
| 0.9375-0.234375 | 0.03 | -0.31 | 0.37 | 1 |
| 0.9375-0.46875 | 0.03 | -0.32 | 0.37 | 1 |

Supplementary Table S10. Tukey's HSD Post-hoc Test Results (95% Confidence Level, Samples vs Controls) for duration assays

| Comparison | Difference | Lower | Upper | Adjusted P-Value |
|---|---|---|---|---|
| 10:Sample-10:Control | 1.41 | 0.77 | 2.06 | 459000 |
| 40:Sample-40:Control | 1.75 | 1.16 | 2.33 | 1500000 |
| 60:Sample-60:Control | 2.66 | 2.08 | 3.25 | 8610000000 |
| 120:Sample-120:Control | 3.2 | 2.62 | 3.79 | 1070000000 |
| 720:Sample-720:Control | 2.96 | 2.32 | 3.6 | 7370000000 |

Supplementary Table S11. The detailed table with all the calculations. Comparison of different aromatic amino acid decarboxylases that have been characterized using L-tyrosine as a substrate. The values in blue have been determined by either a unit conversion or have been calculated based on the data available in each corresponding article. All values have been converted to identical units to facilitate the comparisons. Only the entries for which all values were present or could be calculated were kept in the table.

| Organism | Enzyme / | Km (µ | kcat ($s^{-1}$) | calculated kcat ($s^{-1}$) | kcat calculation | Vmax (as reported) | Vmax (nkat/mg) | Vmax calculation | Molecul | Reactio | Reference |
|---|---|---|---|---|---|---|---|---|---|---|---|
| lycoris radiata | *Lr* TyDC2 | 60 | - | 0.03199 | from 2.64 µM/min, 100 µL, 10 µg, MW 72.7 | 2.64 µM/min | 0.44 | 2.64×0.1 ÷0.01 ÷60 | 72.7 | 100 | Hu et al. 2022 |
| Narcissus pseudonarcissus | *Np* TyDC1 | 109 | 0.023 | 0.02337 | 4.207 µM/min, 100 µL, 30 µg, MW 100 | 4.207 µM/min | 0.23 | 4.207×0.1 ÷0.03 ÷60 | 100 | 100 | This study |
| Rehmannia glutinosa | *Rg* TyDC2 | 250 | - | 0.15 | 6.424 µM/min, 250 µL, 10 µg, MW 56.05 | 6.424 ± 0.131 µM/min | 2.68 | 6.424×0.25 ÷0.01 ÷60 | 56.05 | 250 | Li et al. 2022 |
| Lycoris radiata | *Lr* TyDC1 | 390 | - | 0.03817 | 3.15 µM/min, 100 µL, 10 µg, MW 72.7 | 3.15 µM/min | 0.53 | 3.15×0.1 ÷0.01 ÷60 | 72.7 | 100 | Hu et al. 2021 |
| Petroselinum crispum | *Pc* AAS | 460 | - | 1.06 | 1.117 µmol/min/mg, MW 57 | 1.117 µmol/min/mg | 18.62 | 1.117×1000 ÷60 | 57 | 100 | Torrens-Spence 2012 |
| Lactobacillus brevis IOEB 9809 | TDC | 580 | - | 0.134 | 115 nmol/min/mg, MW 70 | 115 nmol/min/mg | 1.92 | 115 ÷60 | 70 | 2000 | Moreno-Arribas 1999 |
| Lactobacillus brevis CGMCC 1.2028 | r*Lb* TDC | 590 | 343.1 | 343.1 | reported | 147.1 µmol/min/mg | 2451.67 | 147.1×1000 ÷60 | 70 | 1000 | Zhang & [illegible] |
| Lycoris aurea | *Lau* TyDC | 602 | - | 0.2664 | 3.19 nkat/mg, MW 83.5 | 3.19 ± 0.05 nkat/mg | 3.19 | reported | 83.5 | 150 | Wang et al. 2019 |
| Lactobacillus brevis (Sci Rep 2016) | *Lb* TDC | 630 | 124.8 | 124.8 | reported | - | 1783 | 124.8 $s^{-1}$, MW 70 | 70 | 1000 | Zhu et al. 2016 |
| Lactobacillus brevis ATCC 367 | TDC | 670 | - | 0.077 | 66 nmol/min/mg, MW 70 | 66 nmol/min/mg | 1.1 | 66 ÷60 | 70 | 2000 | Moreno-Arribas 1999 |
| Arabidopsis thaliana | *At* TyrDC | 745 | - | 3.99 | 61.35 nkat/mg, MW 65 | 61.35 nkat/mg | 61.35 | reported | 65 | 300 | Lehmann & Pollmann 2009 |
| Papaver somniferum | *Ps* TyDC1 | 1000 | - | 3.36E-08 | 0.59 × $10^{-15}$ × 57,000,000 = 0.0000000336 | 0.59 fkat/mg | 0 | 0.59×1e-6 | 57 | 1000 | Facchini & De Luca 1995 |
| Papaver somniferum | *Ps* TyDC2 | 1002 | - | 7.08E-09 | 0.12 × $10^{-15}$ × 59,000,000 = 0.00000000708 | 0.12 fkat/mg | 0 | 0.12×1e-6 | 59 | 1000 | Facchini & De Luca 1995 |
| Olea europaea | *Oe* TDC2 | 1290 | 23.98 | 23.98 | reported | 9.93 µM/min | 161.46 | 9.93×0.2 ÷0.000205 ÷60 | 56.4 | 200 | Luaces et al. 2024 |
| Olea europaea | *Oe* TDC1 | 1900 | 12.79 | 12.79 | reported | 5.18 µM/min | 187.68 | 5.18×0.2 ÷0.000092 ÷60 | 56.3 | 200 | Luaces et al. 2024 |

Supplementary Table S12. Accession numbers of all BLASTP hits.

| ID | Enzyme | Organism |
|---|---|---|
| XP_042928513.1 | uncharacterized protein CHLRE_01g028423v5 | Chlamydomonas reinhardtii |
| KAL6764535.1 | aromatic-aminoacid decarboxylase | Haematococcus lacustris |
| BHG22473.1 | Tyrosine decarboxylase 1 | Coccomyxa sp. KJ |
| BDA43194.1 | Aromatic-L-amino-acid decarboxylase | Coccomyxa sp. Obi |
| XP_005646768.1 | aromatic-aminoacid decarboxylase | Coccomyxa subellipsoidea C-169 |
| KAA6422859.1 | MAG: tyrosine decarboxylase | Trebouxia sp. A1-2 |
| XP_011401077.1 | Tyrosine decarboxylase 1 | Auxenochlorella protothecoides |
| GAQ86385.1 | aromatic aldehyde synthase | Klebsormidium nitens |
| XP_009102040.1 | tyrosine decarboxylase 1 | Brassica rapa |
| CAA2998143.1 | tyrosine decarboxylase 1 | Olea europaea subsp. europaea |
| QJA07379.1 | aromatic aldehyde synthase | Olea europaea |
| KAG7636800.1 | Pyridoxal phosphate-dependent decarboxylase | Arabidopsis thaliana x Arabidopsis arenosa |
| XP_034689683.1 | tyrosine decarboxylase 1 | Vitis riparia |
| KAG7584508.1 | Pyridoxal phosphate-dependent decarboxylase | Arabidopsis suecica |
| KAL9300046.1 | Tyrosine decarboxylase 1 | Arabidopsis thaliana |
| XP_002884194.2 | tyrosine decarboxylase 1 | Arabidopsis lyrata subsp. lyrata |
| XP_010652425.1 | phenylacetaldehyde synthase | Vitis vinifera |
| XP_020265332.1 | tyrosine decarboxylase 1 | Asparagus officinalis |
| XP_058207624.1 | phenylacetaldehyde synthase | Rhododendron vialii |
| XP_048529018.1 | tryptophan decarboxylase 2 isoform X1 | Triticum urartu |
| XP_071721071.1 | phenylacetaldehyde synthase | Rutidosis leptorrhynchoides |
| KAL3645050.1 | Tyrosine decarboxylase 2 | Castilleja foliolosa |
| XP_068656100.1 | tyrosine decarboxylase 2 | Aristolochia californica |
| 6EEI_A | Chain A, Tyrosine decarboxylase 1 | Arabidopsis thaliana |
| XP_047071867.1 | tryptophan decarboxylase 2 isoform X1 | Lolium rigidum |
| XP_043610472.1 | phenylacetaldehyde synthase | Ericeron canadensis |
| XP_054800292.1 | tyrosine decarboxylase 2 isoform X1 | Prosopis cineraria |
| XP_020163775.1 | tryptophan decarboxylase 2 | Aegilops tauschii subsp. strangulata |
| XP_044396173.1 | tryptophan decarboxylase 2 isoform X1 | Triticum aestivum |
| KAI7991487.1 | Tyrosine decarboxylase 1 | Camellia lanceoleosa |
| GFP82980.1 | tyrosine decarboxylase 1 | Phtheirospermum japonicum |
| KAL2488032.1 | Tyrosine decarboxylase 1 | Forsythia ovata |
| XP_044946747.1 | tryptophan decarboxylase 2 isoform X1 | Hordeum vulgare subsp. vulgare |
| XP_061343436.1 | tyrosine decarboxylase 2 isoform X2 | Gastrolobium bilobum |
| XP_047167178.1 | tyrosine decarboxylase 2 | Vigna umbellata |
| ULR57006.1 | tyrosine decarboxylase | Rehmannia glutinosa |
| XP_017411095.1 | tyrosine decarboxylase 2 | Vigna angularis |
| XP_013742404.2 | phenylacetaldehyde synthase | Brassica napus |
| XP_021893770.1 | tyrosine decarboxylase 1 | Carica papaya |
| KAK4418449.1 | Tyrosine decarboxylase 1 | Sesamum alatum |
| XP_023764054.1 | phenylacetaldehyde synthase | Lactuca sativa |
| KAF5199076.1 | Tyrosine decarboxylase | Thalictrum thalictroides |
| XP_037440286.1 | tryptophan decarboxylase 2 isoform X1 | Triticum cicocceides |
| XP_038995498.1 | phenylacetaldehyde synthase isoform X1 | Hibiscus syriacus |
| GMI73528.1 | aromatic aldehyde synthase | Hibiscus trionum |
| XP_057965229.1 | tyrosine decarboxylase 2 isoform X1 | Malania oleifera |
| XP_020681680.1 | tryptophan decarboxylase 2 | Dendrobium catenatu |
| KAL1546636.1 | Tyrosine decarboxylase 2 | Salvia divinorum |
| XP_017234290.1 | phenylacetaldehyde synthase isoform X2 | Daucus carota subsp. sativus |
| XP_050364044.1 | tyrosine decarboxylase 2 | Argentina anserina |
| UIP35206.1 | tyrosine decarboxylase 2 | Leucojum aestivum |
| XP_006299006.2 | tyrosine decarboxylase 1 | Capsella rubella |
| MFO7279120.1 | pyridoxal-dependent decarboxylase | Thermoanaerobacteras bacterium |
| KAK1353286.1 | Tryptophan decarboxylase | Heracleum sosnowsky |
| AUI41112.1 | aromatic acetaldehyde synthase | Rhodiola rosea |
| XP_027915667.1 | tryptophan decarboxylase 2 | Vigna unguiculata |
| WJX79094.1 | Tyrosine decarboxylase 2 | Trifolium repens |
| XP_057438483.1 | tyrosine decarboxylase 2 | Lotus japonicus |
| XP_016743391.2 | phenylacetaldehyde synthase | Gossypium hirsutum |
| XP_062019397.1 | phenylacetaldehyde synthase isoform X1 | Rosa rugosa |
| KAL1219337.1 | Phenylacetaldehyde synthase | Cardamine amara subsp. amara |
| XP_065615717.1 | phenylacetaldehyde synthase isoform X5 | Quercus suber |
| XP_059660189.1 | tyrosine decarboxylase 2 | Cornus florida |
| CAN1131424.1 | Phenylacetaldehyde synthase | Linum perenne |
| XP_062148052.1 | phenylacetaldehyde synthase | Alnus glutinosa |
| XP_014494710.1 | tyrosine decarboxylase 1 | Vigna radiata var. radiata |
| XP_012484102.1 | phenylacetaldehyde synthase | Gossypium raimondii |
| KAM5563291.1 | phenylacetaldehyde synthase | Rosa sericea |
| XP_002459778.2 | tyrosine decarboxylase 1 | Sorghum bicolor |
| XP_028794633.1 | tyrosine decarboxylase 1 isoform X2 | Neltuma alba |
| KAK1290117.1 | Tyrosine decarboxylase 1 | Acorus calamus |
| XP_058101404.1 | tyrosine decarboxylase 2 isoform X2 | Magnolia sinica |
| XP_009762727.1 | tyrosine decarboxylase 2 isoform X2 | Nicotiana sylvestris |
| XP_065615717.1 | phenylacetaldehyde synthase isoform X5 | Quercus suber |
| XP_059660189.1 | tyrosine decarboxylase 2 | Cornus florida |
| CAN1131424.1 | Phenylacetaldehyde synthase | Linum perenne |
| XP_062148052.1 | phenylacetaldehyde synthase | Alnus glutinosa |
| XP_014494710.1 | tyrosine decarboxylase 1 | Vigna radiata var. radiata |
| XP_012484102.1 | phenylacetaldehyde synthase | Gossypium raimondii |
| KAM5563291.1 | phenylacetaldehyde synthase | Rosa sericea |
| XP_002459778.2 | tyrosine decarboxylase 1 | Sorghum bicolor |
| XP_028794633.1 | tyrosine decarboxylase 1 isoform X2 | Neltuma alba |
| KAK1290117.1 | Tyrosine decarboxylase 1 | Acorus calamus |
| XP_058101404.1 | tyrosine decarboxylase 2 isoform X2 | Magnolia sinica |
| XP_009762727.1 | tyrosine decarboxylase 2 isoform X2 | Nicotiana sylvestris |
| XP_065615717.1 | phenylacetaldehyde synthase isoform X5 | Quercus suber |
| XP_059660189.1 | tyrosine decarboxylase 2 | Cornus florida |
| CAN1131424.1 | Phenylacetaldehyde synthase | Linum perenne |
| XP_062148052.1 | phenylacetaldehyde synthase | Alnus glutinosa |
| XP_014494710.1 | tyrosine decarboxylase 1 | Vigna radiata var. radiata |
| XP_012484102.1 | phenylacetaldehyde synthase | Gossypium raimondii |
| KAM5563291.1 | phenylacetaldehyde synthase | Rosa sericea |
| XP_002459778.2 | tyrosine decarboxylase 1 | Sorghum bicolor |
| XP_028794633.1 | tyrosine decarboxylase 1 isoform X2 | Neltuma alba |
| KAK1290117.1 | Tyrosine decarboxylase 1 | Acorus calamus |
| XP_058101404.1 | tyrosine decarboxylase 2 isoform X2 | Magnolia sinica |
| XP_009762727.1 | tyrosine decarboxylase 2 isoform X2 | Nicotiana sylvestris |
| XP_065615717.1 | phenylacetaldehyde synthase isoform X5 | Quercus suber |
| XP_059660189.1 | tyrosine decarboxylase 2 | Cornus florida |
| CAN1131424.1 | Phenylacetaldehyde synthase | Linum perenne |
| XP_062148052.1 | phenylacetaldehyde synthase | Alnus glutinosa |
| XP_014494710.1 | tyrosine decarboxylase 1 | Vigna radiata var. radiata |
| XP_012484102.1 | phenylacetaldehyde synthase | Gossypium raimondii |
| KAM5563291.1 | phenylacetaldehyde synthase | Rosa sericea |
| XP_002459778.2 | tyrosine decarboxylase 1 | Sorghum bicolor |
| XP_028794633.1 | tyrosine decarboxylase 1 isoform X2 | Neltuma alba |
| KAK1290117.1 | Tyrosine decarboxylase 1 | Acorus calamus |
| XP_058101404.1 | tyrosine decarboxylase 2 isoform X2 | Magnolia sinica |
| XP_009762727.1 | tyrosine decarboxylase 2 isoform X2 | Nicotiana sylvestris |

Supplementary Table S13. Comparisons to negative controls (statistical analysis)

| Comparisons to negative controls | P values |
|---|---|
| Concentration0 none - Concentration16 Tyr 0.2758892 0.03603576 358 7.656 | 0.0001 |
| Concentration0 none - Concentration32 Tyr 0.4769910 0.03603576 358 13.237 | 0.0001 |
| Concentration0 none - Concentration0.5 Tyr -0.0688463 0.03603576 358 -1.911 | 0.7521 |
| Concentration0 none - Concentration0.125 Tyr -0.0547258 0.03603576 358 -1.519 | 0.9347 |
| Concentration0 none - Concentration0.25 Tyr -0.0456626 0.03603576 358 -1.267 | 0.9826 |
| Concentration0 none - Concentration2 Tyr -0.0410335 0.03603576 358 -1.139 | 0.9927 |
| Concentration0 none - Concentration4 Tyr -0.0290709 0.03603576 358 -0.807 | 0.9997 |
| Concentration0 none - Concentration0.75 Tyr -0.0240714 0.03603576 358 -0.668 | 1 |
| Concentration0 none - Concentration1 Tyr -0.0202579 0.03603576 358 -0.562 | 1 |
| Concentration0 none - Concentration1.5 Tyr 0.0028768 0.03603576 358 0.080 | 1 |
| Concentration0 none - Concentration8 Tyr -0.0209151 0.03603576 358 -0.580 | 1 |

Supplementary Table S14. Comparisons to negative controls (statistical analysis)

| Comparisons to negative controls | P values |
|---|---|
| Concentration0 none - Concentration32 Tyr 0.4149879 0.04179367 354 9.929 | 0.0001 |
| Concentration0 none - Concentration16 Tyr 0.1632940 0.04179367 354 3.907 | 0.0062 |
| Concentration0 none - Concentration0.125 Tyr -0.0474014 0.04179367 354 -1.134 | 0.9929 |
| Concentration0 none - Concentration0.25 Tyr -0.0078599 0.04179367 354 -0.188 | 1 |
| Concentration0 none - Concentration0.5 Tyr -0.0212016 0.04491942 354 -0.472 | 1 |
| Concentration0 none - Concentration0.75 Tyr -0.0178885 0.04179367 354 -0.428 | 1 |
| Concentration0 none - Concentration1 Tyr -0.0079967 0.04179367 354 -0.191 | 1 |
| Concentration0 none - Concentration1.5 Tyr -0.0148619 0.04179367 354 -0.356 | 1 |
| Concentration0 none - Concentration2 Tyr 0.0076507 0.04179367 354 0.183 | 1 |
| Concentration0 none - Concentration4 Tyr -0.0037360 0.04179367 354 -0.089 | 1 |
| Concentration0 none - Concentration8 Tyr -0.0189636 0.04179367 354 -0.454 | 1 |

Supplementary Table S15. Comparisons to negative controls and between samples (statistical analysis)

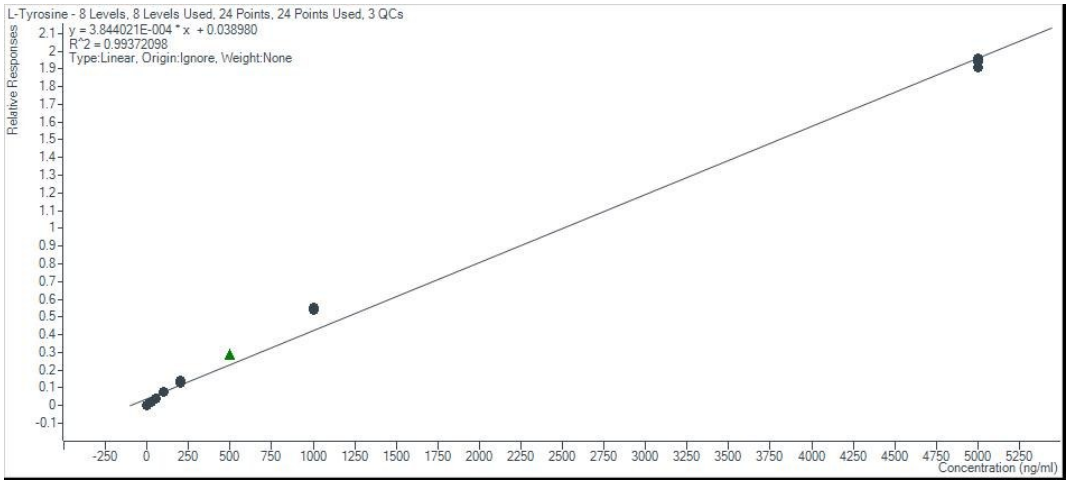
| Comparison | Difference | Lower_95 | Upper_95 | P_adj |
|---|---|---|---|---|
| 4:Tyrosine-4:Control | 9.4553 | 4.4071 | 14.5036 | 0.0001 |
| 3:Tyrosine-3:Control | 9.2886 | 4.2403 | 14.3369 | 0.0002 |
| 5:Tyrosine-5:Control | 9.1775 | 4.1293 | 14.2258 | 0.0002 |
| 4:Tyrosine-3:Tyrosine | 0.1967 | -4.8515 | 5.245 | 1 |
| 5:Tyrosine-3:Tyrosine | 0.1708 | -4.8774 | 5.2191 | 1 |
| 5:Tyrosine-4:Tyrosine | -0.0259 | -5.0742 | 5.0223 | 1 |

Supplementary Table S16. Chlorophyll (430/645) Tukey HSD (vs Negative)

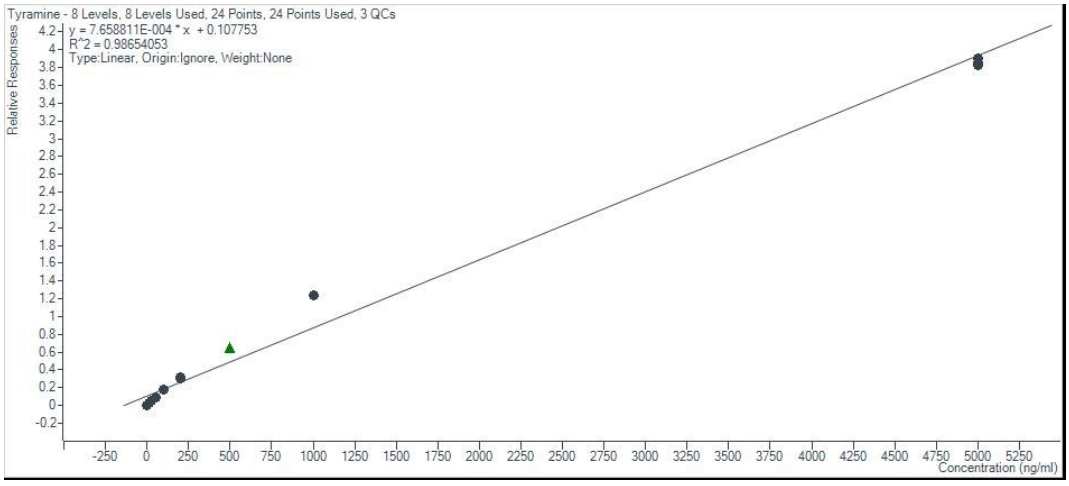
| Comparison | Difference | Lower | Upper | P adjusted |
|---|---|---|---|---|
| 1-Negative | -41.8056 | -171.478 | 87.8669 | 0.9939 |
| 2-Negative | -5.1389 | -134.8113 | 124.5336 | 1 |
| 3-Negative | -15.75 | -145.4224 | 113.9224 | 1 |
| 4-Negative | -45.1111 | -174.7836 | 84.5613 | 0.989 |
| 5-Negative | -48.6389 | -178.3113 | 81.0336 | 0.9806 |
| 6-Negative | -130.4722 | -260.1447 | -0.7998 | 0.0471 |
| 7-Negative | -112.7222 | -242.3947 | 16.9502 | 0.1563 |
| 8-Negative | -13.9167 | -143.5891 | 115.7558 | 1 |
| 9-Negative | 19.0833 | -110.5891 | 148.7558 | 1 |
| Positive-Negative | 13.75 | -115.9224 | 143.4224 | 1 |

Supplementary Table S17. mVenus (500/540) Tukey HSD (vs Positive)

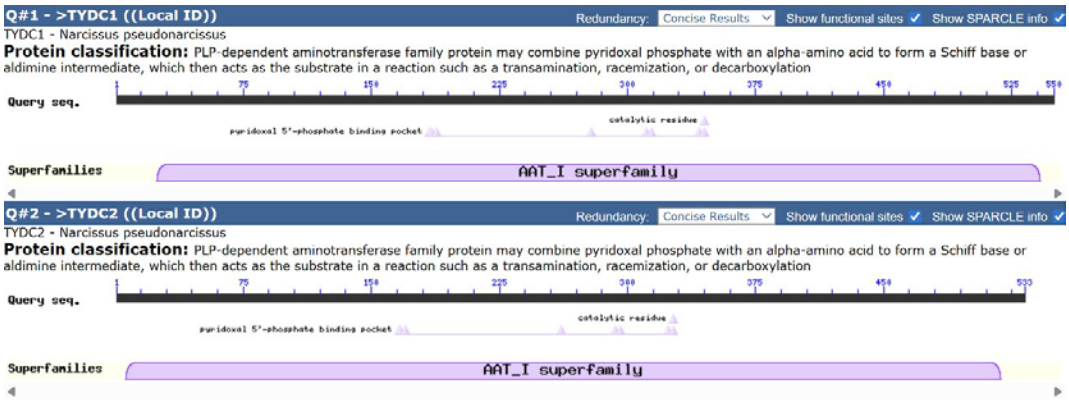
| Comparison | Difference | Lower | Upper | P adjusted |
|---|---|---|---|---|
| 1-Positive | -1128.778 | -1436.757 | -820.7986 | **<2.2251e-308** |
| 2-Positive | -1123.889 | -1431.868 | -815.9097 | **<2.2251e-308** |
| 3-Positive | -1127.639 | -1435.618 | -819.6597 | **<2.2251e-308** |
| 4-Positive | -1126.139 | -1434.118 | -818.1597 | **<2.2251e-308** |
| 5-Positive | -1108.361 | -1416.34 | -800.3819 | **<2.2251e-308** |
| 6-Positive | -1088.306 | -1396.285 | -780.3264 | **<2.2251e-308** |
| 7-Positive | -1077.056 | -1385.035 | -769.0764 | **<2.2251e-308** |
| 8-Positive | -1118.944 | -1426.924 | -810.9653 | **<2.2251e-308** |
| 9-Positive | -1131.583 | -1439.562 | -823.6042 | **<2.2251e-308** |
| Negative-Positive | -1101.833 | -1409.812 | -793.8542 | **<2.2251e-308** |



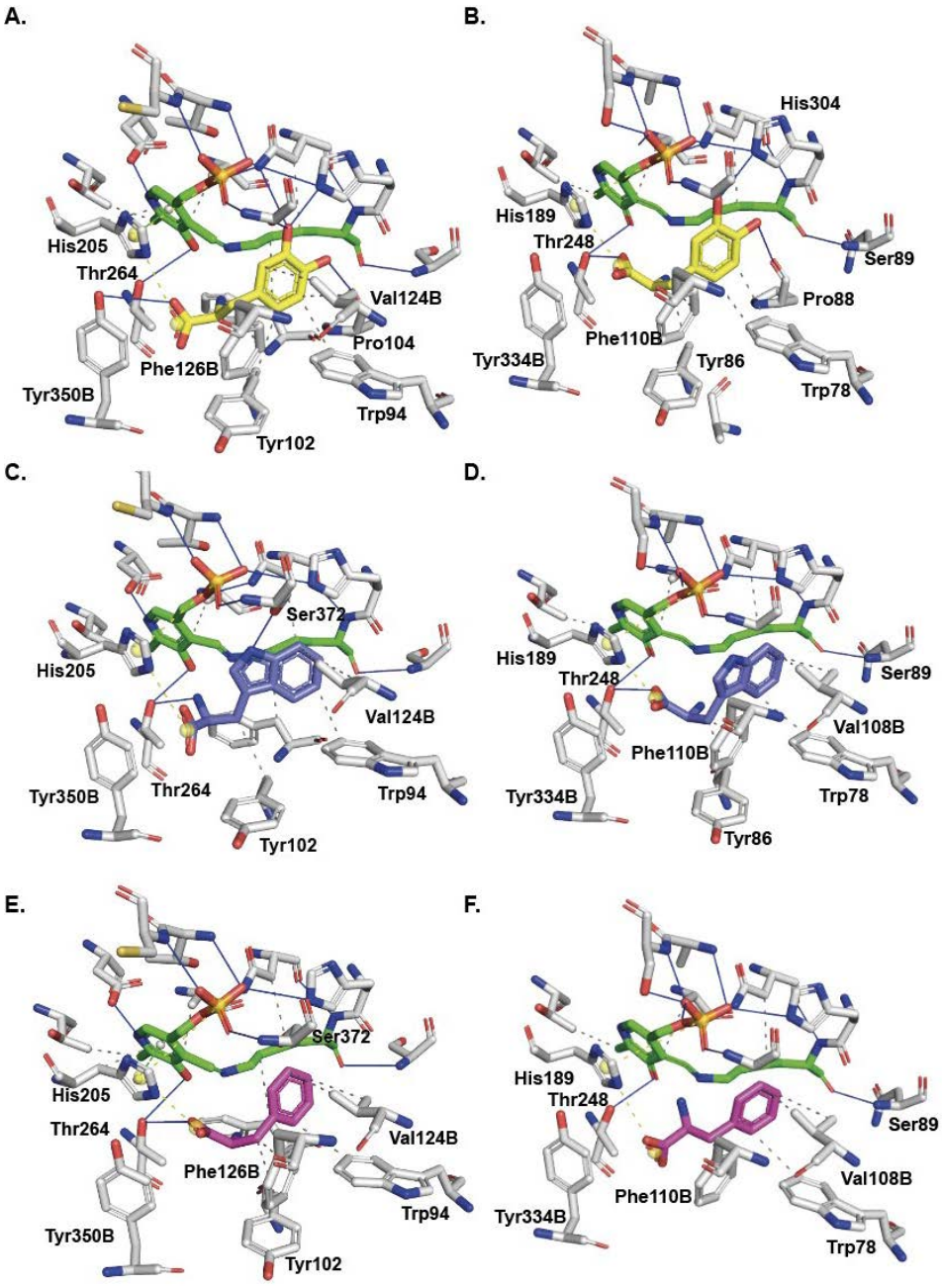

Supplementary Figure S1. The calibration curves obtained by plotting the area ratio for L-tyrosine.




Supplementary Figure S2. The calibration curves obtained by plotting the area ratio for tyramine.



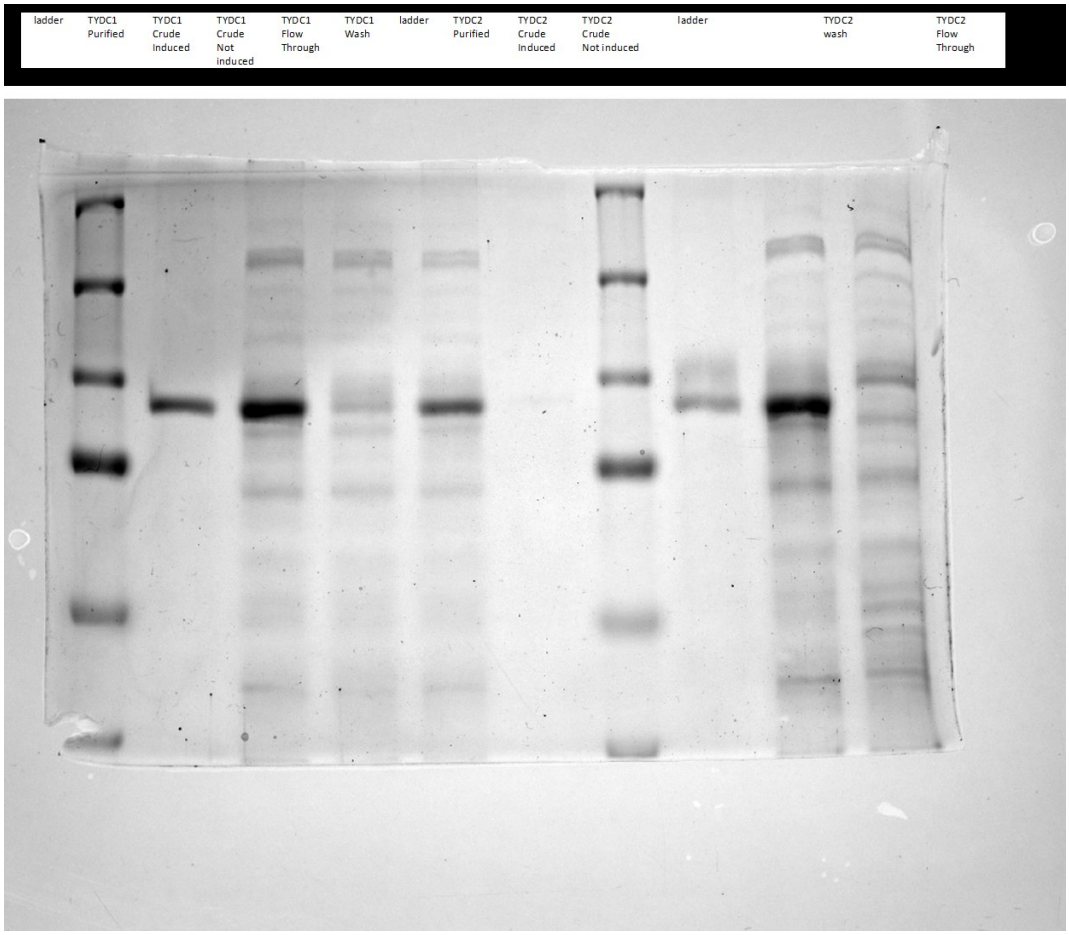

Supplementary Figure S3. Conserved domain analysis of tyrosine decarboxylase isoforms TyDC1 and TyDC2.



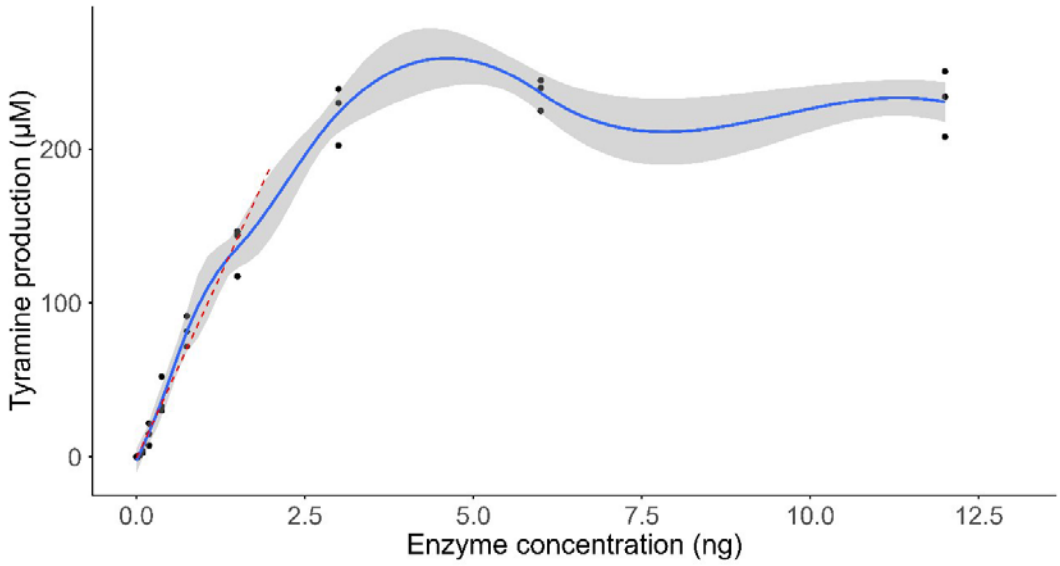

Supplementary Figure S4. *Np*TyDC1 (A, C, E) and *Np*TyDC2 (B, D, F) active site accepts diverse ligands. Active site residues are shown as grey sticks, while LLP is shown as green sticks. H-bonds are shown as blue lines, hydrophobic bonds as dotted grey lines, and salt bridges as dotted yellow lines with yellow spheres. Amino acids from chain B are identified with "B." A. and B.; Yellow sticks: docked $_{L}$-DOPA. C. and D.; Purple sticks: docked $_{L}$-tryptophan. E. and F.; Pink sticks: docked phenylalanine.



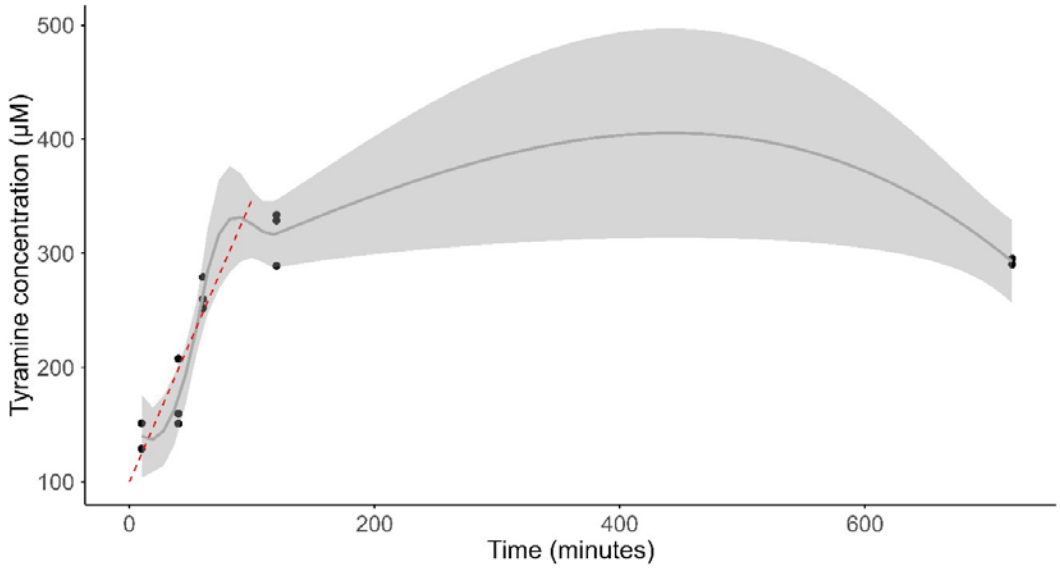
Supplementary Figure S5. Superposition of *Np*TYDC2 (in pink) and *Np*TyDC1 in yellow with the shift in position of Leu355 (red) in *Np*TyDC2



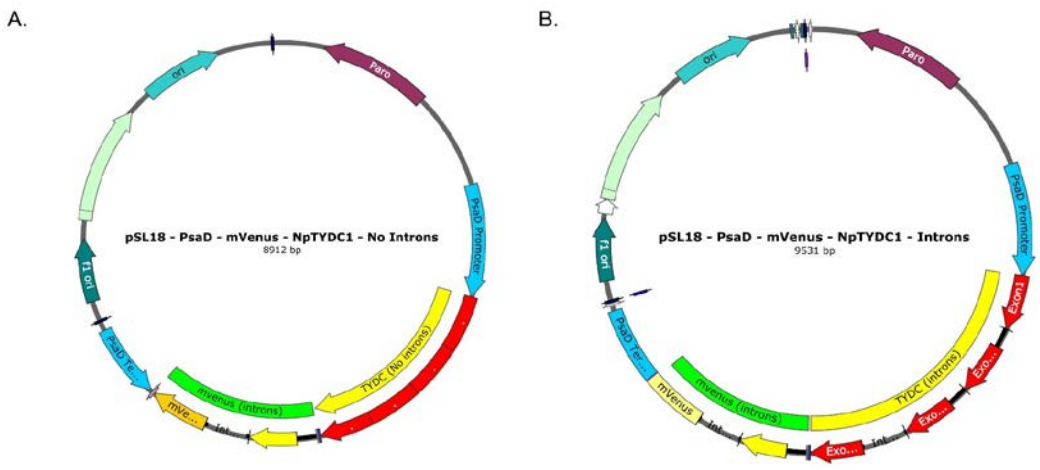

Supplementary Figure S6. SDS_PAGE results.




Supplementary Figure S7. Effect of enzyme concentration on tyramine production by *Np*TyDC1. 95% Confidence level calculated using 3 replicates.

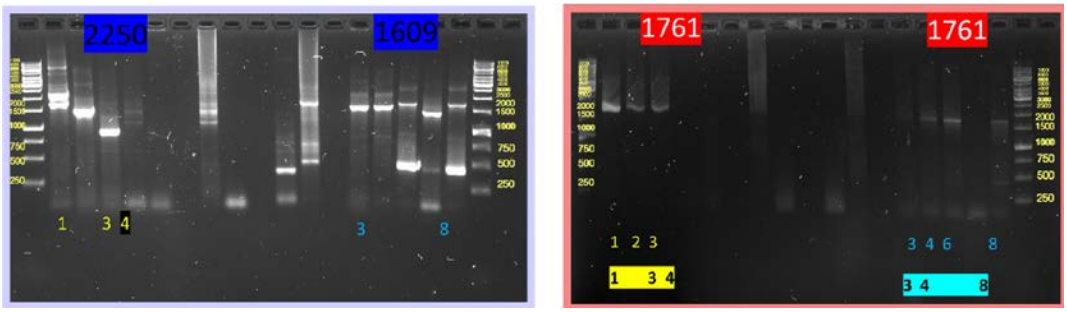



Supplementary Figure S8. Effect of reaction duration on tyramine production by *Np*TyDC1. 95% Confidence level calculated using 3 replicates.

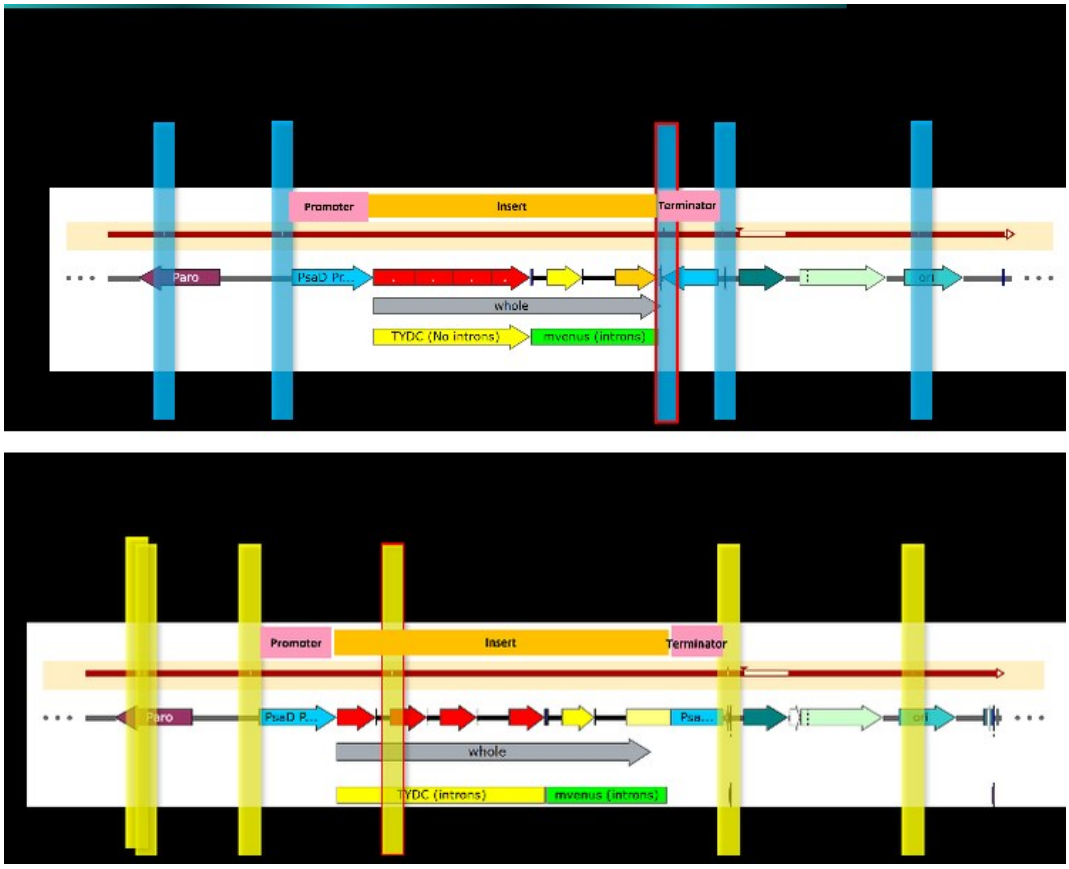



Supplementary Figure S10. Assembly strategy and final Gibson product for the *Np*TyDC1 expression cassette. Schematic representation of Gibson assembly for codon-optimized *Np*TyDC1 constructs designed for expression in *C. reinhardtii*. The plasmid backbone (pSL18) contains an origin of replication (ori, teal) and a paromomycin resistance gene (purple). Expression is driven by the PsaD promoter (blue) and terminated by the PsaD terminator (blue). The coding region includes mVenus (yellow) fused to *Np*TyDC1 (red, with "Exo." or "Exon1" indicating exon blocks), with or without introns (gray segments within mVenus and black segments within *Np*TyDC1). Panel A shows the intron-free construct, while Panel B shows the intron-containing version.

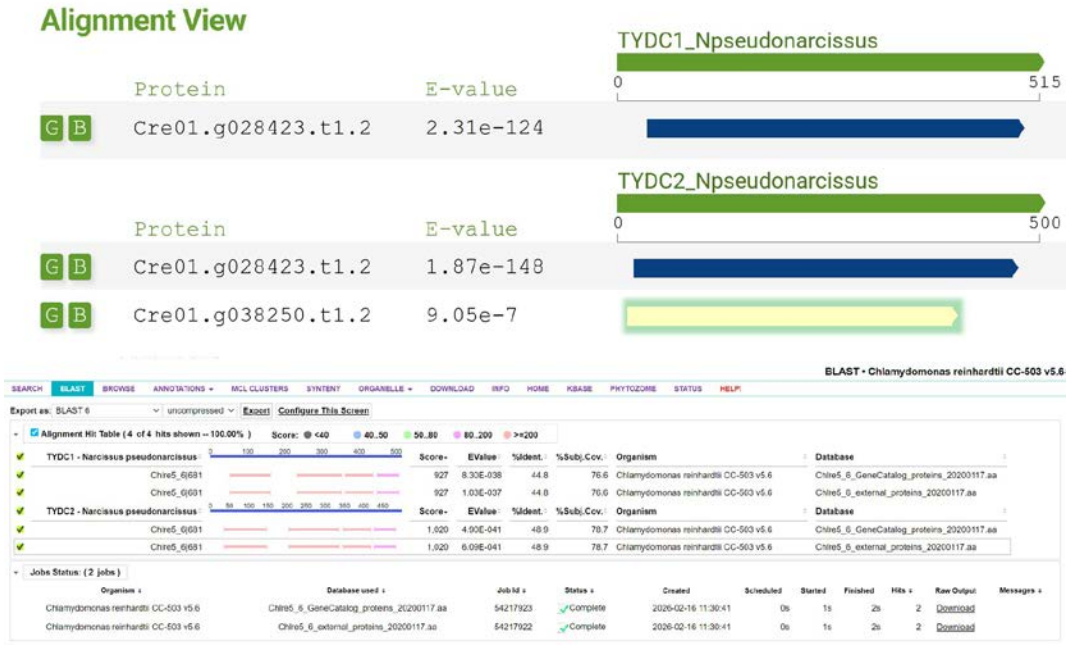
Supplementary Figure S11. Intermediate Gibson assembly validation by gel electrophoresis. Agarose gel images showing intermediate and final Gibson assembly products. Bands correspond to expected fragment sizes at each assembly step.



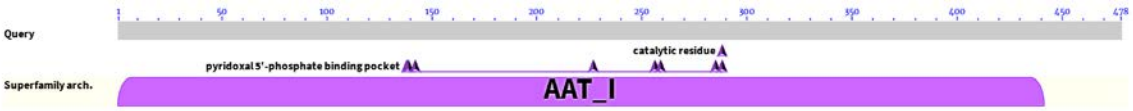

Supplementary Figure S12. Colony PCR screening of intron-containing and intron-free *Np*TyDC1 constructs prior to transformation. The colonies 1,3,4 from the construct with introns and colonies 3,4,8 from the sample without intron were chosen for digestion based on if they had a band present in both colony PCRs (second and third). The middle is negative and positive controls. Negative control 1 is water, negative control 2 is empty vector. Positive controls are the respective diluted Gibson's assembly products.



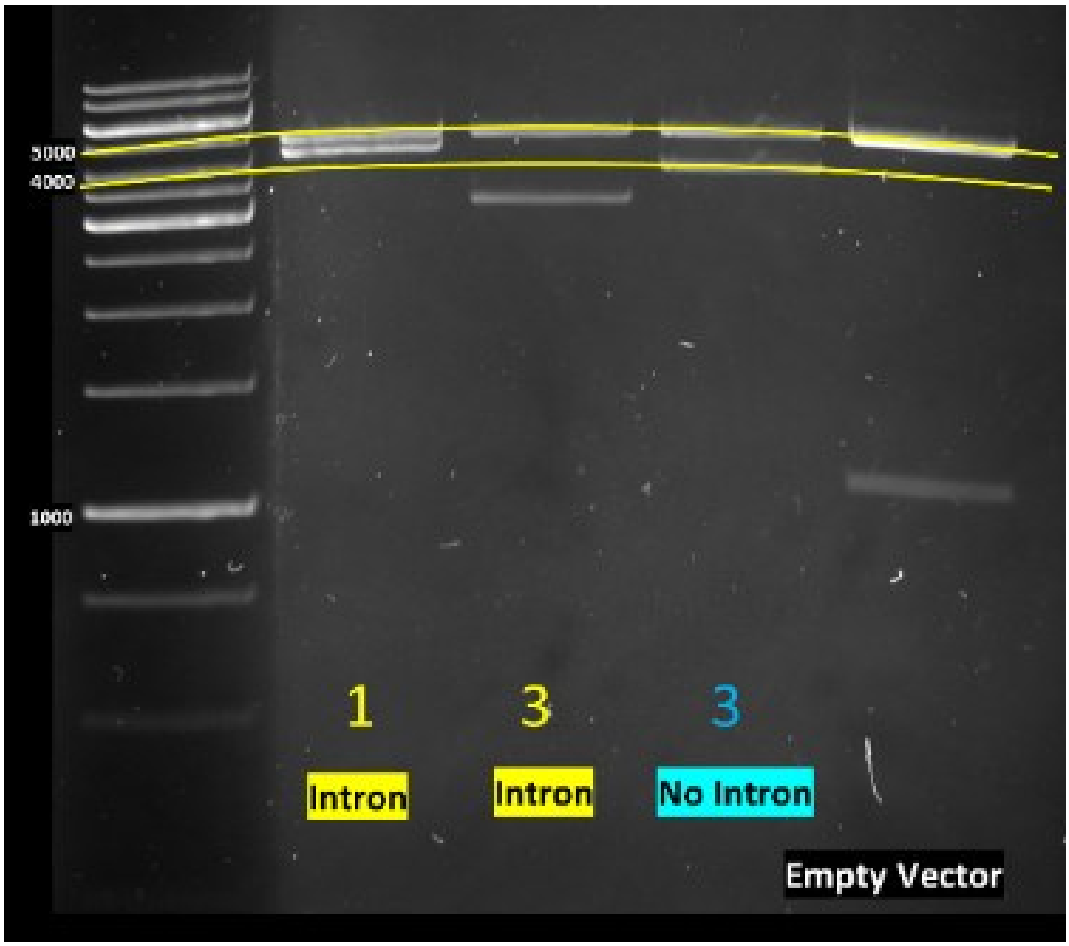

Supplementary Figure S13. Sequencing results confirm a deletion in one intron-containing construct and intact coding sequence in the intron-free construct.




Supplementary Figure S14. C. protein hit data.




Supplementary Figure S15. Conserve Domain of *Cr*AAT.




Supplementary Figure S16. Restriction digestion analysis of validated *Np*TyDC1 construct. Agarose gel showing restriction digestion profiles of selected clones. Fragment sizes match predicted patterns for the correctly assembled *Np*TyDC1 expression cassette.

# Chapter 6 - References

Adasme, Melissa F., Katja L. Linnemann, Sarah Naomi Bolz, Florian Kaiser, Sebastian Salentin, V. Joachim Haupt, and Michael Schroeder. 2021. 'PLIP 2021: expanding the scope of the protein–ligand interaction profiler to DNA and RNA', *Nucleic Acids Research*, 49: W530–W34.

Alcazar, R., M. Bueno, and A. F. Tiburcio. 2020. 'Polyamines: Small Amines with Large Effects on Plant Abiotic Stress Tolerance', *Cells*, 9.

Aniszewski, T. 2007. *Alkaloids - Secrets of Life*.

Ashihara, H., H. Sano, and A. Crozier. 2008. 'Caffeine and related purine alkaloids: biosynthesis, catabolism, function and genetic engineering', *Phytochemistry*, 69: 841–56.

Baghban, R., S. Farajnia, Y. Ghasemi, M. Mortazavi, N. Zarghami, and N. Samadi. 2018. 'New Developments in *Pichia pastoris* Expression System, Review and Update', *Current Pharmaceutical Biotechnology*, 19: 451–67.

Baier, T., N. Jacobebbinghaus, A. Einhaus, K. J. Lauersen, and O. Kruse. 2020. 'Introns mediate post-transcriptional enhancement of nuclear gene expression in the green microalga *Chlamydomonas reinhardtii*', *PLoS Genetics*, 16: e1008944.

Baier, T., J. Wichmann, O. Kruse, and K. J. Lauersen. 2018. 'Intron-containing algal transgenes mediate efficient recombinant gene expression in the green microalga *Chlamydomonas reinhardtii*', *Nucleic Acids Research*, 46: 6909–19.

Bankhead, P., M. B. Loughrey, J. A. Fernandez, Y. Dombrowski, D. G. McArt, P. D. Dunne, S. McQuaid, R. T. Gray, L. J. Murray, H. G. Coleman, J. A. James, M. Salto-Tellez, and P. W. Hamilton. 2017. 'QuPath: Open source software for digital pathology image analysis', *Scientific Reports*, 7: 16878.

Barahimipour, R., D. Strenkert, J. Neupert, M. Schroda, S. S. Merchant, and R. Bock. 2015. 'Dissecting the contributions of GC content and codon usage to gene expression in the model alga *Chlamydomonas reinhardtii*', *Plant Journal*, 84: 704–17.

Barkham, J. P. , and C. E. Hance. 1982. 'Population Dynamics of the Wild Daffodil (*Narcissus Pseudonarcissus*)', *Journal of Ecology*.

Barton, D. H. R., G. W. Kirbi, J. B. Taylor, and Thomas G. M. 1963. 'Phenol oxidation and biosynthesis. Part VI. The biogenesis of Arnaryllidaceae alkaloids', *Journal of the Chemical Society*: 4545–58.

Bastida, J., S. Berkov, L. Torras, N. B. P.  Jean Paulo de Andrade, V. Martínez, C. Codina, and F. Viladomat. 2011. 'Chemical and biological aspects of Amaryllidaceae alkaloids'.

Beauchemin, R., N. Merindol, E. Fantino, P. Lavoie, S. B. Nouemssi, F. Meddeb-Mouelhi, and I. Desgagne-Penix. 2024. 'Successful reversal of transgene silencing in *Chlamydomonas reinhardtii*', *The Biotechnology Journal* 19: e2300232.

Bell, E. A. 2003. 'Nonprotein amino acids of plants: Significance in medicine, nutrition, and agriculture', *Journal of Agriculture and Food Chemistry*, 51: 2854–65.

Bhambhani, S., K. R. Kondhare, and A. P. Giri. 2021. 'Diversity in Chemical Structures and Biological Properties of Plant Alkaloids', *Molecules*, 26.

Bolanos-Martinez, O. C., G. Mahendran, S. Rosales-Mendoza, and S. Vimolmangkang. 2022. 'Current Status and Perspective on the Use of Viral-Based Vectors in Eukaryotic Microalgae', *Marine Drugs*, 20.

Camara, J. S., R. Perestrelo, R. Ferreira, C. V. Berenguer, J. A. M. Pereira, and P. C. Castilho. 2024. 'Plant-Derived Terpenoids: A Plethora of Bioactive Compounds with Several

Health Functions and Industrial Applications-A Comprehensive Overview', *Molecules*, 29.

Cheng, A. X., Y. G. Lou, Y. B. Mao, S. Lu, L. J. Wang, and X. Y. Chen. 2007. 'Plant Terpenoids: Biosynthesis and Ecological Functions', *Journal of Integrative Plant Biology*, 49: 179–86.

Cho, J. S., G. B. Kim, H. Eun, C. W. Moon, and S. Y. Lee. 2022. 'Designing Microbial Cell Factories for the Production of Chemicals', *JACS Au*, 2: 1781–99.

Cortes, N., R. Alvarez, E. H. Osorio, F. Alzate, S. Berkov, and E. Osorio. 2015. 'Alkaloid metabolite profiles by GC/MS and acetylcholinesterase inhibitory activities with binding-mode predictions of five Amaryllidaceae plants', *Journal of Pharmaceutical and Biomedical Analysis*, 102: 222–8.

Demir, S. C., A. B. Yildirim, A. U. Turker, and I. Eker. 2022. 'Seasonal variation in alkaloid content, phenolic constituent and biological activities of some *Leucojum aestivum* L. populations in Turkey', *South African Journal of Botany*, 147: 713–23.

Desgagné-Penix, I. 2021. 'Biosynthesis of alkaloids in Amaryllidaceae plants: a review', *Phytochemistry Reviews*, 20: 409–31.

Dey, P., A. Kundu, H. J. Chakraborty, B. Kar, W. S. Choi, B. M. Lee, T. Bhakta, A. G. Atanasov, and H. S. Kim. 2019. 'Therapeutic value of steroidal alkaloids in cancer: Current trends and future perspectives', *International Journal of Cancer*, 145: 1731–44.

Diamond, A., and I. Desgagné-Penix. 2016. 'Metabolic engineering for the production of plant isoquinoline alkaloids', *Plant Biotechnology Journal*, 14: 1319–28.

Dias, D. A., S. Urban, and U. Roessner. 2012. 'A historical overview of natural products in drug discovery', *Metabolites*, 2: 303–36.

Donovan, C. W. , Robinson N., and B. R. Glick. 1996. 'Review: Optimizing inducer and culture conditions for expression of foreign proteins under the control of the lac promoter', *Journal of Industrial Microbiology*, 16: 145–54.

Dyo, Y. M., and S. Purton. 2018. 'The algal chloroplast as a synthetic biology platform for production of therapeutic proteins', *Microbiology*, 164: 113–21.

Eichhorn, J, T Takada, Y Kita, and M. H. Zenk. 1998. 'Biosynthesis of the Amaryllidaceae Alkaloid Galanthamine', *Phytochemistry*, 49.

Eijkman, J. F. 1885. 'Sur les principes constituants de l'Illicium religiosum (Sieb.) (Shikimi-no-ki en japonais)'.

Einhaus, A., J. Steube, R. A. Freudenberg, J. Barczyk, T. Baier, and O. Kruse. 2022. 'Engineering a powerful green cell factory for robust photoautotrophic diterpenoid production', *Metabolic Engineering*, 73: 82–90.

El Tahchy, A., A. Ptak, M. Boisbrun, E. Barre, C. Guillou, F. Dupire, F. Chretien, M. Henry, Y. Chapleur, and D. Laurain-Mattar. 2011. 'Kinetic study of the rearrangement of deuterium-labeled 4'-O-methylnorbelladine in *Leucojum aestivum* shoot cultures by mass spectrometry. Influence of precursor feeding on amaryllidaceae alkaloid accumulation', *Journal of Natural Products*, 74: 2356–61.

Ettl, H. 1976. 'Die Gattung Chlamydomonas Ehrenberg', *Beihefte zur Nova Hedwigia*.

Facchini, P. J., J. Bohlmann, P. S. Covello, V. De Luca, R. Mahadevan, J. E. Page, D. K. Ro, C. W. Sensen, R. Storms, and V. J. Martin. 2012. 'Synthetic biosystems for the production of high-value plant metabolites', *Trends Biotechnology*, 30: 127–31.

Facchini, P. J., and V. De Luca. 1994. 'Differential and tissue-specific expression of a gene family for tyrosine/dopa decarboxylase in opium poppy', *Journal of Biological Chemistry*, 269: 26684–90.

Facchini, P.J., K.L. Huber-Allanach, and L.W. Tari. 2000. 'Plant aromatic L-amino acid decarboxylases: evolution, biochemistry, regulation, and metabolic engineering applications', *Phytochemistry*.

Facchini, Peter J., A. G. Johnson, J. Poupart, and Vincenzo De Luca. 1994. 'Expression in Escherichia coli and partial characterization of two tyrosine/dopa decarboxylases from opium poppy', *Phytochemistry*, 38: 1119–26.

Ferdausi, A., X. Chang, A. Hall, and M. Jones. 2020. 'Galanthamine production in tissue culture and metabolomic study on Amaryllidaceae alkaloids in *Narcissus pseudonarcissus* cv. Carlton', *Industrial Crops and Products*, 144.

Ferrer, J. L., J. M. Jez, M. E. Bowman, R. A. Dixon, and J. P. Noel. 1999. 'Structure of chalcone synthase and the molecular basis of plant polyketide biosynthesis', *Nature*.

Fischer, N., and J. D. Rochaix. 2001. 'The flanking regions of PsaD drive efficient gene expression in the nucleus of the green alga *Chlamydomonas reinhardtii*', *Molecular Genetics and Genomics*, 265: 888–94.

Fossati, E., A. Ekins, L. Narcross, and Y. Zhu. 2014. 'Reconstitution of a 10-gene pathway for synthesis of the plant alkaloid dihydrosanguinarine in *Saccharomyces cerevisiae*', *Nature Communications*.

Fuhrmann, M., W. Oertel, and P. Hegemann. 1999. 'A synthetic gene coding for the green fluorescent protein (GFP) is a versatile reporter in *Chlamydomonas reinhardtii*', *Plant Journal*, 19: 353–61.

Galanie, S. M., K. Thodey, I. F. Interrante, C. J. Trenchard, and D. Smolke. 2015. 'Complete biosynthesis of opioids in yeast', *Synthetic Biology*.

Gallaher, S. D., S. T. Fitz-Gibbon, A. G. Glaesener, M. Pellegrini, and S. S. Merchant. 2015. '*Chlamydomonas* Genome Resource for Laboratory Strains Reveals a Mosaic of Sequence Variation, Identifies True Strain Histories, and Enables Strain-Specific Studies', *Plant Cell*, 27: 2335–52.

Gallaher, S. D., S. T. Fitz-Gibbon, D. Strenkert, S. O. Purvine, M. Pellegrini, and S. S. Merchant. 2018. 'High-throughput sequencing of the chloroplast and mitochondrion of *Chlamydomonas reinhardtii* to generate improved de novo assemblies, analyze expression patterns and transcript speciation, and evaluate diversity among laboratory strains and wild isolates', *Plant Journal*, 93: 545–65.

Gálvez-Valdivieso, Gregorio, Manuel Pineda, and Miguel Aguilar. 2010. 'Functional Characterization and Expression Analysis Ofp-Hydroxyphenylpyruvate Dioxygenase from the Green Alga *Chlamydomonas Reinhardtii* (Chlorophyta)', *Phycological Society of America*, 46: 297–308.

Garagounis, C., N. Delkis, and K. K. Papadopoulou. 2021. 'Unraveling the roles of plant specialized metabolites: using synthetic biology to design molecular biosensors', *New Phytologist*, 231: 1338–52.

Georgiev, V., I. Ivanov, and A. Pavlov. 2020. 'Recent Progress in Amaryllidaceae Biotechnology', *Molecules*, 25.

Gershenzon, J., and N. Dudareva. 2007. 'The function of terpene natural products in the natural world', *Nature Chemical Biology*, 3: 408–14.

Gleadow, R. M., and B. L. Moller. 2014. 'Cyanogenic glycosides: synthesis, physiology, and phenotypic plasticity', *Annual review of plant biology*, 65: 155–85.

Gnanasekaran, T., D. Karcher, A. Z. Nielsen, H. J. Martens, S. Ruf, X. Kroop, C. E. Olsen, M. S. Motawie, M. Pribil, B. L. Moller, R. Bock, and P. E. Jensen. 2016. 'Transfer of the cytochrome P450-dependent dhurrin pathway from *Sorghum bicolor* into *Nicotiana tabacum* chloroplasts for light-driven synthesis', *Journal of Experimental Botany*, 67: 2495–506.

Goodenough, U. W. , and J. E. Heuser. 1985. 'The *Chlamydomonas* Cell Wall Glycoproteins and Its Constituent Analyzed by the Quick-Freeze, Deep-Etch Technique'.

Greger, H. 2015. 'Alkamides: a critical reconsideration of a multifunctional class of unsaturated fatty acid amides', *Phytochemistry Reviews*, 15: 729–70.

Grigoriev, I. V., R. D. Hayes, S. Calhoun, B. Kamel, A. Wang, S. Ahrendt, S. Dusheyko, R. Nikitin, S. J. Mondo, A. Salamov, I. Shabalov, and A. Kuo. 2021. 'PhycoCosm, a comparative algal genomics resource', *Nucleic Acids Research*, 49: D1004–D11.

Hanks, Gordon R. 2002. *Medicinal and Aromatic Plants - Industrial Profiles - Narcissus and Daffodil The Genus Narcissus*.

Hanus, L. O., S. M. Meyer, E. Munoz, O. Taglialatela-Scafati, and G. Appendino. 2016. 'Phytocannabinoids: a unified critical inventory', *Natural Product Reports*, 33: 1357–92.

Harris, E. 2001. '*Chlamydomonas* As a Model Organism'.

Heitzer, M., and B. Zschoernig. 2007. 'Construction of modular tandem expression vectors for the green alga *Chlamydomonas reinhardtii* using the Cre/lox-system', *Biotechniques*, 43: 324, 26, 28 passim.

Henikoff, S., and J. G. Henikoff. 1992. 'Amino acid substitution matrices from protein blocks', *Biochemistry*.

Herrmann, K. M., and L. M. Weaver. 1999. 'The Shikimate Pathway'.

Hnin, S. Y. Y., Y. Nakashima, and H. Morita. 2024. 'Substrate Flexibilities of Norbelladine Synthase and Noroxomaritidine/Norcraugsodine Reductase for Hydroxylated and/or Methoxylated Aldehydes', *Chemical and Pharmaceutical Bulletin*, 72: 507–11.

Holsters, M. , and B. Silva. 1980. 'The Functional Organization of the Nopaline *A. tumerfaciens* Plasmid pTiC58', *Plasmid*, 3: 212–30.

Hotchandani, T., J. de Villers, and I. Desgagne-Penix. 2019. 'Developmental Regulation of the Expression of Amaryllidaceae Alkaloid Biosynthetic Genes in *Narcissus papyraceus*', *Genes*, 10.

Hu, J., W. Li, Z. Liu, G. Zhang, and Y. Luo. 2021. 'Molecular cloning and functional characterization of tyrosine decarboxylases from galanthamine-producing *Lycoris radiata*', *Acta Physiologiae Plantarum*, 43.

Huang, T., G. Jander, and M. de Vos. 2011. 'Non-protein amino acids in plant defense against insect herbivores: representative cases and opportunities for further functional analysis', *Phytochemistry*, 72: 1531–7.

Hyun, M. W., Y. H. Yun, J. Y. Kim, and S. H. Kim. 2011. 'Fungal and Plant Phenylalanine Ammonia-lyase', *Mycobiology*, 39: 257–65.

Iannone, R, Cheng J, Schloerke B, Hughes E, Lauer A, Seo J, and Roy O Brevoort K. 2025. "gt: Easily Create Presentation-Ready Display Tables." In.

Irwin, J. J., K. G. Tang, J. Young, C. Dandarchuluun, B. R. Wong, M. Khurelbaatar, Y. S. Moroz, J. Mayfield, and R. A. Sayle. 2020. 'ZINC20-A Free Ultralarge-Scale Chemical Database for Ligand Discovery', *J Chem Inf Model*, 60: 6065–73.

James W. Byng, Mark W. Chase, Maarten J. M. Christenhusz, Michael F. Fay, Walter S. Judd, David J. Mabberley, Alexander N. Sennikov, Douglas E. Soltis, Pamela S. Soltis and Peter F. Stevens. 2016. 'An update of the Angiosperm Phylogeny Group classification for the orders and families of flowering plants', *Botanical Journal of the Linnean Society*, 181: 1–20.

Jarvis, P. 2008. 'Targeting of nucleus-encoded proteins to chloroplasts in plants', *New Phytologist*, 179: 257–85.

Jayawardena, T. U., N. Merindol, N. S. Liyanage, and I. Desgagne-Penix. 2024. 'Unveiling Amaryllidaceae alkaloids: from biosynthesis to antiviral potential - a review', *Natural Product Reports*, 41: 721–47.

Jiang, Y., N. Xia, X. Li, W. Shen, L. Liang, C. Wang, R. Wang, F. Peng, and B. Xia. 2011. 'Molecular cloning and characterization of a phenylalanine ammonia-lyase gene (LrPAL) from *Lycoris radiata*', *Molecular Biology Reports*, 38: 1935–40.

Ka, S., N. Merindol, A. A. Sow, A. Singh, K. Landelouci, M. B. Plourde, G. Pepin, M. Masi, R. Di Lecce, A. Evidente, M. Seck, L. Berthoux, L. Chatel-Chaix, and I. Desgagne-Penix. 2021. 'Amaryllidaceae Alkaloid Cherylline Inhibits the Replication of Dengue and Zika Viruses', *Antimicrobial Agents and Chemotherapy*, 65: e0039821.

Karimzadegan, V., M. Koirala, S. Sobhanverdi, N. Merindol, B. B. Majhi, S. E. Gelinas, V. I. Timokhin, J. Ralph, M. Dastmalchi, and I. Desgagne-Penix. 2024. 'Characterization of cinnamate 4-hydroxylase (CYP73A) and p-coumaroyl 3'-hydroxylase (CYP98A) from *Leucojum aestivum*, a source of Amaryllidaceae alkaloids', *Plant Physiology and Biochemistry*, 210: 108612.

Kawalleck, P., H. Keller, K. Hahlbrock, D. Scheel, and I. E. Somssich. 1993. 'A pathogen-responsive gene of parsley encodes tyrosine decarboxylase', *Journal of Biological Chemistry*, 268: 2189–94.

Kilgore, M. B., M. M. Augustin, C. M. Starks, M. O'Neil-Johnson, G. D. May, J. A. Crow, and T. M. Kutchan. 2014. 'Cloning and characterization of a norbelladine 4'-O-methyltransferase involved in the biosynthesis of the Alzheimer's drug galanthamine in *Narcissus* sp. aff. *pseudonarcissus*', *PLoS One*, 9: e103223.

Kilgore, M. B., C. K. Holland, J. M. Jez, and T. M. Kutchan. 2016. 'Identification of a Noroxomaritidine Reductase with Amaryllidaceae Alkaloid Biosynthesis Related Activities', *Journal of Biological Chemistry*, 291: 16740–52.

Kilgore, M. B., and T. M. Kutchan. 2016. 'The Amaryllidaceae alkaloids: biosynthesis and methods for enzyme discovery', *Phytochemistry Reviews*, 15: 317–37.

Kilgore, Matthew B., Megan M. Augustin, Courtney M. Starks, Mark O'Neil-Johnson, Gregory D. May, John A. Crow, and Toni M. Kutchan. 2014. 'Cloning and Characterization of a Norbelladine 4′-O-Methyltransferase Involved in the Biosynthesis of the Alzheimer's Drug Galanthamine in Narcissus sp. aff. pseudonarcissus', *PLOS ONE*, 9: e103223.

Kindle, K. L. 1990. 'High-frequency nuclear transformation of *Chlamydomonas reinhardtii*'.

Kington, S. . 2008. *The international daffodil register and classified list* (THE ROYAL HORTICULTURAL SOCIETY).

Kitney, R., and P. Freemont. 2012. 'Synthetic biology - the state of play', *FEBS Letters*, 586: 2029–36.

Koirala, M., V. Karimzadegan, N. S. Liyanage, N. Merindol, and I. Desgagne-Penix. 2022. 'Biotechnological Approaches to Optimize the Production of Amaryllidaceae Alkaloids', *Biomolecules*, 12.

Koirala, Manoj, Natacha Merindol, Vahid Karimzadegan, Sarah-Eve Gélinas, Nuwan Sameera Liyanage, Basanta Lamichhane, Maria Camila García Tobón, Patrick Lagüe, and Isabel Desgagné-Penix. 2024. 'Kinetic and in silico structural characterization of norbelladine O-methyltransferase of Amaryllidaceae alkaloids biosynthesis', *Journal of Biological Chemistry*, 300: 107649.

Kruse, T., C. Gehl, M. Geisler, M. Lehrke, P. Ringel, S. Hallier, R. Hansch, and R. R. Mendel. 2010. 'Identification and biochemical characterization of molybdenum cofactor-binding proteins from *Arabidopsis thaliana*', *Journal of Biological Chemistry*, 285: 6623–35.

Kumar, A., V. R. Falcao, and R. T. Sayre. 2013. 'Evaluating nuclear transgene expression systems in *Chlamydomonas reinhardtii*', *Algal Research*, 2: 321–32.

Lamichhane, B., S. E. Gelinas, N. Merindol, M. Koirala, K. C. G. Dos Santos, H. Germain, and I. Desgagne-Penix. 2025. 'Elucidating the enzyme network driving Amaryllidaceae alkaloids biosynthesis in *Leucojum aestivum*', *Plant Biotechnology Journal*, 23: 1988–2005.

Landymore, A.r F., and N. J. Antia. 2008. 'Growth of a Marine Diatom and a Haptophycean Alga on Phenylalanine or Tyrosine Serving as Sole Nitrogen Source', *Journal of Phycology*, 13: 231–38.

Lauersen, K. J., T. Baier, J. Wichmann, R. Wordenweber, J. H. Mussgnug, W. Hubner, T. Huser, and O. Kruse. 2016. 'Efficient phototrophic production of a high-value sesquiterpenoid from the eukaryotic microalga *Chlamydomonas reinhardtii*', *Metabolic Engineering* 38: 331–43.

Lauersen, K. J., H. Berger, J. H. Mussgnug, and O. Kruse. 2013. 'Efficient recombinant protein production and secretion from nuclear transgenes in *Chlamydomonas reinhardtii*', *Journal of Biotechnology*, 167: 101–10.

Lauersen, K. J., J. Wichmann, T. Baier, S. C. Kampranis, I. Pateraki, B. L. Moller, and O. Kruse. 2018. 'Phototrophic production of heterologous diterpenoids and a hydroxy-functionalized derivative from *Chlamydomonas reinhardtii*', *Metabolic Engineering*, 49: 116–27.

Lehmann, T., and S. Pollmann. 2009. 'Gene expression and characterization of a stress-induced tyrosine decarboxylase from *Arabidopsis thaliana*', *FEBS Letters* 583: 1895–900.

Letunic, I., and P. Bork. 2024. 'Interactive Tree of Life (iTOL) v6: recent updates to the phylogenetic tree display and annotation tool', *Nucleic Acids Research*, 52: W78–W82.

Li, Q., J. Xu, Y. Zheng, Y. Zhang, and Y. Cai. 2021. 'Transcriptomic and Metabolomic Analyses Reveals That Exogenous Methyl Jasmonate Regulates Galanthamine Biosynthesis in *Lycoris longituba* Seedlings', *Frontiers in Plant Science*, 12: 713795.

Li, W., C. Qiao, J. Pang, G. Zhang, and Y. Luo. 2019. 'The versatile O-methyltransferase LrOMT catalyzes multiple O-methylation reactions in amaryllidaceae alkaloids biosynthesis', *International Journal of Biological Macromolecules*, 141: 680–92.

Li, Y., B. Guo, J. Yang, Y. Li, B. Chen, and Y. Zheng. 2025. 'Physiological and Molecular Regulation of Amaryllidaceae Alkaloid Biosynthesis in *Lycoris* Species', *Russian Journal of Plant Physiology*, 72.

Li, Y., J. Li, B. Qian, L. Cheng, S. Xu, and R. Wang. 2018. 'De Novo Biosynthesis of p-Coumaric Acid in *E. coli* with a trans-Cinnamic Acid 4-Hydroxylase from the Amaryllidaceae Plant *Lycoris aurea*', *Molecules*, 23.

Li, Y., S. Li, K. Thodey, I. Trenchard, A. Cravens, and C. D. Smolke. 2018. 'Complete biosynthesis of noscapine and halogenated alkaloids in yeast', *Proceedings of the National Academy of Sciences of the United States of America*, 115: E3922–E31.

Li, Y., Y. Wang, L. Huang, C. Chen, N. An, and X. Zheng. 2022. 'Identification and Functional Characterization of Tyrosine Decarboxylase from *Rehmannia glutinosa*', *Molecules*, 27.

Lim, A. W. Y., L. Schneider, and C. Loy. 2024. 'Galantamine for dementia due to Alzheimer's disease and mild cognitive impairment', *The Cochrane Database of Systematic Reviews*, 11: CD001747.

Liu, H., and T. Lu. 2015. 'Autonomous production of 1,4-butanediol via a de novo biosynthesis pathway in engineered *Escherichia coli*', *Metabolic Engineering*, 29: 135–41.

Liu, J., X. Yin, C. Kou, R. Thimmappa, X. Hua, and Z. Xue. 2024. 'Classification, biosynthesis, and biological functions of triterpene esters in plants', *Plant Communications*, 5: 100845.

Lively, Mark. O., and James C. Powers. 1978. 'Specificity And Reactivity Of Human Granulocyte Elastase And Cathepsin G, Porcine Pancreatic Elastase, Bovine Chymotrypsin And Trypsin Toward Inhibition With Sulfonyl Fluorides. ', *Biochimica et Biophysica Acta*, 525: 171–79.

Liyanage, N. S., F. Awwad, K. C. G. dos Santos, T. U. Jayawardena, N. Mérindol, and I. Desgagné-Penix. 2024. 'Navigating Amaryllidaceae alkaloids: Bridging gaps and charting biosynthetic territories', *Journal of Experimental Botany*.

Liyanage, N. S., B. Lamichhane, E. Fantino, N. Merindol, S. E. Gelinas, M. C. Garcia Tobon, and I. Desgagne-Penix. 2025. 'Coclaurine N-methyltransferase-like enzymes drive the final biosynthetic reaction of the anti-Alzheimer's drug galanthamine in Amaryllidaceae', *Plant Physiology and Biochemistry*, 226: 110067.

Luaces, P., R. Sánchez, J. Expósito, A. J. Pérez-Pulido, A. G. Pérez, and C. Sanz. 2024. 'Functional and Physiological Characterization of Tyrosine Decarboxylases from *Olea europaea* L. Involved in the Synthesis of the Main Phenolics in Olive Fruit and Virgin Olive Oil', *International Journal of Molecular Sciences*, 25.

Lumbreras, V., D. R. Stevens, and S. Purton. 2002. 'Efficient foreign gene expression in *Chlamydomonas reinhardtii* mediated by an endogenous intron', *Plant Journal*, 14: 441–47.

Luo, J., J. Deng, L. Cui, P. Chang, X. Dai, C. Yang, N. Li, Z. Ren, and X. Zhang. 2020. 'The potential assessment of green alga *Chlamydomonas reinhardtii* CC-503 in the biodegradation of benz(a)anthracene and the related mechanism analysis', *Chemosphere*, 249: 126097.

Maeda, H., and N. Dudareva. 2012. 'The shikimate pathway and aromatic amino Acid biosynthesis in plants', *Annual review of plant biology*, 63: 73–105.

Majhi, B. B., S. E. Gelinas, N. Merindol, S. Ricard, and I. Desgagne-Penix. 2023. 'Characterization of norbelladine synthase and noroxomaritidine/norcraugsodine reductase reveals a novel catalytic route for the biosynthesis of Amaryllidaceae alkaloids including the Alzheimer's drug galanthamine', *Frontiers in Plant Science*, 14: 1231809.

Marshall, W. F. 2024. '*Chlamydomonas* as a model system to study cilia and flagella using genetics, biochemistry, and microscopy', *Frontiers in Cell and Developmental Biology*, 12: 1412641.

Masi, A., F. Leonelli, V. Scognamiglio, G. Gasperuzzo, A. Antonacci, and M. A. Terzidis. 2023. '*Chlamydomonas reinhardtii*: A Factory of Nutraceutical and Food Supplements for Human Health', *Molecules*, 28.

Matsuda, F., K. Morino, R. Ano, M. Kuzawa, K. Wakasa, and H. Miyagawa. 2005. 'Metabolic flux analysis of the phenylpropanoid pathway in elicitor-treated potato tuber tissue', *Plant Cell Physiology*, 46: 454–66.

Matthew, T., W. Zhou, J. Rupprecht, L. Lim, S. R. Thomas-Hall, A. Doebbe, O. Kruse, B. Hankamer, U. C. Marx, S. M. Smith, and P. M. Schenk. 2009. 'The metabolome of *Chlamydomonas reinhardtii* following induction of anaerobic H2 production by sulfur depletion', *Journal of Biological Chemistry*, 284: 23415–25.

Meerow, A.W. 2023. 'Classification and phylogeny of Amaryllidaceae, the modern synthesis and the road ahead: a review', *Boletín de la Sociedad Argentina de Botánica*, 58.

Meerow, A.W., and D.A. Snijman. 1998. 'Amaryllidaceae.' in, *The Families and Genera of Vascular Plants - Flowering Plants. Monocotyledons Lilianae (except Orchidaceae)* (Springer).

Mehta, N., Y. Meng, R. Zare, R. Kamenetsky-Goldstein, and E. Sattely. 2024. 'A developmental gradient reveals biosynthetic pathways to eukaryotic toxins in monocot geophytes', *Cell*, 187: 5620–37 e10.

Mellor, S. B., Jbyh Behrendorff, J. O. Ipsen, C. Crocoll, T. Laursen, E. M. J. Gillam, and M. Pribil. 2022. 'Exploiting photosynthesis-driven P450 activity to produce indican in tobacco chloroplasts', *Frontiers in Plant Science*, 13: 1049177.

Mendez-Bravo, A., C. Calderon-Vazquez, E. Ibarra-Laclette, J. Raya-Gonzalez, E. Ramirez-Chavez, J. Molina-Torres, A. A. Guevara-Garcia, J. Lopez-Bucio, and L. Herrera-Estrella. 2011. 'Alkamides activate jasmonic acid biosynthesis and signaling pathways and confer resistance to *Botrytis cinerea* in *Arabidopsis thaliana*', *PLoS One*, 6: e27251.

Merchant, S. S., S. E. Prochnik, O. Vallon, E. H. Harris, S. J. Karpowicz, G. B. Witman, A. Terry, A. Salamov, L. K. Fritz-Laylin, L. Marechal-Drouard, W. F. Marshall, L. H. Qu, D. R. Nelson, A. A. Sanderfoot, M. H. Spalding, V. V. Kapitonov, Q. Ren, P. Ferris, E. Lindquist, H. Shapiro, S. M. Lucas, J. Grimwood, J. Schmutz, P. Cardol, H. Cerutti, G. Chanfreau, C. L. Chen, V. Cognat, M. T. Croft, R. Dent, S. Dutcher, E. Fernandez, H. Fukuzawa, D. Gonzalez-Ballester, D. Gonzalez-Halphen, A. Hallmann, M. Hanikenne, M. Hippler, W. Inwood, K. Jabbari, M. Kalanon, R. Kuras, P. A. Lefebvre, S. D. Lemaire, A. V. Lobanov, M. Lohr, A. Manuell, I. Meier, L. Mets, M. Mittag, T. Mittelmeier, J. V. Moroney, J. Moseley, C. Napoli, A. M. Nedelcu, K. Niyogi, S. V. Novoselov, I. T. Paulsen, G. Pazour, S. Purton, J. P. Ral, D. M. Riano-Pachon, W. Riekhof, L. Rymarquis, M. Schroda, D. Stern, J. Umen, R. Willows, N. Wilson, S. L. Zimmer, J. Allmer, J. Balk, K. Bisova, C. J. Chen, M. Elias, K. Gendler, C. Hauser, M. R. Lamb, H. Ledford, J. C. Long, J. Minagawa, M. D. Page, J. Pan, W. Pootakham, S. Roje, A. Rose, E. Stahlberg, A. M. Terauchi, P. Yang, S. Ball, C. Bowler, C. L. Dieckmann, V. N. Gladyshev, P. Green, R. Jorgensen, S. Mayfield, B. Mueller-Roeber, S. Rajamani, R. T. Sayre, P. Brokstein, I. Dubchak, D. Goodstein, L. Hornick, Y. W. Huang, J. Jhaveri, Y. Luo, D. Martinez, W. C. Ngau, B. Otillar, A. Poliakov, A. Porter, L. Szajkowski, G. Werner, K. Zhou, I. V. Grigoriev, D. S. Rokhsar, and A. R. Grossman. 2007. 'The *Chlamydomonas* genome reveals the evolution of key animal and plant functions', *Science*, 318: 245–50.

Milne, N., P. Thomsen, N. Molgaard Knudsen, P. Rubaszka, M. Kristensen, and I. Borodina. 2020. 'Metabolic engineering of *Saccharomyces cerevisiae* for the de novo production of psilocybin and related tryptamine derivatives', *Metabolic Engineering*, 60: 25–36.

Mladenovic, D., J. Brealey, B. Peacock, K. Koort, and N. Zarovni. 2025. 'Quantitative fluorescent nanoparticle tracking analysis and nano-flow cytometry enable advanced characterization of single extracellular vesicles', *ournal of Extracellular Biology*, 4: e70031.

Mora-Vasquez, S., G. G. Wells-Abascal, C. Espinosa-Leal, G. A. Cardineau, and S. Garcia-Lara. 2022. 'Application of metabolic engineering to enhance the content of alkaloids in medicinal plants', *Metabolic Engineering Communications*, 14: e00194.

Moreno-Arribas, V. , and A. Lonvaud-Funel. 1999. 'Tyrosine decarboxylase activity of *Lactobacillus brevis* IOEB 9809 isolated from wine and *L. brevis* ATCC 367', *FEMS Microbiology Letters* 180: 55–60.

Motyka, S., K. Jafernik, H. Ekiert, J. Sharifi-Rad, D. Calina, B. Al-Omari, A. Szopa, and W. C. Cho. 2023. 'Podophyllotoxin and its derivatives: Potential anticancer agents of natural origin in cancer chemotherapy', *Biomedicine & Pharmacotherapy*, 158: 114145.

Nair, J. J., J Bastida, and J Van Stadena. 2016. 'In vivo Cytotoxicity Studies of Amaryllidaceae Alkaloids'.

Neupert, J., S. D. Gallaher, Y. Lu, D. Strenkert, N. Segal, R. Barahimipour, S. T. Fitz-Gibbon, M. Schroda, S. S. Merchant, and R. Bock. 2020. 'An epigenetic gene silencing pathway selectively acting on transgenic DNA in the green alga *Chlamydomonas*', *Nature Communications*, 11: 6269.

Neupert, J., D. Karcher, and R. Bock. 2009. 'Generation of *Chlamydomonas* strains that efficiently express nuclear transgenes', *The Plant Journal* 57: 1140–50.

Nickelsen, J, and U Kück. 2000. 'The Unicellular Green Alga *Chlamydomonas reinhardtii* as an Experimental System to Study Chloroplast RNA Metabolism', *Naturwissenschaften*.

Niemeyer, J., L. Fischer, F. O. Aylward, and M. Schroda. 2023. 'Analysis of Viral Promoters for Transgene Expression and of the Effect of 5'-UTRs on Alternative Translational Start Sites in *Chlamydomonas*', *Genes (Basel)*, 14.

Noda, S., T. Shirai, K. Mochida, F. Matsuda, S. Oyama, M. Okamoto, and A. Kondo. 2015. 'Evaluation of *Brachypodium distachyon* L-Tyrosine Decarboxylase Using L-Tyrosine Over-Producing *Saccharomyces cerevisiae*', *PLoS One*, 10: e0125488.

Orouji, N., S. K. Asl, Z. Taghipour, S. Habtemariam, S. M. Nabavi, and R. Rahimi. 2023. 'Glucosinolates in cancer prevention and treatment: experimental and clinical evidence', *Medical Oncology*, 40: 344.

Ortiz, A., and E. Sansinenea. 2023. 'Phenylpropanoid Derivatives and Their Role in Plants' Health and as antimicrobials', *Current Microbiology*, 80: 380.

Overton, T. W. 2014. 'Recombinant protein production in bacterial hosts', *Drug Discovery Today*, 19: 590–601.

Park, C.H., H.J. Yeo, Y.E. Park, S.A. Baek, J.K. Kim, and S.U. Park. 2019. 'Transcriptome Analysis and Metabolic Profiling of *Lycoris Radiata*', *Biology*, 8.

Park, J. B. 2014. 'Synthesis and characterization of norbelladine, a precursor of Amaryllidaceae alkaloid, as an anti-inflammatory/anti-COX compound', *Bioorganic & Medicinal Chemistry Letters*, 24: 5381–4.

Patil, H., A. Baviskar, J. Dinore, and A. Yelwande. 2025. 'Advances in Terpenoid Biosynthesis: Chemical Diversity and Emerging Industrial Applications', *Sciences of Phytochemistry*, 4: 62–75.

Perozeni, F., S. Cazzaniga, T. Baier, F. Zanoni, G. Zoccatelli, K. J. Lauersen, L. Wobbe, and M. Ballottari. 2020. 'Turning a green alga red: engineering astaxanthin biosynthesis by intragenic pseudogene revival in *Chlamydomonas reinhardtii*', *Plant Biotechnology Journal*, 18: 2053–67.

Phillips, D. R., J. M. Rasbery, B. Bartel, and S. P. Matsuda. 2006. 'Biosynthetic diversity in plant triterpene cyclization', *Current Opinion in Plant Biology*, 9: 305–14.

Pirselova, B., and J. Jakubcinova. 2025. 'Plant cyanogenic glycosides: from structure to properties and potential applications', *Frontiers in Plant Science*, 16: 1612132.

Planells-Carcel, A., E. Valera-Garcia, G. Quintas, J. L. Martinez, S. Muniz-Calvo, and J. M. Guillamon. 2025. 'Metabolic Engineering of a Serotonin Overproducing *Saccharomyces cerevisiae* Strain', *Microbial Biotechnology*, 18: e70140.

Poethe, S. S., N. Junker, F. Meyer, and V. F. Wendisch. 2024. 'Sustainable production of the drug precursor tyramine by engineered *Corynebacterium glutamicum*', *Applied Microbiology and Biotechnology*, 108: 499.

Ptak, A., M. Warchol, E. Moranska, D. Laurain-Mattar, R. Spina, F. Dupire, P. Waligorski, and M. Simlat. 2026. 'Amaryllidaceae Alkaloids and Phenolic Acids Identification in *Leucojum aestivum* L. Plant Cultures Exposed to Different Temperature Conditions', *Molecules*, 31.

Pyne, M. E., L. Narcross, and V. J. J. Martin. 2019. 'Engineering Plant Secondary Metabolism in Microbial Systems', *Plant Physiology*, 179: 844–61.

Qu, Y., O. Safonova, and V. De Luca. 2019. 'Completion of the canonical pathway for assembly of anticancer drugs vincristine/vinblastine in *Catharanthus roseus*', *Plant Journal*, 97: 257–66.

R Core Team. 2024. "R: A language and environment for statistical computing." In.: R Foundation for Statistical Computing.

Rasala, B. A., S. S. Chao, M. Pier, D. J. Barrera, and S. P. Mayfield. 2014. 'Enhanced genetic tools for engineering multigene traits into green algae', *PLoS One*, 9: e94028.

Rasala, B. A., and S. P. Mayfield. 2015. 'Photosynthetic biomanufacturing in green algae; production of recombinant proteins for industrial, nutritional, and medical uses', *Photosynthesis Research*, 123: 227–39.

Renda, G., I. Gokkaya, and D. Sohretoglu. 2022. 'Immunomodulatory properties of triterpenes', *Phytochemistry Reviews*, 21: 537–63.

Robert, X., C. Guillon, and P. Gouet. 2025. 'FoldScript: a web server for the efficient analysis of AI-generated 3D protein models', *Nucleic Acids Research*, 53: W277–W82.

Roy, M., L. Liang, X. Xiao, P. Feng, M. Ye, and J. Liu. 2018. 'Lycorine: A prospective natural lead for anticancer drug discovery', *Biomedicine & Pharmacotherapy*, 107: 615–24.

Salim, V., S. A. Jarecki, M. Vick, and R. Miller. 2023. 'Advances in Metabolic Engineering of Plant Monoterpene Indole Alkaloids', *Biology (Basel)*, 12.

Salome, P. A., and S. S. Merchant. 2019. 'A Series of Fortunate Events: Introducing Chlamydomonas as a Reference Organism', *Plant Cell*, 31: 1682–707.

Sandmeier, Erika, Terence Hale, and Philipp; Christen. 1994. 'Multiple evolutionary origin of pyridoxal-5'-phosphate-dependent amino acid decarboxylases', *European Journal of Biochemistry*, 221: 997–1002.

Santos, G. S., S. B. P. Sinoti, F. T. C. de Almeida, D. Silveira, L. A. Simeoni, and K. K. P. Gomes-Copeland. 2020. 'Use of galantamine in the treatment of Alzheimer's disease and strategies to optimize its biosynthesis using the *in vitro* culture technique', *Plant Cell, Tissue and Organ Culture (PCTOC)*, 143: 13–29.

Sarvananda, L, H. D. T. Madhuranga, B. L. N. K. Madhurangi, A. D. Premarathna, and M. Saravanan. 2025. 'Alkaloids unveiled: A comprehensive analysis of novel therapeutic properties, mechanisms, and plant-based innovations', *Intelligent Pharmacy*, 3: 268–76.

Sayers, E. W., J. Beck, E. E. Bolton, J. R. Brister, J. Chan, R. Connor, M. Feldgarden, A. M. Fine, K. Funk, J. Hoffman, S. Kannan, C. Kelly, W. Klimke, S. Kim, S. Lathrop, A. Marchler-Bauer, T. D. Murphy, C. O'Sullivan, E. Schmieder, Y. Skripchenko, A. Stine, F. Thibaud-Nissen, J. Wang, J. Ye, E. Zellers, V. A. Schneider, and K. D. Pruitt. 2025. 'Database resources of the National Center for Biotechnology Information in 2025', *Nucleic Acids Research*, 53: D20–D29.

Scaife, M. A., Gtdt Nguyen, J. Rico, D. Lambert, K. E. Helliwell, and A. G. Smith. 2015. 'Establishing *Chlamydomonas reinhardtii* as an industrial biotechnology host', *Plant Journal*, 82: 532–46.

Schroda, M. 2019. 'Good News for Nuclear Transgene Expression in *Chlamydomonas*', *Cells*, 8.

Schroda, M., C. F. Beck, and O. Vallon. 2002. 'Sequence elements within an HSP70 promoter counteract transcriptional transgene silencing in *Chlamydomonas*', *Plant Journal*, 31: 445–55.

Schroda, M., D. Blocker, and C. F. Beck. 2000. 'The HSP70A promoter as a tool for the improved expression of transgenes in *Chlamydomonas*', *Plant Journal*, 21: 121–31.

Scranton, Melissa A., Joseph T. Ostrand, D. Ryan Georgianna, Shane M. Lofgren, Daphne Li, Rosalie C. Ellis, David N. Carruthers, Andreas Dräger, David L. Masica, and Stephen P. Mayfield. 2016. 'Synthetic promoters capable of driving robust nuclear gene expression in the green alga *Chlamydomonas reinhardtii*', *Algal Research*, 15: 135–42.

Shahar, N., S. Landman, I. Weiner, T. Elman, E. Dafni, Y. Feldman, T. Tuller, and I. Yacoby. 2019. 'The Integration of Multiple Nuclear-Encoded Transgenes in the Green Alga *Chlamydomonas reinhardtii* Results in Higher Transcription Levels', *Frontiers in Plant Science*, 10: 1784.

Sharifi-Rad, J., C. Quispe, J. K. Patra, Y. D. Singh, M. K. Panda, G. Das, C. O. Adetunji, O. S. Michael, O. Sytar, L. Polito, J. Zivkovic, N. Cruz-Martins, M. Klimek-Szczykutowicz, H. Ekiert, M. I. Choudhary, S. A. Ayatollahi, B. Tynybekov, F. Kobarfard, A. C. Muntean, I. Grozea, S. D. Dastan, M. Butnariu, A. Szopa, and D. Calina. 2021. 'Paclitaxel: Application in Modern Oncology and Nanomedicine-Based Cancer Therapy', *Oxidative Medicine and Cellular Longevity*, 2021: 3687700.

Shen, J., P. Liu, B. Zhang, B. Ye, S. Xu, W. Su, and X. Chu. 2025. 'Expanding the application of tyrosine: engineering microbes for the production of tyrosine and its derivatives', *Frontiers in Bioengineering and Biotechnology*, 13: 1519764.

Shende, V. V., K. D. Bauman, and B. S. Moore. 2024. 'The shikimate pathway: gateway to metabolic diversity', *Natural Product Reports*, 41: 604–48.

Shimogawara, K., S. Shoko Fujiwara, A. Arthur Grossman, and H. Hideaki Usuda. 1998. 'High-Efficiency Transformation of *Chlamydomonas reinhardtii* by Electroporation'.

Sievers, F., and D. G. Higgins. 2018. 'Clustal Omega for making accurate alignments of many protein sequences', *Protein Science*, 27: 135–45.

Singh, A., and I. Desgagné-Penix. 2017. 'Transcriptome and metabolome profiling of *Narcissus pseudonarcissus* 'King Alfred' reveal components of Amaryllidaceae alkaloid metabolism', *Scientific Reports*, 7.

Singh, A., M. A. Massicotte, A. Garand, L. Tousignant, V. Ouellette, G. Berube, and I. Desgagne-Penix. 2018. 'Cloning and characterization of norbelladine synthase catalyzing the first committed reaction in Amaryllidaceae alkaloid biosynthesis', *BMC Plant Biology*, 18: 338.

Singh, A.; Isabel Desgagné-Penix. 2018. 'Discovery of novel genes and enzymes involved in amaryllidaceae alkaloid biosynthesis using integrated metabolomics and transcriptomics in *Narcissus*', *Scientific Reports*.

Slattery, S. S., A. Diamond, H. Wang, J. A. Therrien, J. T. Lant, T. Jazey, K. Lee, Z. Klassen, I. Desgagne-Penix, B. J. Karas, and D. R. Edgell. 2018. 'An Expanded Plasmid-Based Genetic Toolbox Enables Cas9 Genome Editing and Stable Maintenance of Synthetic Pathways in *Phaeodactylum tricornutum*', *ACS Synthetic Biology*, 7: 328–38.

Sproles, Ashley E., Francis J. Fields, Tressa N. Smalley, Chau H. Le, Amr Badary, and Stephen P. Mayfield. 2021. 'Recent advancements in the genetic engineering of microalgae', *Algal Research*, 53.

Sreenikethanam, A., S. Raj, R. B. J, P. Gugulothu, and A. K. Bajhaiya. 2022. 'Genetic Engineering of Microalgae for Secondary Metabolite Production: Recent Developments, Challenges, and Future Prospects', *Frontiers in Bioengineering and Biotechnology*, 10: 836056.

Stern, D., and G. Witman. 2009. *The Chlamydomonas Sourcebook*.

Suhadolnik, R. J. , A. G. Fischer, and J. Zulalia. 1963. 'Biogenesis of the Amaryllidaceae Alkaloids. Part III. L-Phenylahine and Protocatechuic Aldehyde as C,C,

Precursors of Haemanthamine and Lycorine'.

Sun, B., P. Wang, R. Wang, Y. Li, and S. Xu. 2018. 'Molecular Cloning and Characterization of a meta/para-O-Methyltransferase from *Lycoris aurea*', *International Journal of Molecular Sciences*, 19.

Takos, A. M., and F. Rook. 2013. 'Towards a molecular understanding of the biosynthesis of amaryllidaceae alkaloids in support of their expanding medical use', *International Journal of Molecular Sciences*, 14: 11713–41.

Thawabteh, A. M., A. W. Ghanem, S. AbuMadi, D. Thaher, W. Jaghama, R. Karaman, L. Scrano, and S. A. Bufo. 2024. 'Antibacterial Activity and Antifungal Activity of Monomeric Alkaloids', *Toxins (Basel)*, 16.

Torrens-Spence, M. P., Y. C. Chiang, T. Smith, M. A. Vicent, Y. Wang, and J. K. Weng. 2020a. 'Structural basis for divergent and convergent evolution of catalytic machineries in plant aromatic amino acid decarboxylase proteins', *Proc Natl Acad Sci U S A*, 117: 10806–17.

———. 2020b. 'Structural basis for divergent and convergent evolution of catalytic machineries in plant aromatic amino acid decarboxylase proteins', *Proceedings of the National Academy of Sciences*, 117: 10806–17.

Torrens-Spence, M. P., G. Gillaspy, B. Zhao, K. Harich, R. H. White, and J. Li. 2012. 'Biochemical evaluation of a parsley tyrosine decarboxylase results in a novel 4-hydroxyphenylacetaldehyde synthase enzyme', *Biochemical And Biophysical Research Communications*, 418: 211–6.

Torrens-Spence, M. P., M. Lazear, R. von Guggenberg, H. Ding, and J. Li. 2014. 'Investigation of a substrate-specifying residue within *Papaver somniferum* and *Catharanthus roseus* aromatic amino acid decarboxylases', *Phytochemistry*, 106: 37–43.

Torrens-Spence, M. P., P. Liu, H. Ding, K. Harich, G. Gillaspy, and J. Li. 2013. 'Biochemical evaluation of the decarboxylation and decarboxylation-deamination activities of plant aromatic amino acid decarboxylases', *Journal of Biological Chemistry*, 288: 2376–87.

Torres-Tiji, Y., F. J. Fields, and S. P. Mayfield. 2020. 'Microalgae as a future food source', *Biotechnology Advances*, 41: 107536.

Tousignant, L., A. M. Diaz-Garza, B. Majhi, S. Gélinas, A. Singh, and I. Desgagné-Penix. 2022. 'Transcriptome analysis of Leucojum aestivum and identification of genes involved in norbelladine biosynthesis', *Planta*, 255.

Tousignant, Laurence, Aracely Maribel Diaz-Garza, Bharat Bhusan Majhi, Sarah-Eve Gélinas, Aparna Singh, and Isabel Desgagne-Penix. 2022. 'Transcriptome analysis of Leucojum aestivum and identification of genes involved in norbelladine biosynthesis', *Planta*, 255: 30.

Tran, N. T., and R. Kaldenhoff. 2020. 'Achievements and challenges of genetic engineering of the model green alga *Chlamydomonas reinhardtii*', *Algal Research*, 50.

Vogt, T. 2010. 'Phenylpropanoid biosynthesis', *Molecular Plant*, 3: 2–20.

Wang, R., X. Han, S. Xu, B. Xia, Y. Jiang, Y. Xue, and R. Wang. 2019. 'Cloning and characterization of a tyrosine decarboxylase involved in the biosynthesis of galanthamine in *Lycoris aurea*', *PeerJ*, 7: e6729.

Wang, X., J. Xin, L. Sun, Y. Sun, Y. Xu, F. Zhao, C. Niu, and S. Liu. 2024. 'Exploring the Biomedical Potential of Terpenoid Alkaloids: Sources, Structures, and Activities', *Molecules*, 29.

Wichmann, J., T. Baier, E. Wentnagel, K. J. Lauersen, and O. Kruse. 2018. 'Tailored carbon partitioning for phototrophic production of (E)-alpha-bisabolene from the green microalga *Chlamydomonas reinhardtii*', *Metabolic Engineering*, 45: 211–22.

Wink, M., M. Ashour, and F. Botschen. 2010. *Biochemistry of plant secondary metabolism* (Blackwell Publishing Ltd.: Annual plant reviews).

Wurtzel, E. T. 2019. 'Changing Form and Function through Carotenoids and Synthetic Biology', *Plant Physiology*, 179: 830–43.

Xiang, C., J. Liu, L. Ma, and M. Yang. 2020. 'Overexpressing codon-adapted fusion proteins of 4-coumaroyl-CoA ligase (4CL) and stilbene synthase (STS) for resveratrol production in *Chlamydomonas reinhardtii*', *Journal of Applied Phycology*, 32: 1669–76.

Xie, Q., and C. Wang. 2022. 'Polyacetylenes in herbal medicine: A comprehensive review of its occurrence, pharmacology, toxicology, and pharmacokinetics (2014-2021)', *Phytochemistry*, 201: 113288.

Yang, W. , X. Chen, Y. Li, S. Guo, Z. Wang, and Yu. X. 2020. 'Advances in Pharmacological Activities of Terpenoids', *Natural Product Communications*.

Yang, X., X. Miao, L. Dai, X. Guo, J. Jenis, J. Zhang, and X. Shang. 2024. 'Isolation, biological activity, and synthesis of isoquinoline alkaloids', *Natural Product Reports*, 41: 1652–722.

Yu, O., and J. M. Jez. 2008. 'Nature's assembly line: biosynthesis of simple phenylpropanoids and polyketides', *Plant Journal*, 54: 750–62.

Zhang, J., L. G. Hansen, O. Gudich, K. Viehrig, L. M. M. Lassen, L. Schrubbers, K. B. Adhikari, P. Rubaszka, E. Carrasquer-Alvarez, L. Chen, V. D'Ambrosio, B. Lehka, A. K. Haidar,

S. Nallapareddy, K. Giannakou, M. Laloux, D. Arsovska, M. A. K. Jorgensen, L. J. G. Chan, M. Kristensen, H. B. Christensen, S. Sudarsan, E. A. Stander, E. Baidoo, C. J. Petzold, T. Wulff, S. E. O'Connor, V. Courdavault, M. K. Jensen, and J. D. Keasling. 2022. 'A microbial supply chain for production of the anti-cancer drug vinblastine', *Nature*, 609: 341–47.

Zhang, K., and Y. Ni. 2014. 'Tyrosine decarboxylase from *Lactobacillus brevis*: soluble expression and characterization', *Protein Expression and Purification*, 94: 33–9.

Zhang, M. P., M. Wang, and C. Wang. 2021. 'Nuclear transformation of *Chlamydomonas reinhardtii*: A review', *Biochimie*, 181: 1–11.

Zhang, X., and C. J. Liu. 2015. 'Multifaceted regulations of gateway enzyme phenylalanine ammonia-lyase in the biosynthesis of phenylpropanoids', *Molecular Plant*, 8: 17–27.

Zhao, Y., G. Liu, F. Yang, Y. Liang, Q. Gao, C. Xiang, X. Li, R. Yang, G. Zhang, H. Jiang, L. Yu, and S. Yang. 2023. 'Multilayered regulation of secondary metabolism in medicinal plants', *Molecular Horticulture*, 3: 11.

Zhu, H., G. Xu, K. Zhang, X. Kong, R. Han, J. Zhou, and Y. Ni. 2016. 'Crystal structure of tyrosine decarboxylase and identification of key residues involved in conformational swing and substrate binding', *Scientific Reports*, 6: 27779.

Zhu, X., X. Zeng, C. Sun, and S. Chen. 2014. 'Biosynthetic pathway of terpenoid indole alkaloids in *Catharanthus roseus*', *Frontiers Medicine*, 8: 285–93.

Ziegler, J., and P. J. Facchini. 2008. 'Alkaloid biosynthesis: metabolism and trafficking', *Annual review of plant biology*, 59: 735–69.

Zong, X., X. Yan, J. L. Wu, Z. Liu, H. Zhou, N. Li, and L. Liu. 2019. 'Potentially Cardiotoxic Diterpenoid Alkaloids from the Roots of *Aconitum carmichaelii*', *Journal of Natural Products*, 82: 980–89.